

**Overexpression and isolation of the
intermediate state of serotonin transporter
from *Echinococcus multilocularis*
— the ER localized HSP complexes of the
folding trajectory**

Inaugural-Dissertation

zur Erlangung des Doktorgrades
der Mathematisch-Naturwissenschaftlichen Fakultät
der Heinrich-Heine-Universität Düsseldorf

vorgelegt von

Weihou Guo
aus Xinjiang, China

Hamburg, June 2021

aus dem Institut für Physikalische Biologie
der Heinrich-Heine-Universität Düsseldorf

Gedruckt mit der Genehmigung der
Mathematisch-Naturwissenschaftlichen Fakultät der
Heinrich-Heine-Universität Düsseldorf

Berichtersteller:

1. Referent: Prof. Dr. Jörg Labahn
2. Korreferent: Prof. Dr. Henrike Heise

Tag der mündlichen Prüfung: 06.08.2021

Contents

List of Figure	IV
List of Table	VII
1 Introduction	1
1.1 The alveolar hydatid disease	1
1.2 The life cycle of <i>Echinococcus multilocularis</i>	2
1.3 Serotonergic pathway	4
1.4 Serotonin transporter	7
1.5 The extended chaperone/COPII exchange model	9
1.6 Aim of this study.....	11
2 Materials and methods	12
2.1 Materials and instruments	12
2.1.1 Consumables and Instruments.....	12
2.1.2 Biological materials.....	14
2.1.3 Purification, Assay and Gel Electrophoresis Buffers.....	18
2.2 Cloning	20
2.2.1 Site-directed mutagenesis.....	21
2.3 Cell-free expression with the continuous exchange cell-free system (CECF).....	24
2.3.1 Plasmid preparation	25
2.3.2 Nanodiscs preparation	25
2.3.3 CECF reaction set-up.....	26
2.4 <i>In vivo</i> emST expression	28
2.4.1 Bacterial expression	28
2.4.2 Insect cell expression.....	29
2.4.3 Mammalian cell expression.....	32
2.5 emST purification.....	33
2.5.1 Cell lysis and membrane preparation.....	33
2.5.2 Affinity chromatography	35

2.5.3	Ion exchange chromatography	36
2.5.4	Size exclusion chromatography	36
2.6	Deglycosylation assay	36
2.7	Protein Identification and Characterization.....	37
2.7.1	Mass spectrometry	37
2.7.2	Circular dichroism spectroscopy	38
2.8	Subcellular localization	39
2.8.1	Confocal microscopy	39
2.8.2	Cell fractionation and organelle isolation	42
3	Results	45
3.1	Bacterial system.....	45
3.1.1	In vitro expression and purification of emST by CECF	45
3.1.2	In vivo expression and purification of emST	50
3.1.3	Mass spectrometric analysis of emST.....	57
3.1.4	CD spectroscopic analysis	58
3.2	Insect cell expression system	59
3.2.1	Expression of emST-rho in Sf9 cells	59
3.2.2	Expression of emST in High 5 cells	60
3.3	Mammalian expression system	60
3.3.1	Expression analysis of emST	60
3.3.2	Detergent screening for solubilization of emST	62
3.3.3	Purification of emST-rho and its variants	64
3.3.4	Analysis of emST glycosylation	71
3.3.5	Mass spectrometric analysis of emST.....	72
3.3.6	CD spectroscopic analysis	74
3.3.7	Subcellular localization of emST	77
4	Discussion	82
4.1	Unfolded emST from <i>E.coli</i> and in-vitro expression.....	82
4.2	EmST was isolated in form of HSP complexes	84
4.3	The conformation of the emST-HSP complexes	88

4.4	Difference for emST with regard to the extended chaperone/COPII exchange model	89
4.5	Ex-vivo reconstitution of the PM state of emST	90
4.6	The role of glycosylation	92
4.7	Transport process and degradation pathway	95
4.8	Perspectives	97
	Summary	98
	Zusammenfassung	99
	Bibliography	101
	Abbreviations	117
	Appendix I: DNA and protein sequences	119
	Appendix II: Alignment of ST	123
	Appendix III: Primers	124
	Appendix IV: Protocols	127
	Acknowledgments	128
	Erklärung	129

List of Figure

Figure 1.1 Approximate global distribution of alveolar hydatid disease (Adapted from [16]).....	1
Figure 1.2 <i>E. multilocularis</i> adults isolated from a fox in Erzurum province (stereomicroscope) (adopted from [35]).....	2
Figure 1.3 Life cycle of the <i>E. multilocularis</i>	3
Figure 1.4 Putative serotonin pathway in <i>Echinococcus species</i> (adopted from [56]).	4
Figure 1.5 Lifecycle of a serotonin molecule(Figure adapted from [65])	5
Figure 1.6 The biochemical pathway of serotonin synthesis and metabolism (adopted from [65, 69])	6
Figure 1.7 Schematic representation of key steps in the physiological transport cycle of hST (adopted from [73]) and prediction of emST three conformations states	7
Figure 1.8 The architecture of the human serotonin transporter (adopted from [86]) ..	8
Figure 1.9 hST transmembrane topology comprises 12 membrane-spanning helices bound by intracellular and extracellular loops (adopted from [73]).....	9
Figure 1.10 Extended chaperone/COPII exchange model (Resource [57]).....	10
Figure 2.1 Schematic depiction of an MSP nanodisc	25
Figure 2.2 CECF reaction in a two-chamber dialysis device.....	27
Figure 2.3 Intracellular Transport Pathways (adapt from [166]).....	41
Figure 3.1 Without a solubilizer, anti-His western blot of cell-free expressed emST .	46
Figure 3.2 Western blot of cell-free expressed emST without a solubilizer	46
Figure 3.3 emST expressed into nanodiscs anti-his western blot	48
Figure 3.4 Expression and purification of emST-nanodisc in in-vitro system	49
Figure 3.5 emST in BL21(DE3) strains with pET27b _{emST-his} expression	50
Figure 3.6 Expression analysis of emST in different strains with pET27b _{emST-his}	51
Figure 3.7 emST expressed in RP cells with pET27b _{emST-his} (ZY-CAIM).....	51
Figure 3.8 emST expressed in RP cells with pET27b _{emST-his} (TB-CAIM).....	52
Figure 3.9 Expression analysis of emST in RIL cells with pET27b _{emST-his}	53
Figure 3.10 Expression analysis of emST in RIL and RP cells with pQE2 _{emST-his}	54
Figure 3.11 Expression analysis of emST in BL21(DE3) cells with pQE2 _{emST-his}	55
Figure 3.12 Purification analysis of emST in BL21(DE3) cells with pQE2 _{emST-his}	56
Figure 3.13 SEC analysis of emST in BL21(DE3) cells with pQE2 _{emST-his}	56

Figure 3.14 Expression analysis of emST in BL21(DE3) cells with pET20a _{emST-rho}	57
Figure 3.15 Peptides identification of emST by LC-MS/MS analysis	58
Figure 3.16 CD spectra of emST-his	58
Figure 3.17 Anti-Rho western blot of <i>Sf9</i> cell expressed emST	59
Figure 3.18 Anti-Rho western blot of <i>High 5</i> cell expressed emST	60
Figure 3.19 Mammalian expressions for different construct of emST.....	61
Figure 3.20 Anti-Rho western blot of mammalian cell expressed emST mutants	62
Figure 3.21 Detergent screening of mammalian expressed emST	63
Figure 3.22 Fos-12 and DIBMA solubilization of emST	64
Figure 3.23 Rho-tag Purification of <i>Expi 293</i> expressed emST	65
Figure 3.24 SEC Purification of <i>Expi 293</i> expressed emST	65
Figure 3.25 DIBMA Purification of <i>Expi 293</i> expressed wild type emST	66
Figure 3.26 DIBMA SEC Purification of <i>Expi 293</i> expressed wild type emST.....	67
Figure 3.27 Fos12 Purification of <i>Expi 293</i> expressed wild type emST.....	67
Figure 3.28 Fos12 SEC Purification of <i>Expi 293</i> expressed wild type emST	68
Figure 3.29 DDM Purification of <i>Expi 293</i> expressed emST-tm2 emST	68
Figure 3.30 DDM SEC Purification of <i>Expi 293</i> expressed emST-tm2 emST	69
Figure 3.31 Rho-tag Purification of <i>Expi 293</i> expressed emST-mCherry	70
Figure 3.32 SEC Purification of <i>Expi 293</i> expressed emST-mCherry	70
Figure 3.33 SEC profile of Superdex 200pg	71
Figure 3.34 SDS-PAGE analysis of emST digested with endo H or PNGase F	71
Figure 3.35 Peptides identified of emST by LC-MS/MS.....	72
Figure 3.36 Peptides identified of HSP by LC-MS/MS	73
Figure 3.37 Sequence and extracted ion chromatogram (XIC) diagram	74
Figure 3.38 CD spectra of emST-rho	75
Figure 3.39 CD spectra of emST-tm2-rho and emST-mCherry-rho	76
Figure 3.40 Co-localization of VAP-A, ERGIC-53 and emST-mCherry in transfected <i>Expi293</i> cells.	78
Figure 3.41 Co-localization of GM130, EEA1 Rab7 Rab11 LAMP1, and emST-mCherry in transfected <i>Expi293</i> cells.	79
Figure 3.42 Fractional image acquired during isolation.....	80
Figure 3.43 Intracellular distribution of emST and other markers.....	81

Figure 4.1 Native folding and trafficking from ER to the plasma membrane. (adopted from [106]).....	87
Figure 4.2 Cryo-EM reconstructions of occluded hST conformations.....	91
Figure 4.3 emST model and hST structure	93
Figure 4.4 Oligosaccharide synthesis of synthesized glycoproteins in ER.....	94
Figure 4.5 Sequences alignment of C-terminal hST and emST	96
Figure II.0.1 MUSCLE alignment of emST and hST sequences.	123

List of Table

Table 2.1 Instruments	13
Table 2.2 Consumables.....	12
Table 2.3 Bacterial strains and genotypes.	14
Table 2.4 Insect and mammalian cell strains	15
Table 2.5 Expression Vector.....	16
Table 2.6 Antibodies used for immunodetection.	16
Table 2.7 Composition of bacterial culture medium.....	16
Table 2.8 Auto-induction medium for bacterial culture.	17
Table 2.9 Antibiotics and stock solutions for bacterial culture.....	17
Table 2.10 Antibiotics and stock solutions for bacterial culture.	17
Table 2.11 Gel electrophoresis buffer	18
Table 2.12 Composition of SDS-PAGE.....	18
Table 2.13 Composition of purification buffers	18
Table 2.14 PCR reaction components.	20
Table 2.15 The cycling conditions for Phusion Hot Start II DNA Polymerase.	21
Table 2.16 DNA constructs for expression. (primers in Appendix III, generated by SDM)	22
Table 2.17 Nanodiscs preparation buffer.....	26
Table 2.18 CECF reaction buffer preparation (50 μ L)	27
Table 2.19 CECF reaction set up (50 μ L).....	28
Table 2.20 Strain and medium used for bacteria expression	29
Table 2.21 Detergents used in solubilization.	35
Table 2.22 Protein sample and CD buffer	38
Table 2.23 Microscope.....	40
Table 2.24 Primary antibodies.....	42
Table 2.25 Secondary antibodies.....	42
Table 2.26 Antibodies of subcellular marker proteins.....	44
Table 3.1 Constructs of emST	45
Table 3.2 Predicted and measured secondary structure contents of BL21(DE3) derived emST-his.....	59
Table 3.3 The molecular weight of emST variants and HSPs.....	70

Table 3.4 Molecular weights of the three variants of emST after PNGaseF treatment	72
Table 3.5 Predicted and measured secondary structure contents of <i>Expi293</i> derived emST-rho	75
Table 3.6 Predicted and measured secondary structure contents of <i>Expi293</i> derived emST-tm2-rho	77
Table 4.1 Strain and medium used for bacteria expression	83
Table 4.2 The oligomer state of DDM purified emST and its variants.	85
Table 4.3 Protein similarity	89
Table III.0.1 Primers for cloning	124

1 Introduction

1.1 The alveolar hydatid disease

Alveolar hydatid disease (AHD) is a zoonotic disease, a chronic parasitic disease caused by the genus *Echinococcus multilocularis* (Figure 1.2)(*E. multilocularis*). The distribution of *E. multilocularis* is expanding in the northern hemisphere. (Figure 1.1) [1-4]. About 18,200 human cases per annum of AHD distribute all over the world, resulting in approximately 666,000 disability-adjusted life year (DALY, 37 DALYs per case) [5]. The disease is most prevalent in central Asia, central and northern Europe, northern Russia, northwestern Alaska, north-central United States, northern Japan and northwestern Canada [6-12]. An estimated 90% of cases and 95% of the DALYs are occurring in China [6]. In Europe, including Russia, there are about 1600 cases of AHD each year, resulting in 33,000 DALYs [6-12]. It is worth noting that in the last few decades, the disease's distribution has expanded in Europe. [13]. 559 people were diagnosed in Europe between 1982 and 2000. [13]. Remarkably, in Switzerland the total burden is about 78 DALYs a year which is ten times lower than the global average [14]. In the Americas *E. multilocularis* is found primarily in northwestern Canada, North America, the northcentral United States and northwestern Alaska i.e. In the United States, only one indigenous case has been registered. [12, 15].

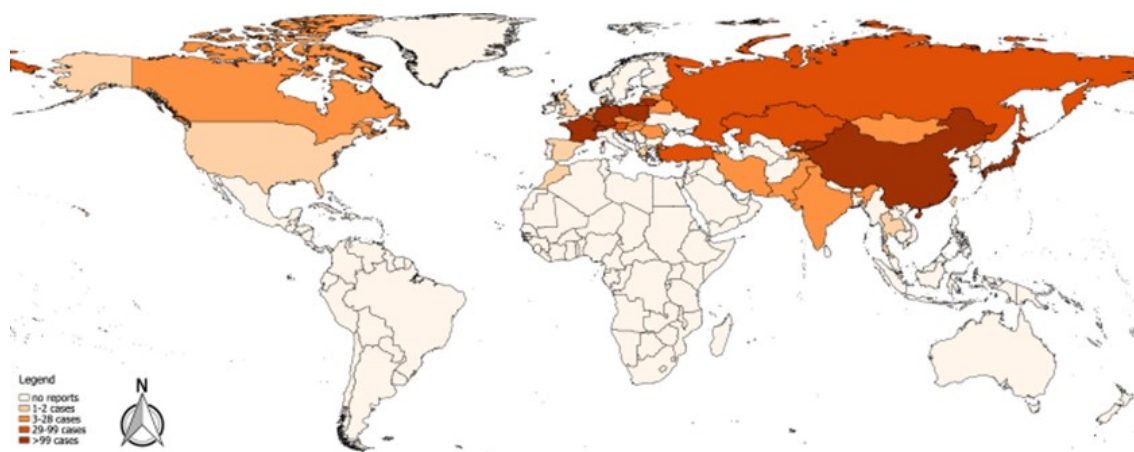


Figure 1.1 Approximate global distribution of alveolar hydatid disease (Adapted from [16])

Humans can be infected by *Echinococcus* eggs as an intermediate host [17-19]. Whereas the related cystic echinococcosis (*E. granulosus*) causes death by the formation of parasite cysts, the alveolar echinococcosis (*E. multilocularis*) progresses relentlessly by metastasizing through different organs [17-19]. The metacestodes (hydatid cysts) develop typically in the liver, lung or brain [20]. They are difficult to distinguish from cancer by imaging alone [21, 22]. Wherefore, the cysts have also been called "tapeworm tumours" [23].

Current treatment includes surgery for removal of the infected tissue and/or a life-long treatment with benzimidazole derivatives (e.g. Albendazole) [19, 24-29]. Unfortunately, these drugs possess only a parasitostatic effect, and can cause severe side effects i.e. damage to liver tissue [17, 30, 31].

1.2 The life cycle of *Echinococcus multilocularis*

The cause of AHD, the small parasitic flatworm (*E. multilocularis*), is dwelling in the intestines of canids [32-34]. In comparison to *E. granulosus*, *E. multilocularis*' adult stage is characterized by its small size, which allows differentiation of the two *Echinococcus* species (Figure 1.2) [35, 36]. As shown in Figure 1.2, *E. multilocularis* has five segments that include a sack-like scolex and other four proglottids. [37, 38].



Figure 1.2 *E. multilocularis* adults isolated from a fox in Erzurum province (stereomicroscope) (adopted from [35])

The transmission of *E. multilocularis* involves two different stages in the sylvatic cycle: the definitive host (i.e. foxes, dogs and cats) and the intermediate hosts (i.e. small mammals) (Figure 1.3) [3, 35, 39, 40]. Humans, not being a definite host, do not allow completion of the *E. multilocularis* life cycle [41, 42].

The adult *E. multilocularis* lives in the small bowel of the final hosts, mostly foxes, (i.e. the Red fox (*Vulpes vulpes*) and the Arctic fox (*Alopex lagopus*)) [43, 44]. Other wild canids, including such raccoon dogs (*Nyctereutes procyonoides*), coyotes (*Canis*

latrans), wild Felidae (*wild cats and also house cats*) and/or wolves (*Canis lupus familiaris*) can act as definitive hosts in certain regions [45-48].

In the sylvatic cycle, *E. multilocularis* resides in the small bowel of the definitive host where gravid proglottids produce infective eggs that are carried in the feces [49-51]. Infection proceeds when an intermediary host consumes these eggs. There are over 40 species of small mammals that seem to be susceptible towards *E. multilocularis* under normal conditions, with members of the families Cricetidae (i.e. *hamsters, related rodents and gerbils*) and Arvicolidae (*voles and lemmings*) being especially important [42, 52, 53].

In the small intestine, an egg hatches, releasing an oncosphere that penetrates the intestinal wall. The oncosphere migrates through the systemic circulation, settling in various organs, most notably the liver and lungs [1]. The oncosphere develops into an infective hydatid cyst in the liver or lungs [1]. This cyst enlarges gradually and produces daughter cysts and protoscolices, which occupy the cyst's interior [1]. After ingestion of the infected tissue by the definitive host, the protoscolices evaginate and migrate to the mucosa of the intestine [1]. In 32-80 days, the protoscolices mature into adult stages [54]. Humans can be infected as the intermediate host by *E. multilocularis* eggs, after having hand-to-mouth contact with feces contaminated food, i.e. egg-contaminated dog hair or mud, or by consuming contaminated food or drink [55].

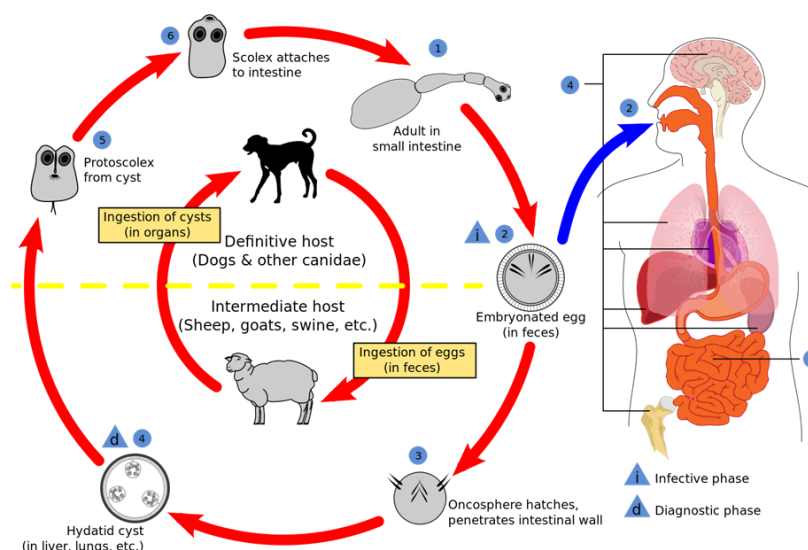


Figure 1.3 Life cycle of the *E. multilocularis*
(adopted from [Echinococcus Wikipedia])

The intermediate and definite hosts are depicted in red for cystic *E. multilocularis*, and blue for

human infection.

1.3 Serotonergic pathway

Serotonin (5-hydroxytryptamine, 5HT) is a phylogenetically old molecule and widely distributed in metazoans including *Echinococcus*. It regulates a diverse range of processes, particularly cell proliferation and differentiation. Especially, serotonin and serotonin uptake play a significant role in *E. multilocularis* survival and development [56, 57].

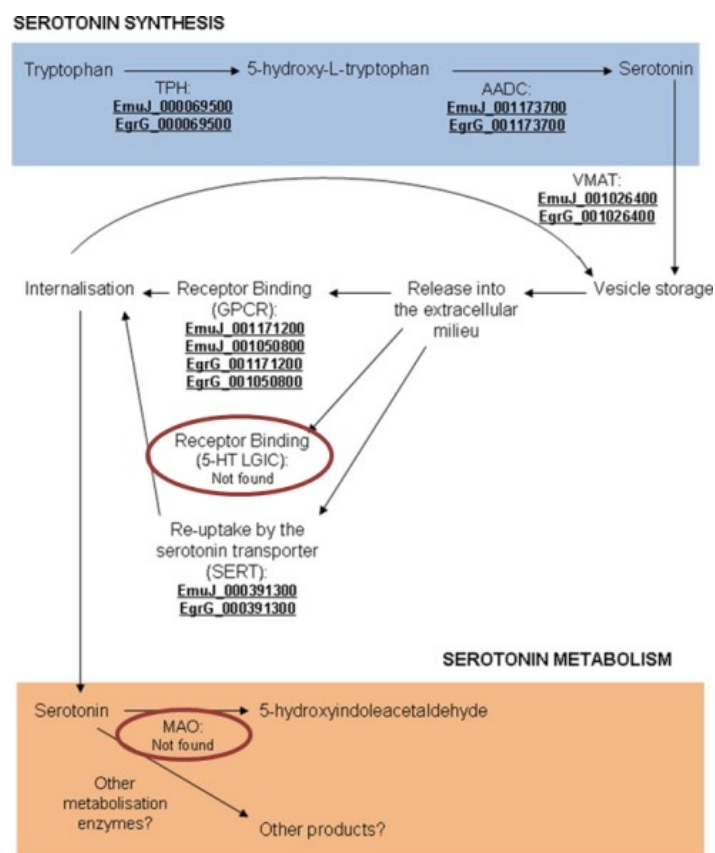


Figure 1.4 Putative serotonergic pathway in *Echinococcus* species (adopted from [56])

The canonical serotonergic pathway is almost completely encoded in the *Echinococcus* genome (Figure 1.4). Serotonin can be synthesized in *Echinococcus*, and is able to be transported and perceived with receptors. However, the monoamine oxidase (MAO) is missing in the *E. multilocularis* genome. The MAO is mainly acting as a degradation reagent of monoamines in vertebrates (Figure 1.6). According to

Sloley (2004), unlike the vertebrates, invertebrates have various ways of monoamine degradation [58]. But according to recent reports, MAO activity was detected in other parasites i.e. the trematode *S. mansoni* [59] and the cestode *H. diminuta* [60, 61]. In *Echinococcus* the processing of Serotonin is still unclear because the genetic characterization of this organism is still incomplete.

In general, the different physiological roles of 5-HT are due to various 5-HT receptors, but for most invertebrates the genes, respectively the 5-HT₃ receptors, are not identified.

The multiple effects of the neurotransmitter serotonin are best known for the human body. It affects the gastrointestinal tract (intestinal movement), cardiovascular system (vasoconstriction, haemostasis) and the nervous system (mood, appetite, sleep) via binding to different 5-HT receptors (Figure 1.6 A) [62, 63]. The main function of the serotonin transporter is the removal of serotonin from the synaptic cleft and thus the termination of 5-HT mediated signal transduction (Figure 1.5). Depression is a disease that can be attributed to the lack of serotonin in the synaptic cleft [64].

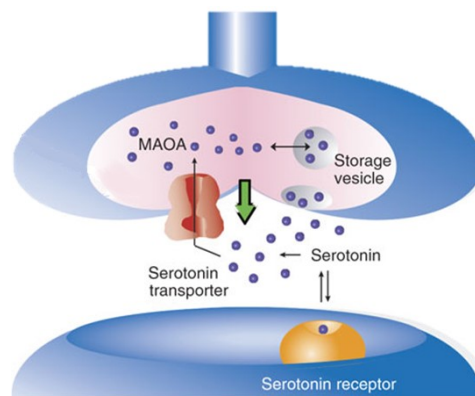


Figure 1.5 Lifecycle of a serotonin molecule(Figure adapted from [65])

In more simple species like *Caenorhabditis elegans* a new type of ionotropic serotonin receptor had been found encoded in the genome [66]. This receptor is not permeable for cations like the canonical 5-HT₃ receptor but rather acts as a 5-HT-gated chloride channel. Therefore, it is likely that serotonin gated ion channel genes are also encoded in *Echinococcus* [56, 67, 68].

In *Echinococcus* not much is known about the role of serotonin and serotonin transport. The few investigations point at an important role for serotonin in *Echinococcus* as a neurotransmitter, and it also acts as a morphogen by regulation of developmental processes [56]. It had been proved that high concentrations of serotonin will ultimately

lead to the death of protozoa due to constant muscle contraction [62]. Therefore, the Serotonergic pathway can be considered as a target wrt the hydatid disease.

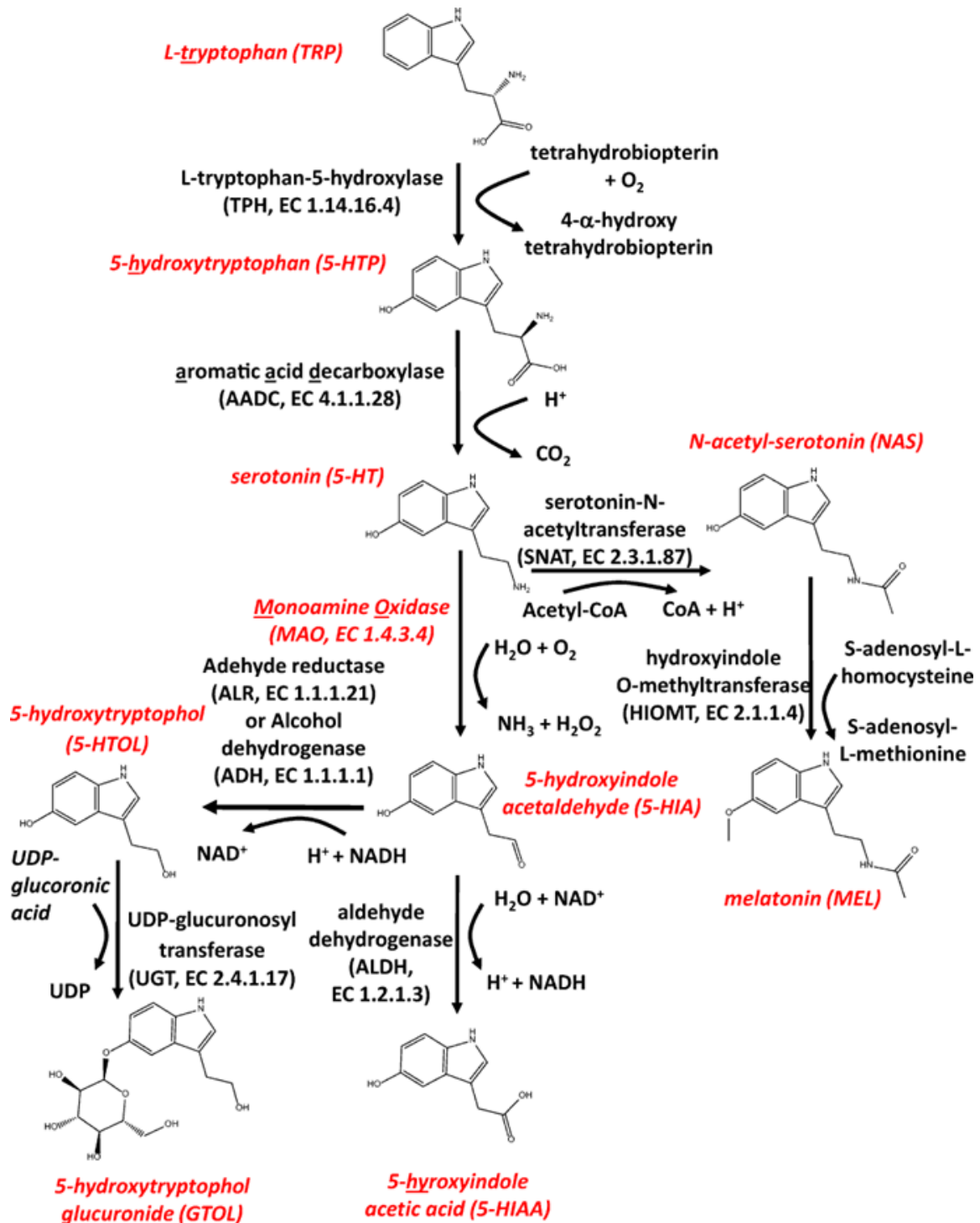


Figure 1.6 The biochemical pathway of serotonin synthesis and metabolism (adopted from [65, 69])

1.4 Serotonin transporter

The development of pharmaceuticals that specifically bind to serotonin transporter of *E. multilocularis*, requires a comprehensive understanding of its function and structure that currently is only available for the human serotonin transporter. Both these serotonin transporters belong to the membrane protein family - secondary active solute carrier 6 (SLC6) [70-72].

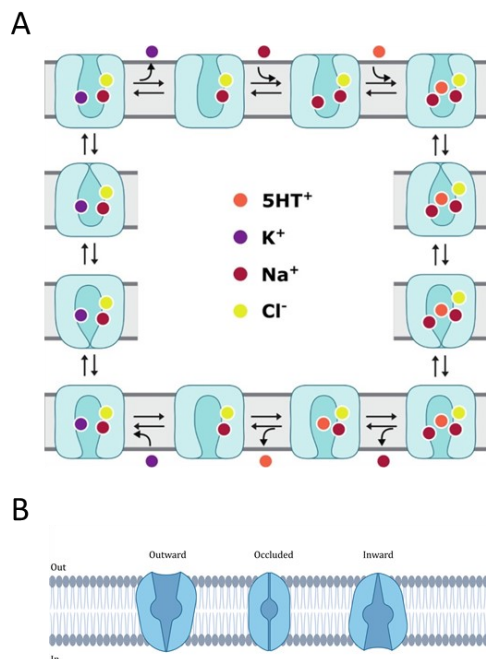


Figure 1.7 Schematic representation of key steps in the physiological transport cycle of hST (adopted from [73]) and prediction of emST three conformational states

A: the physiological transport cycle of hST. Orange circle: serotonin; Purple circle: Potassium ion; Red circle: sodium ion; Yellow circle: chloride ion. B: Left, outward-facing open conformation. Middle, occluded conformation. Right, inward-facing open conformation.

The SLC transporter family encompassed over 400 transporters organized into 66 families of the SLC series [74-79]. Serotonin (ST) Norepinephrine (NET) and dopamine (DAT) transporters belong to the SCL6 transporter family, the largest SLC families, containing 20 genes [80-82]. The alternating-access system roughly describes the mechanism of the serotonin transport cycle (Figure 1.8) [83]. Biochemical experiments, structural modeling, more recently X-ray crystallography and cryo-EM fully support that mechanism [73, 84-88].

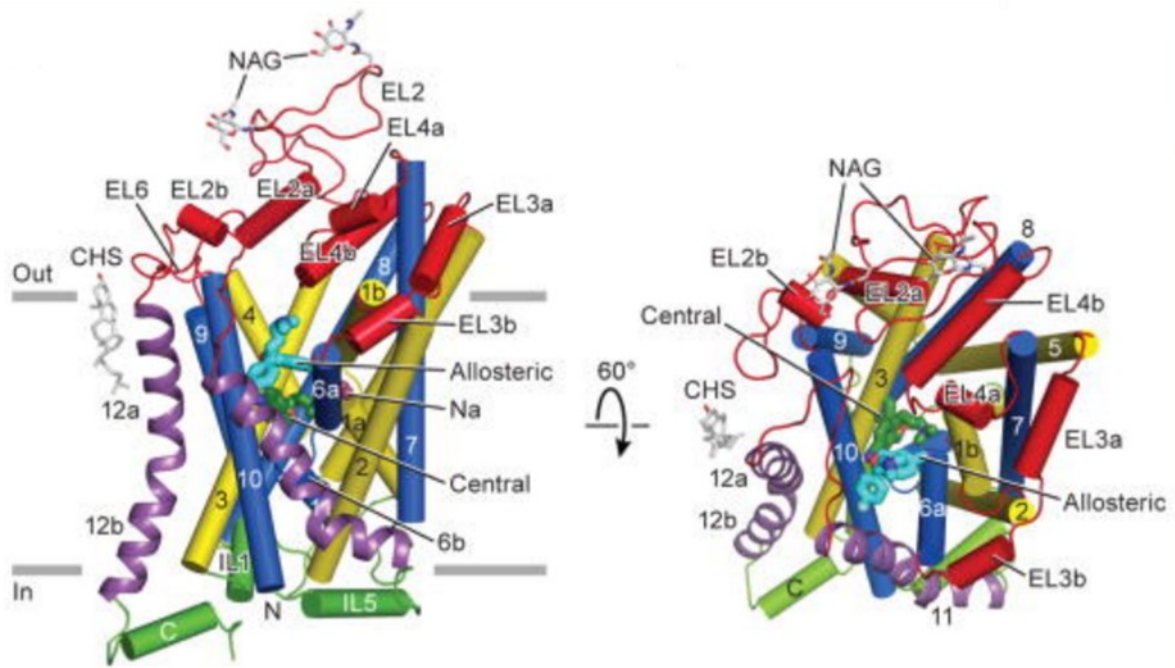


Figure 1.8 The architecture of the human serotonin transporter (adopted from [86])

The serotonin transporters are membrane proteins that belong to a family of transporters that share the LeuT structural fold [89-94]. It is shared by the neurotransmitter/ Na^+ symporter LeuT, the dopamine transport/ Na^+ symporter DAT and the serotonin/ Na^+ symporter ST [86]. The LeuT fold consists of 10 transmembrane helices (TMs) with a pseudo-symmetry axis and an anti-parallel orientation in the membrane, each of which contains a structural inverted repeat TM1-5 and TM6-10 [96, 97]. The EL2 (extracellular loop) closely interacts with EL4 and EL6 and forms the extracellular surface of the transporter. For this loop in dDAT it was suggested that excessive shortening leads to a loss of transport activity [98]. Nevertheless, in most structural studies the region of EL2 was trimmed to make it as short as possible without impairing transport activity [86, 95]. A disulfide bridge is commonly observed in EL2 of NSS members. The zinc ion binding site in the hDAT is formed by the EL2 (H193, D206) and EL4 (H375, E396) loops [99, 100]. The presence of bound Zn^{2+} inhibited substrate translocation, implying that transport activity is controlled by metal ions. [99]. The Zn^{2+} binding site, however, is specific to mammalian DATs and has not been found in other sodium and substrate symporters [95].

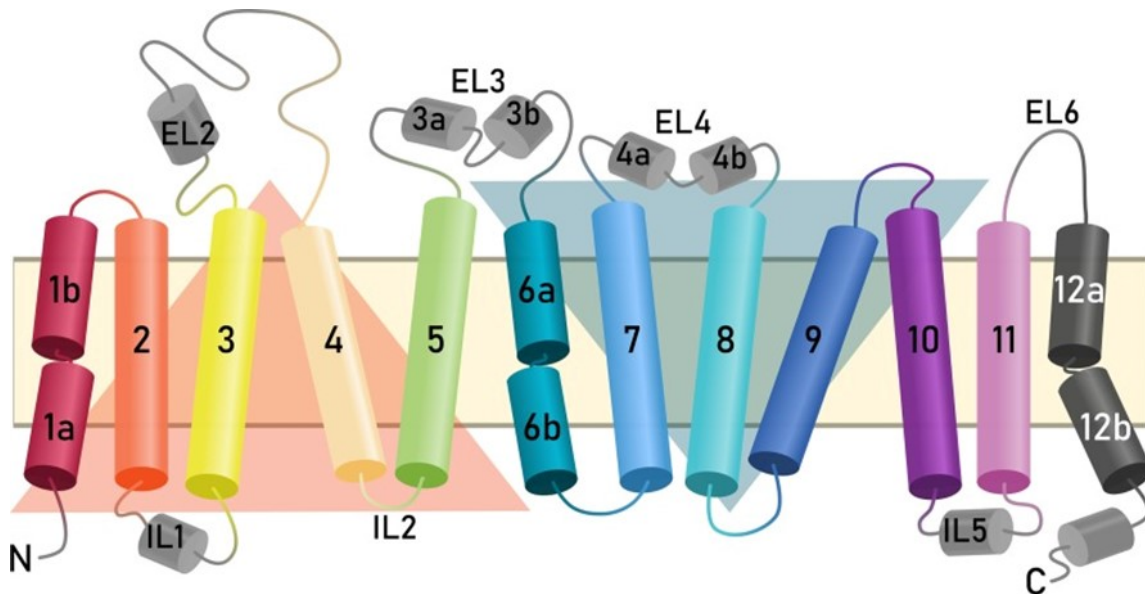


Figure 1.9 hST transmembrane topology comprises 12 membrane-spanning helices bound by intracellular and extracellular loops (adopted from [73])

1.5 The extended chaperone/COPII exchange model

In the model calnexin shields the monomeric hST via binding the sugar moieties by lectin domains. (Figure 1.10) [101]. Co-expression of this luminal chaperon increased the yield of mature hST by three times in heterologous expression systems [102]. Upon release from calnexin, the hST should dimerize and sequentially engage the heat shock proteins (HSPs) with its C-terminus [103]. Upon adopting a final stable conformation, it should release the HSPs from the C-terminus. The hST protein in the ER membrane exchanges HSPs for SEC-24 that drives the subsequent export of the complex as COP-II vesicle to the ER-Golgi intermediate compartment (ERGIC) [104]. Subsequently, the protein is transported to the cis-Golgi for post-translation modifications [103, 105, 106].

Misfolded or unfolded hST was supposed to be detected by ER's quality management machinery i.e. HSP40, HSP70, and HSP90 [105]. The misfolded ST was predicted to switch quickly between different states involving the binding of different HSPs [107]. The endoplasmic reticulum-associated protein degradation (ERAD) proteasome should degrade the protein after it was ubiquitinated i.e. E3-ligase (Figure 1.10) [108].

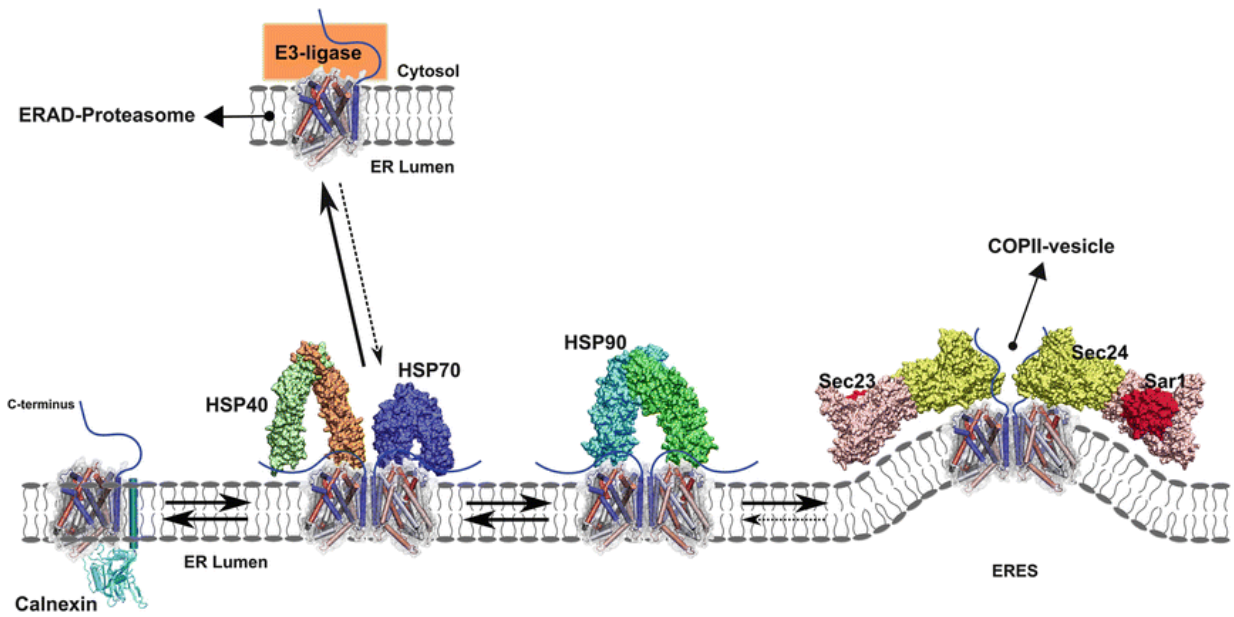


Figure 1.10 Extended chaperone/COPII exchange model (Resource [57])

1.6 Aim of this study

This project aimed at heterogenic expression, purification, and characterization of emST. For the research plan, the following objectives were established: The overexpression of emST was planned in three different expression systems (i.e. bacteria, insect and mammalian) in order to obtain enough material for the subsequent biochemical and biophysical studies, especially the structural characterization.

The mCherry tagged construct was planned as a possible tool for monitoring the expression level (ERIC-Ultra project). The localization and deglycosylation assays were planned to gain an understanding of the folding trajectory of heterologous expression of emST.

For analysis of the primary and secondary structure of the target protein CD-spectroscopy and mass spectrometry was to be employed

This work was supposed to provide a basis for further studies targeting pharmaceutically relevant inhibitors that specifically inhibits the serotonin transporter from *E. multilocularis*.

2 Materials and methods

2.1 Materials and instruments

2.1.1 Consumables and Instruments

Table 2.1 Consumables.

Consumables	Company
Acetyl phosphate lithium potassium salt (ACP)	Sigma-Aldrich
Amino acids for cell-free expression	Sigma-Aldrich
Antarctic phosphatase	ThermoScientific
Bench Marker TM protein ladder	Invitrogen
Complete EDTA-free protease inhibitor	Roche Applied Science
Complete protease inhibitor cocktail	Roche
Cytidine 5'-triphosphate di-sodium salt (CTP)	Sigma-Aldrich
Detergents (DDM etc.)	Anatrace
Detergents (Fos-12,)	Cube Biotech
Dialysis tubing spectra/por® 7	Spectrumlabs
<i>E.coli</i> lysate for cell-free protein expression	Cube Biotech
Folinic acid calcium salt	Sigma-Aldrich
Gel extraction kit	Qiagen
Gel Red	Biotium
Gelfiltration calibration HMW kit	GE Healthcare
GeneJET plasmid miniprep kit	Thermo Scientific
Glas capillaries	NanoTemper
Guanosine 5'-triphosphate di-sodium salt (GTP)	Sigma-Aldrich
Lipids	Avanti Polar Lipids, Inc.
Magnesium acetate tetrahydrate (Mg(oAc)2)	Sigma-Aldrich
MassRuler™ DNA ladder	ThermoScientific
Monoclonal anti-polyHistidine–peroxidase	Sigma-Aldrich
Ni-NTA/Ni indigo resin	Cube Biotech

PD-10 empty column and desalting column	GE Healthcare Life Science
Phosphoenol pyruvic acid monopotassium salt (PEP)	Sigma-Aldrich
Phusion hot start DNA-polymerase	ThermoScientific
Plasmid mini/midi kit	Qiagen
Prestained protein marker	Jena Bioscience
PureCube rho1D4 agarose, peptide, antibodies	Cube Biotech
PVDF membrane amersham hybond	GE Healthcare
Pyruvate kinase (PK)	Roche
Q agarose	Cube Biotech
Rapid ligation kit	ThermoScientific
RED-NHS NT-115 labeling kit	NanoTemper
Restriction enzymes	ThermoScientific
RiboLock RNase inhibitor	Thermo Scientific
Sodium azide (NaN ₃)	Sigma-Aldrich
Superdex 200 10/300 gl	GE Healthcare
Superdex 200 16/60 pg	GE Healthcare
TGX stain-free fastcast	Bio-Rad
tRNA <i>E.coli</i> MRE 600	Roche
Uridine 5'-triphosphate tri-sodium salt (UTP)	Sigma-Aldrich
Whatman gel blot paper	GE Healthcare

Table 2.2 Instruments

Instruments	Company
Akta explorer 100	GE Healthcare Life Science
AVIV model CD 425	AVIV
Benchtop centrifuge (HERMLE Z 233 M-2)	Thermo Scientific
Benchtop centrifuge 5417R	Eppendorf
Cell disruptor (EmulsiFlex-C3)	Avestin
Centrifuge 5804R	Eppendorf

ChemiDoc XRS gel system	Bio-Rad
DuoFlow 10 chromatography system	Bio-Rad
Heraeus biofuge stratos	Thermo Scientific
Incubator shaker	INFORS Unitron
Maxisafe 2020	Thermo Scientific
Micro-centrifuge	Sigma
Mini-PROTEAN tetra cell	Bio-Rad
Mixing block	BIOER(MB-102)
Monolith NT.115	Nanotemper
Optima XPN-90	Beckmann Coulter
Refrigerated incubator shaker	INNOVA (423L)
Multitron standard	Infors HT
Sigma 1-14K	SIGMA
Spectrafuge mini	Labnet
Sub-cell GT	Bio-Rad
Thermal cycler	BIO-RAD (T100)
Thermomixer R	Eppendorf
T80/T80+ UV-VIS spectrophotometer	PG INSTRUMENTS
Trans-Blot® SD semi-dry electrophoretic transfer cell	Bio-Rad
Ultracentrifuge (SORVAL LYNX 6000)	Thermo Scientific

2.1.2 Biological materials

Table 2.3 Bacterial strains and genotypes.

<i>E. coli</i> strain	Genotype	Origin, Purpose
	<i>F⁻ mcr A Δ(mrr-hsdRMS-mcrBC) φ80lacZΔM15</i>	Invitrogen, plasmid amplification
Top 10	<i>ΔlacX74 recA1 araD139 Δ(ara-leu)7697 galU galK λ⁻ rpsL (Str^R) endA1 nupG</i>	

BL21(DE3)	<i>F⁻ ompT hsdS_B (r_B⁻, m_B⁻) gal dcm (DE3)</i>	Invitrogen, Protein Expression
Lemo21	<i>fhuA2 [lon] ompT gal (λ DE3) [dcm] ΔhsdS/ pLemo(Cam^R) λ DE3 = λ sBamHlo ΔEcoRI-B</i> <i>int:(lacI:PlacUV5:T7 gene1)</i> <i>i21 Δnin5</i> <i>pLemo = pACYC184-PrhaBAD-lysY</i>	New England Biolabs, Protein Expression
C43(DE3)	<i>F⁻ ompT hsdS_B (r_B⁻ m_B⁻) gal dcm (DE3)</i>	Lucigen, Protein Expression
C41(DE3)	<i>F⁻ ompT hsdS_B (r_B⁻ m_B⁻) gal dcm (DE3)</i>	Lucigen, Protein Expression

Table 2.4 Insect and mammalian cell strains

Strain	Species of origin	Origin, Purpose
IPLB-SF-9AE	Spodoptera frugiperda	Oxford technologies, expression and baculovirus amplification
BTI-TN-5B1-4	Trichoplusia ni	Oxford technologies, expression
HEK293-6E	Homo sapiens	Oxford technologies, expression
Expi293F GnTI	Homo sapiens	Thermofisher scientific protein expression

Table 2.5 Expression Vector.

Vector	Antibiotic Resistance	Expression system	Origin, Purpose
pET 20b	Kanamycin	Bacteria	Invitrogen, protein expression
pQE-2	Kanamycin	Bacteria	Qiagen, protein expression
pET 27b	Kanamycin	Bacteria	Invitrogen, protein expression Oxford expression
pOET-2	Ampicillin	Insect	technologies, protein expression Oxford expression
pOET-4	Ampicillin	Insect	technologies, protein expression
pOpiE-2	Ampicillin	Insect	Thermofisher scientific protein expression
pTT-5	Ampicillin	Mammalian	Thermofisher scientific protein expression

Table 2.6 Antibodies (immunodetection)

Antibody	Description	Supplier
α -Penta-His	Mouse monoclonal against Penta-His epitope; HRP conjugated working dilution: 1:10,000	Qiagen, Hilden
α -Rho1D4	Mouse monoclonal against Rho1D4 epitope; working dilution: 1:5,000	Cube Biotech, Monheim
Goat α -mouse HRP conjugate	Secondary antibody against mouse; HRP conjugated working dilution: 1:5,000	Sigma-Aldrich, Darmstadt

Table 2.7 Composition of bacterial culture medium.

Medium	Composition (for one liter)
SOB	5 g Yeast Extract, 20 g Tryptone, 0.5 g NaCl, 10 mM MgCl ₂ , 2.5 mM KCl, 10 mM MgSO ₄

DYT	10 g Yeast Extract, 16 g Tryptone, 5 g NaCl
LB	5 g Yeast Extract, 10 g Tryptone, 10 g NaCl
TB	24 g Yeast Extract, 12 g Tryptone, 4 mL Glycerol
Phosphate Buffer for TB medium	0.72 M K ₂ HPO ₄ , 0.17 M KH ₂ PO ₄

Table 2.8 Auto-induction medium

Component	Composition (for one liter)
20 × NPS	25 mM (NH ₄) ₂ SO ₄ , 50 mM KH ₂ PO ₄ , 50 mM Na ₂ HPO ₄
50 × 5052	0.05 % (w/v) Glucose, 0.5 % (w/v) Glycerol, 0.2 % (w/v) α-Lactose
MgSO ₄	2 mM MgSO ₄
ZY medium	0.5 % (w/v) Yeast extract, 1 % (w/v) Tryptone
1000 × trace elements	20 mM CaCl ₂ , 50 mM FeCl ₃ , 10 mM MnCl ₂ , 2 mM CoCl ₂ , 2 mM CuCl ₂ , 10 mM ZnSO ₄ , 2 mM NiCl ₂

Table 2.9 Antibiotics and stock solutions for bacterial culture.

Stock solutions	Concentration
Chloramphenicol	25 mg/mL
Ampicillin sodium salt	200 mg/mL
IPTG	0.2 M
Kanamycin sulfate	50 mg/mL
Glucose	40% (w/v)

Table 2.10 Antibiotics and stock solutions for bacterial culture.

Stock solutions	Concentration
Kanamycin sulfate	50 mg/mL
Ampicillin sodium salt	200 mg/mL
Chloramphenicol	25 mg/mL
IPTG	0.2 M
Glucose	40% (w/v)

2.1.3 Purification, Assay and Gel Electrophoresis Buffers

Table 2.11 Gel electrophoresis buffer

Buffer	Composition
SDS-PAGE	
SDS-Sample loading buffer	2 % (w/v) SDS, 62 mM Tris, 5 % (v/v) β -Mercaptoethanol, 0.2 % (w/v) Bromophenol blue, 20%(w/v) Glycerol,
Laemmli buffer	192 mM Glycine, 25 mM Tris, 0.1 % (w/v) SDS
MES running buffer	1mM EDTA, 50mM Tris-Base, 50mM MES, 0.1% SDS, pH7.3
Blue silver staining solution (1L)	200 mL Methanol, 10% Ammonium sulphate, 10% Phosphoric acid, 1.2g Coomassie G-250
Western Blot	
Transfer Buffer	20% Methanol, 48 mM Tris base, 39 mM Glycine
Blocking buffer	5% milk powder in TBS-T buffer
TBS/TBS-T buffer	w/o 0.1% Tween 20, 137 mM NaCl, 20 mM Tris base pH 7.6
Agarose gel	
TAE	1 mM EDTA, 40 mM Tris, pH 8.0

Table 2.12 Composition (SDS-PAGE)

SDS-PAGE (Home-Made) Solution components	5 % Stacking gel (10 mL)	8 % Resolving gel (25 mL)	12 % Resolving gel (25 mL)
H ₂ O	6.8	11.5	8.2
1.5 M Tris, pH8.8		6.3	6.3
30 % Acrylamide	1.7	6.7	10.0
1.0 M Tris, pH 6.8	1.25		
10 % ammonium persulfate	0.1	0.25	0.25
10 % SDS	0.1	0.25	0.25
TEMED	0.01	0.015	0.01

Table 2.13 Composition of purification buffers

Buffer	Composition
--------	-------------

Osmotic stock	
Sucrose Buffer	1 mM EDTA, 20% Sucrose, 50 mM HEPES, pH 7.9.
MgSO4 Buffer	5 mM MgSO4
Membrane preparation	
Lysis Buffer (<i>E.coli</i>)	150 mM NaCl; 20 mM TRIS (pH 7); 10 % (w/v) Glycerol; 10 μ M E-64; 2 mM MgCl ₂ ; 1 μ M Pepstatin A; 1 mM Pefabloc SC; 10 μ M Leupeptin; 2 mM Benzamidine; 1 mg mL ⁻¹ Lysozyme; 2 mM β -ME; 30 U/mL DNase I
Membrane storage buffer	500 mM NaCl; 20 mM TRIS (pH 7); 30 % (w/v) Glycerol; 10 μ M E-64; 0.5 mM TCEP; 1 μ M Pepstatin A; 1 mM Pefabloc SC; 10 μ M Leupeptin; 2 mM Benzamidine
Lysis Buffer (Insect and mammalian cell)	1 tablet/100 mL EDTA-free protease inhibitor (Roche), PBS pH 7.5;
Purification buffer	
Solubilization buffer (<i>E.coli</i>)	500 mM NaCl; 20 mM TRIS (pH 6.5, 7 or 8); 10 % (w/v) Glycerol; 1 % (w/v) Fos-choline 12; 0.5 mM TCEP; 0.1 mM EDTA; 1 μ M Pepstatin A; 10 μ M E-64; 10 μ M Leupeptin; 1 mM Benzamidine; 1 mM Pefabloc SC
Solubilization buffer (Insect and mammalian cell)	300 mM NaCl; 20 mM HEPES (pH 7.5 or 7); 10 % (w/v) Glycerol; 2 % (w/v) DDM or 1 % (w/v) Fos-choline 12; 0.5 mM TCEP; 0.1 mM EDTA; 1 tablet/100 mL EDTA-free protease inhibitor (Roche)
Solubilization buffer (DIBMA)	150 mM NaCl; 20 mM TRIS pH 7; 0.5 mM TCEP; 7.5mM MgCl ₂ ; 7% DIBMA; 10mM CaCl ₂ ; 1 tablet/100 mL EDTA-free protease inhibitor (Roche)
NTA Wash Buffer 1	150 mM NaCl; 20 mM TRIS (pH 6.5, 7 or 8); 10 % (w/v) Glycerol; 1 % (w/v) Fos-choline 12; 5 mM Imidazole; 0.5 mM TCEP; 1 mM Benzamidine; 1 μ M E-64; 1 μ M Pepstatin A; 1 μ M Leupeptin; 1 mM Pefabloc SC
NTA Wash Buffer 2	150 mM NaCl; 20 mM TRIS (pH 6.5, 7 or 8); 10 % (w/v) Glycerol; 1 % (w/v) Fos-choline 12; 30 mM Imidazole; 0.5 mM TCEP
NTA Wash Buffer 3	150 mM NaCl; 20 mM TRIS (pH 6.5, 7 or 8); 10 % (w/v) Glycerol; 1 % (w/v) Fos-choline 12; 90 mM Imidazole; 0.5 mM TCEP;
Rho Wash Buffer	500 mM NaCl; 20 mM HEPES (pH 7.5 or 7); 10 % (w/v) Glycerol; 0.1 % (w/v) DDM or Fos-choline 12; 0.5 mM TCEP;
NTA Elution Buffer	150 mM NaCl; 20 mM TRIS (pH 6.5, 7 or 8); 10 % (w/v) Glycerol; 1 % (w/v) Fos-choline 12; 250 mM Imidazole; 0.5 mM TCEP;
Rho Elution Buffer	500 mM NaCl; 20 mM HEPES (pH 7.5 or 7); 10 % (w/v) Glycerol; 0.1 % (w/v) DDM or Fos-choline 12; 0.5 mM TCEP; 200 μ M Rho peptide

SEC buffer (<i>E.coli</i>)	150 mM NaCl; 20 mM TRIS (pH 6.5, 8); 10 % (w/v) Glycerol; 0.1 % (w/v) Fos-choline 12; 0.5 mM TCEP
SEC buffer (Insect and mammalian cell)	150 mM NaCl; 20 mM HEPES (pH 7.5 or 7); 10 % (w/v) Glycerol; 0.1 % (w/v) or DDM Fos-choline 12; 0.5 mM TCEP
SEC DIBMA buffer	150 mM NaCl; 20 mM TRIS pH 7.5

2.2 Cloning

Cloning involves the synthesis of the DNA sequence of interest, restriction digestion of the DNA, and subsequent introduction of the ligated product to a suitable host to get enough amounts of target molecules. [109]. A central tool of modern cloning is the polymerase chain reaction (PCR) invented in 1983. [110]. PCR stands for polymerase chain reaction and is a strategy for selectively amplifying DNA segments. PCR was performed in a thermal cycler with all the components needed and their respective concentrations (Appendix I: DNA and protein sequences and Appendix III: Primers).

All DNA constructs (Table 2.16) were generated using one of three approaches described below:

For this work, C-terminus rho tagged emST (pMA-T_{emST-rho}) was ordered from GeneART Thermo Fisher Scientific, Regensburg, Germany (see Appendix I: DNA and protein sequences). All the primers used were synthesized by BioTeZ Berlin Buch GmbH in Germany. A deca-histidine tag was placed at the C-terminus of the emST gene sequence (emST-his) by using respective forward and reverse primers which containing the desired restriction sites and tag-specific sequences (see Appendix III: Primers) during PCR and subsequently, cloned into the desired vector (Appendix III: Primers). Preliminary PCR reactions were used (20 µL reaction volume) and later scaled up to 50 µL reaction volume (Table 2.14).

Table 2.14 PCR reaction components.

Component	20 µL reaction	50 µL reaction	Final conc.
Autoclaved milli-Q H ₂ O	add to 20 µL	add to 50 µL	
10 mM dNTPs	0.4 µL	1 µL	200 µM each
5 × Phusion HF Buffer	4 µL	10 µL	1x
Primer A	0.4 µL	1 µL	2 µM

Template DNA	0.4 μ L	1 μ L	1 pg –10 ng per 50 μ L
Primer B	0.4 μ L	1 μ L	2 μ M
DMSO 100 %	1 μ L	2.5 μ L	5 %
Phusion Hot Start II DNA Polymerase (2 U/ μ L)	0.2 μ L	0.5 μ L	0.02 U/ μ L

Table 2.15 The Phusion Hot Start II DNA Polymerase cycling conditions.

Steps	3 steps	2 steps	No. Of Cycles
Initial denaturation	98 °C, 30 s		1
Denaturation	98 °C, 5-10 s		
Annealing	50 °C-64°C, 10 s		25-35
Extension	72 °C, \times s	72 °C, \times s	
Final extension	72 °C, 5 min, 4 °C Hold		1

Two constructs i.e pOET2_{emST-rho} and pOET4_{emST-rho} were generated by recloning the gene from the synthesized construct (pMA-T_{emST-rho}) to pOET2 and pOET4, respectively. The gene (emST-rho) was released using restriction enzymes EcoRI and BamHI and ligated into the pOET2 and pOET4 digested with same enzymes using Rapid T4 DNA ligase kit. After which the product was used for transformation and clonal screening.

2.2.1 Site-directed mutagenesis

The site-directed mutagenesis has been used to create specific, targeted changes (insertions, deletions, and substitutions) in double-stranded plasmid DNA [111-114]. Here the targeted changes (either insertion or deletion or substitution) were included in the primers, which were designed to amplify a desired DNA fragment along with the expected changes (mutagenic primers). Respective restriction enzymes were used to digest the product and ligated into a vector of interest cleaved with the same set of enzymes followed by transformation and clonal screening. DNA constructs pQE2_{emST-his}, pET27b_{emST-his}, pET20a_{emST-rho} and pOpiE2_{emST-rho} were generated using this approach.

Table 2.16 DNA constructs for expression. (primers in Appendix III, generated by SDM)

DNA constructs for bacterial cell expression			
Construct generated	Template (used during PCR)	Restriction sites used	Changes included
pQE2 _{emST-his}	pMA-T _{emST-rho}	EcoRI / HindIII	rho tag replaced by his tag
pQE2 _{ΔN-emST-his}	pQE2 _{emST-his}	EcoRI / HindIII	Residues 1-34 deletion
pQE2 _{ΔNL-emST-his}	pQE2 _{ΔN-emST-his}	EcoRI / HindIII	Residues 1-34 deletion Residues 182-192 (EL2) deletion
pQE2 _{ΔNL-emST-tm2-his}	pQE2 _{ΔNL-emST-his}	EcoRI / HindIII	Residues 1-34 deletion Residues 182-192 (EL2) deletion Y69A and I273A mutation
pET27b _{emST-his}	pMA-T _{emST-rho}	NdeI / HindIII	rho tag replaced by his tag
pET20a _{emST-rho}	pMA-T _{emST-rho}	NdeI / BamHI	--
DNA constructs for Insect cell expression			
pOpiE2 _{emST-rho}	pMA-T _{emST-rho}	SpeI / BamHI	--
pOpiE2 _{emST-I273A-rho}	pOpiE2 _{emST-rho}	SpeI / BamHI	I273A mutation
pOpiE2 _{emST-tm2-rho}	pOpiE2 _{emST-I273A-rho}	SpeI / BamHI	Y69A and I273A mutation
pOET2 _{emST-rho}	pMA-T _{emST-rho}	EcoRI / BamHI	--
pOET4 _{emST-rho}	pMA-T _{emST-rho}	EcoRI / BamHI	--
DNA constructs for mammalian cell expression			
pTT5 _{emST-rho}	pMA-T _{emST-rho}	AvrII / BamHI	
pTT5 _{emST-I273A-rho}	pTT5 _{emST-rho}	AvrII / BamHI	Y69A mutation
pTT5 _{emST-tm2-rho}	pTT5 _{emST-I273A-rho}	AvrII / BamHI	Y69A and I273A mutation
pTT5 _{emST-mCherry-rho}	pTT5 _{emST-rho}	AvrII / BamHI	C-terminus mCherry tag insertion
Miscellaneous DNA constructs			
pQE2 _{emST-his}	pMA-T _{emST-rho}	EcoRI / HindIII	rho tag replaced by his tag
pQE2 _{ΔN-emST-his}	pQE2 _{emST-his}	EcoRI / HindIII	Residues 1-34 deletion
pQE2 _{ΔL-emST-his}	pQE2 _{emST-his}	EcoRI / HindIII	Residues 182-192 (EL2) deletion

pQE2 Δ C-emST-his	pQE2 _{emST-his}	EcoRI / HindIII	Residues 605-644 deletion
pQE2 _{emST-Y69A-his}	pQE2 _{emST-his}	EcoRI / HindIII	Y69A mutation
pQE2 _{emST-I273A-his}	pQE2 _{emST-his}	EcoRI / HindIII	I273A mutation
pQE2 Δ NC-emST-his	pQE2 Δ N-emST-his	EcoRI / HindIII	Residues 1-34 deletion Residues 605-644 deletion
pQE2 Δ NC-emST-Y69A-his	pQE2 Δ NC-emST-his	EcoRI / HindIII	Residues 1-34 deletion Residues 605-644 deletion. Y69A mutation
pQE2 Δ NC-emST-I273A-his	pQE2 Δ NC-emST-his	EcoRI / HindIII	Residues 1-34 deletion Residues 605-644 deletion. I273A mutation
pQE2 Δ NC-emST-tm2-his	pQE2 Δ NC-emST-Y69A-his	EcoRI / HindIII	Residues 1-34 deletion Residues 605-644 deletion. Y69A and I273A mutation
pQE2 Δ NLC-emST-his	pQE2 Δ NC-emST-I273A-his	EcoRI / HindIII	Residues 1-34 deletion Residues 182-192 (EL2) deletion Residues 605-644 deletion Residues 1-34 deletion
pQE2 Δ NLC-emST-Y69A-his	pQE2 Δ NLC-emST-his	EcoRI / HindIII	Residues 182-192 (EL2) deletion Residues 605-644 deletion. Y69A mutation
pQE2 Δ NLC-emST-I273A-his	pQE2 Δ NLC-emST-his	EcoRI / HindIII	Residues 1-34 deletion Residues 182-192 (EL2) deletion Residues 605-644 deletion. I273A mutation
pQE2 Δ NLC-emST-tm2-his	pQE2 Δ NLC-emST-Y69A-his	EcoRI / HindIII	Residues 1-34 deletion Residues 182-192 (EL2) deletion Residues 605-644 deletion. Y69A and I273A mutation
pQE2 Δ NL-emST-his	pQE2 Δ N-emST-his	EcoRI / HindIII	Residues 1-34 deletion Residues 182-192 (EL2) deletion
pQE2 Δ NL-emST-Y69A-his	pQE2 Δ NL-emST-his	EcoRI / HindIII	Residues 1-34 deletion Residues 182-192 (EL2) deletion. Y69A mutation
pQE2 Δ NL-emST-I273A-his	pQE2 Δ NL-emST-his	EcoRI / HindIII	Residues 1-34 deletion Residues 182-192 (EL2) deletion. I273A mutation
pQE2 Δ NL-emST-tm2-his	pQE2 Δ NL-emST-Y69A-his	EcoRI / HindIII	Residues 1-34 deletion Residues 182-192 (EL2) deletion. Y69A and I273A mutation

2.3 Cell-free expression with the continuous exchange cell-free system (CECF)

In vitro expression is a relatively old technique, which is also known as cell-free expression [115]. The cell-free expression system has been extensively used for membrane protein production because of its uncomplicated operation with high success rates and large flexibility, which often provides a sufficient amount for structural applications [116].

An improved version of this cell expression system i.e continuous exchange cell-free system (CECF) has eliminated problems of in vivo expression like toxicity, limited membrane space and inefficient transport and membrane insertion [119-122]. This CECF is set up in a dialysis chamber, which provides the advantage of delivering components (ATP) to the reaction and removing byproduct such as ADP by dialysis, while the reaction is being continued. This way reaction times up to 24 hours are which possible increase the total protein yield compared to the standard approach [121]. Addition of lipid bi-layers to such a cell free expression system for the co-translational incorporation of membrane protein directly into a defined lipidic environment (eg. nanodisc) had been used successfully (Figure 2.2) [117, 118].

Membranes with integrated membrane proteins are solubilized with different kinds of detergents for solubilization and subsequent purification, which in many cases is detrimental to protein stability. This problem can be avoided using nanodisc integration (Figure 2.1), (which are MSP1D1 and MSPE3D1). This approach allows in vitro expression of membrane proteins into a detergent free environment [123]. Two different sizes of nanodisc assemblies i.e. with MSP1D1 (9-10 nm) and MSPE3D1 (12-14 nm) were used in CECF for emST production.

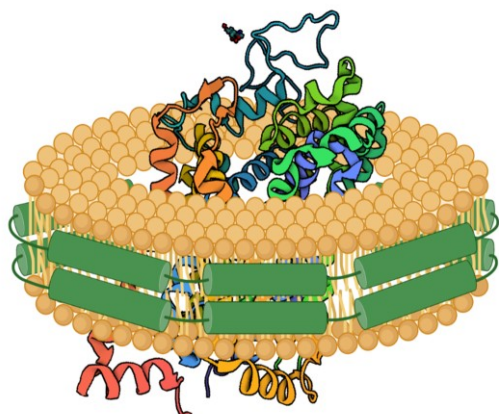


Figure 2.1 Schematic depiction of an MSP nanodisc

The membrane protein (orange) The phospholipids (grey). The membrane scaffolding proteins (green).

2.3.1 Plasmid preparation

For the CECF reaction set up plasmids are required in a concentration range between 0.7–1.0 $\mu\text{g}/\mu\text{L}$. For this, a 25-50 mL culture volumes of respective transformants of Top10 competent cells were used for plasmid preparation. GeneJET Plasmid Midiprep Kit (Table 2.1) was used for the plasmid extraction. Whenever the plasmid concentration was lower than 0.7 $\mu\text{g}/\mu\text{L}$ an additional isopropanol precipitation or SpeedVac evaporator step was used to concentrate the plasmids. Six different constructs, pQE2_{emST-his}, pQE2 ΔN -emST-his, pQE2 ΔNL -emST-his, pQE2 ΔNL -emST-tm2-his, pET27b_{emST-his} and pET20a_{emST-rho} (Table 2.16), were processed this way.

2.3.2 Nanodiscs preparation

11 mg of lyophilized MSP1D1 or MSPE3D1 protein (MSP) was resuspended in 5.5 mL MiliQ to reach a final concentration of 2.2 mg/mL for nanodiscs assembly. For the reconstitution, an MSP to lipid mole ratio of 1:69 was chosen. POPC lipids were unfrozen at room temperature and mixed with lipid buffer (Table 2.17) to a final lipid concentration of 50 mM before being incubated at 37 °C for 20 minutes to fully dissolve. In a 15 mL falcon tube lipids and MSP were combined and incubated at 4 and 37 °C alternatively for three times (with each incubation period of 20 min) [124, 125]. This mixture was dialyzed against a freshly prepared dialysis buffer (Table 2.17) using an MWCO 1000 Da membrane in the cold room for 3-4 days with two buffer changes per day. The dialyzed sample was concentrated and loaded onto a preequilibrated HiLoad Superdex 200 column (Table 2.1) with 2 mL injection volume at 0.25 ml/min flowrate. For further usage, the elution fractions were accumulated and concentrated by

ultrafiltration to a concentration of 10 mg/mL [124, 125].

Table 2.17 Nanodiscs preparation buffer

Buffer	Composition
Lipid Buffer	pH 7.4; 100 mM Na Cholate; 20 mM Tris-HCl
10 × Dialysis Buffer	pH 7.4; 1 M NaCl; 200 mM Tris-HCl
SEC Buffer	pH 7.4; 150 mM NaCl, 10 mM Na ₂ HPO ₄

2.3.3 CECF reaction set-up

The CECF reaction (Table 2.19) consists of two components i.e. reaction solution (Table 2.19) and feeding solution (Table 2.19) [121]. The reaction setup was a 24 well plate with feeding solution in each well to which a dialyzer bag with the reaction solution was added (Table 2.18). The 24 well plates were subsequently incubated at 30°C for 16 hours on an incubator shaking with 600 rpm. The reaction mixtures in the dialyzers were collected and centrifuged for 15 minutes at 20,000 × g to separate the insoluble and the soluble fractions.

Separately, the pellet and supernatant fractions were collected. The pellets were washed by resuspending them in a Wash Buffer (Table 2.13) and centrifugation (15 minutes at 20,000 g).

The pellet and the supernatant fractions were collected separately. The pellets were washed by resuspending in a Wash Buffer (Table 2.13) and centrifuged for 15 min at 20,000 × g. Aliquots of the washed pellets and the earlier supernatant fractions were supplemented with SDS loading Buffer and incubated for 10 min at 46 °C before loading onto an SDS-PAGE and subsequent western blotting.

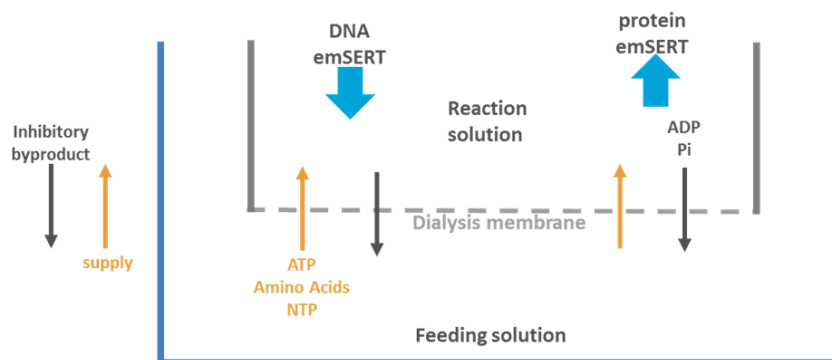


Figure 2.2 CECF reaction in a two-chamber dialysis device.

The preparation of the reaction solution and the feeding solution is described in Table 2.18 and Table 2.19

The above introduced six constructs were analyzed in initial test expressions for which a reaction volume of 50 μL was used. Different amounts of plasmid in the in vitro expression setup (i.e., 0.75, 1.0, 1.25 and 1.5 μg) were used to determine the plasmid amount for optimal expression. Construct pET20a_{emST-rho} was further scaled up to a 100 μL reaction volume.

Table 2.18 CECF reaction buffer preparation (50 μL)

Buffer	Chemical	Stock conc.	final conc.	Volume (μL)
Master mix	RCWMDE	16.67 mM	1 mM	3
	AA-Mix	25 mM	0.55 mM	1.1
	Li ⁺ , K ⁺ Acetyl phosphate (ACP)	1000 mM	20 mM	1
	Phosphoenolpyruvate	1000 mM	20 mM	1
	NTP	75x	1x	0.68
	1,4 Dithiothreitol (DTT)	500 mM	2 mM	0.2
	Folinic acid	10 mg/ml	0.1 mg/ml	0.5
	Proteinase inhibitor	50x	1x	1
	HEPES/EDTA buffer	24x	1x	2.08
	Magnesium acetate	1000 mM	12 mM	0.6
	Potassium acetate	10 M	270 mM	1.35
	Polyethylene glycol 8000	40 %	2 %	2.5

	Sodium azide	10 %	0.05 %	0.25
	RNase-free water	--	--	0.25
Extract mix	S30-Extrakt (BL21 DE3) [Zubay, G, Kigawa, T]	1x	0.35x	17.5
	Plasmid	1.5 mg/ml	0.03 mg/ml	1
	Riboblock	40 U/ μ l	0.3 U/ μ l	0.375
	RNase-free water	0.7 mg/ml	0.05 mg/ml	3.6
	tRNA <i>E.coli</i>	40 mg/ml	0.5 mg/ml	0.63
	Pyruvat Kinase	10 mg/ml	0.04 mg/ml	0.2

Table 2.19 CECF reaction set up (50 μ L)

Reaction	Component	Volume (μ L)
Feeding mix	Master mix	249.76
	S30-buffer	289
	RNase-free water	250
	AA-Mix	16
Reaction mix	Master mix	14.8
	Extract mix	23.3
	RNase-free water + plasmid	12

2.4 *In vivo* emST expression

2.4.1 Bacterial expression

The expression constructs wild type emST protein with C-terminus his-tag in pET27b vector (Table 2.16 (primers in Appendix III: Primers, generated by SDM)) was used to analyze protein expression in different strains of *E.coli* i.e., BL21(DE3), C41, C43, RP, RIL and Lemo21 (Table 2.20) [126-130]. The construct using the pQE2 vector (Table 2.16 and Appendix III: Primers) was used for BL21(DE3), RP and RIL cells (Table 2.20). The plasmids were transformed into 100 μ L aliquots of the respective competent cells by 42 °C heat shock treatment using ~0.2 μ g DNA. The transformants were grown and selected on LB agar plates with 50 μ g/ml kanamycin. After a 37 °C overnight incubation,

several colonies were picked and inoculated into either TB medium or ZY-CAIM (auto-induction medium) for setting up overnight pre-cultures. All bacterial pre-cultures were grown with 50 µg/ml kanamycin and 2% glucose at 30 °C with 250 rpm. Main cultures of 200 ml per 2L baffled flask were prepared using respective pre-cultures and their respective media. Inoculations with 50 µg/ml kanamycin were prepared with a final OD600 of 0.2 from the respective pre-culture. These main cultures were grown at 30 °C until they reach an OD600 of ~0.6. In main cultures with TB media protein expression was induced chemically by adding Isopropyl β-d-1-thiogalactopyranoside (IPTG) at a final concentration of 1 mM, whereas auto-induction experiments did not require IPTG as they are induced by lactose, which is present in the media after the preferred carbon source i.e. glucose is depleted. After the main culture reached an OD600 of 0.6 the temperature of the main cultures was reduced to 18 °C before inducing protein expression i.e. addition of IPTG for cultures with TB media (Table 2.20). TB media-based cultures were induced continuously for 16 h at 18 °C and 110 rpm. The cultures were harvested by centrifuging at 6000 ×g for 10 min at 4 °C. For auto-induction cultures were grown for 22 h after they reached 18 °C. For the production of emST with rho-tag in the BL21(DE3) strain a pET20a_{emST-rho} plasmid was used.

Table 2.20 Strain and medium used for bacteria expression

Construct	Strain	Expression medium
pET27b _{emST-his}	BL21(DE3)	TB-CAIM
	RP	TB-CAIM
		ZY-CAIM
	RIL	TB-CAIM
		ZY-CAIM
	Lemo21	TB-CAIM
	C41	TB-CAIM
pQE2 _{emST-his}	C43	TB-CAIM
	BL21(DE3)	TB-IPTG
	RP	ZY-CAIM
pET20a _{emST-rho}	RIL	ZY-CAIM
	BL21(DE3)	TB-IPTG

2.4.2 Insect cell expression

Recombinant protein expression in insect cells offers high levels of protein with post-

translational modification similar to that of mammalian cells and allows easy scale-up to high-density suspension culture. Two approaches were used for insect cell expression: Baculovirus expression vector system (BEVS) using the flashBAC™ expression system (flashBAC ULTRA™) and the virus free plasmid DNA-based transient gene expression system (TGE) (PEI-mediated transfection) [53, 131-137]. A baculovirus expression vector is a genetically modified baculovirus that contains a specific gene of interest and can be transmitted in insect cells through the baculovirus promoter. Autographa californica nucleopolyhedrovirus (AcMNPV) is the most widely used baculovirus, with a super-coiled, double stranded, circular DNA genome within a rod-shaped nucleocapsid [138]. It has a biphasic life cycle with two virus phenotypes of which the budded virus (BV) form is more infectious toward cultured insect cells than the other form i.e. occlusion-derived virus (ODV) [139, 140]. In BEVS the gene to be expressed replaces the polyhedrin gene, which is non-essential for viral replication in insect cells, thereby letting the insect cells produce the protein of interest with the aid of the powerful polyhedrin gene promoter. In the TGE system DNA containing the target gene is endocytosed by the cells and enters the nucleus by escaping the endosomal pathway [141, 142]. DNA can be incorporated into a host cell by transfection with the assistance of stable cationic polymer e.g. polyethylenimine (PEI) or Lipofectamine which act as transfection reagents [143]. The cationic polymer binds and condenses it to positively charged particles which adhere to anionic cell surfaces and thereby enhance the probability to be picked-up by endocytosis. The PEI-mediated transfection was used for all expressions in High 5 cells.

BTI-Tn-5B1-4 (*Trichoplusia ni*, High5) cells and Sf9 (*Spodoptera frugiperda*) cells were used for the expression of emST-rho by BEVS and the TGE system, respectively [144, 145]. Sf9 cells and High5 cells were grown in Insect-EXPRESS serum free media and ExCell 405 media, respectively, at 27 °C and 120 rpm [136]. Frozen Sf9 cells were unfrozen and resuspended with 5 ml of Insect-XPRESS serum-free media in a T25 flask and incubated at 27 °C for 24 h. Initial cell viability was about 65 %, whereas for the transfection procedure above 90 % is generally required. Viability was determined by counting cells with a hemocytometer after combining equivalent volumes of trypan blue solution and culture sample [146]. To achieve viability above 90 % several passages were made by replacing the exhausted media with fresh media. Once the cell viability of above 90 % was reached suspension cultures were prepared by adding

the cells from the T25 flask to a 25 ml Erlenmeyer flask to a final cell count of 0.4-0.6×10⁶ cells/mL of fresh media and incubated in a shaker at 27 °C and 225 rpm. When the cell count reached 3-6×10⁶ cells/mL, which generally took 2-3 days, a new passage was made to maintain the cultures in the exponential growth phase by diluting the culture in fresh medium to a cell count of 0.4-0.6×10⁶ cells / mL. High5 cells were obtained directly as suspension culture from the protein sample production facility of the Helmholtz center for infection (Braunschweig). and maintained with the same procedure as described for sf9 cell above. All the procedures were handled under aseptic conditions. These suspension cultures were used for emST protein production using BEVS and TGE in Sf9 and High5 cells, respectively.

The flashBAC ULTRA™ was used for expressing emST in Sf9 cells. The flashBAC ULTRA™ includes deletion of non-essential baculovirus genes (chitinase, cathepsin, p26, p10 and p74) [53, 147, 148]. These deletions increase insect cell stability and lower the burden on virus-infected cells, allowing the expression of recombinant membrane proteins [149]. A standard flashBAC ULTRA™ protocol was used for the production of emST-rho using pOET2_{emST-rho} plasmids. Sf9 cultures with a minimum cell viability of 95 percent have been plated in a 6-well plate with 2 mL Insect-XPRESS serum-free medium at a 0.5 × 10⁶ cells/mL density and incubated for 1 h at 27 °C. After the cells had adhered to the surface, 1 mL medium was discarded and 10 mL of Insect GeneJuice added to the transfection mix (5 mL flashBAC ULTRA virus DNA; 100 mL serum-free medium; 100 mL Insect GeneJuice; 500 ng transfer pOET2 vector containing emST-rho (pOET2_{emST-rho})). After 16 hours of incubation at 27 °C, 1 mL of serum-free medium was added to the cells. The supernatant was removed from the well after five days of incubation and maintained as a P0 virus stock in the dark at 4°C. 0.5 mL P0 virus stock was applied to 100 mL Sf9 suspension culture to obtain a higher virus particle concentration. In a 500 mL suspension flask, cells were growth for 3 to 5 days at 27 °C and 200 rpm. Typically, the cells were extracted 3 days after cell growth arrest, when the maximum increase in cell diameter had been attained or when the cell viability had dropped below 80%. The suspension was centrifuged for 15 minutes at 3,000 rpm, and the supernatant was maintained at 4 °C in the dark as an operating P1 virus stock.

Expression of emST-rho in high5 cells using the TGE system was performed at the

protein sample production facility of the Helmholtz center for infection (Braunschweig). The facility provided the High5 cells. A fresh passage was made with a cell density of 0.5×10^6 cells / mL and grown at 27 °C for 24 h. Cells were counted with a hemocytometer and fractions of the cell culture containing 4×10^6 Hi5 cells were centrifuged at $180 \times g$, RT for 4 min, then resuspended with 2 mL fresh EX-CELL 405 medium, and finally a mixture of the DNA and a linear 40 kDa polyethylenimine (PEI 40 kDa) was added. The mixture contained 95 % pOpiE2_{emST-rho} plasmid and 5 % pOpiE2_{eGFP-HA} and 4 µg PEI 40 kDa (in deionised water with pH 7.0) per 1×10^6 cells/mL. The cells were grown with 180 rpm at 27 °C. Every 24 h 2mL fresh medium was added to maintain the exponential growth. The fluorescence of eGFP was measured after 48 h of transfection using the cytometer (Cytoflex, Beckmann Coulter). Centrifugation at 4000 g for 20 min at 4 °C was used to harvest the cultures. Cell pellets were maintained at -80 °C until further processing.

2.4.3 Mammalian cell expression

Different variants of emST i.e., emST-rho, emSTI273A-rho, emST-tm2-rho and emST-mCherry-rho were expressed in the *HEK293-6E* cell line (Human embryonic kidney 293, *HEK293*) and the *Expi293F GnTI-* cell line (Human embryonic kidney, *Expi293*) (Table 2.16) employing the virus-free TGE system using lipofectamine-mediated transfection [150, 151]. These expression experiments were performed at the protein sample production facility of Helmholtz center of infection (Braunschweig). Suspension cultures of *HEK293* and *Expi293* were provided by the facility.

A fresh passage was made with a cell density of 1.5×10^6 cells / mL and grown at 37 °C and 5% CO₂ for 24 h. Cells were counted using a hemocytometer, and a fraction of the cell culture containing 4×10^6 *HEK293* cells was centrifuged at $180 \times g$, RT for 4 min and resuspended in 2 mL fresh FreeStyle™ F-17 medium. This cell resuspension was added with a mixture of the DNA mixture and a 25 kDa polyethylenimine (PEI 25 kDa). The DNA mixture contained 95 % pTT5_{emST-rho} plasmid and 5 % pTT5_{GFP} and a final concentration is 4 µg PEI per 1×10^6 cells/mL. The PEI 25 kDa solution was prepared in deionized water with an adjusted pH of 7.0. The cells were cultivated at 37 °C, 5% CO₂ and 180 rpm. Exponential growth was maintained by the addition of 2mL of fresh medium after 24 h. The fluorescence of eGFP was measured after 48 h of transfection by cytometer (Cytoflex, Beckmann Coulter). Centrifugation at 4000 g for

20 min at 4 °C was used to harvest the cultures. Cell pellets were maintained at -80 °C until used.

A fresh passage was made at a cell density of $2.5\text{-}3.0 \times 10^6$ viable cells / mL and grown at 37 °C with $\geq 80\%$ relative humidity and 8 % CO₂, 125 rpm overnight. The culture containing 6×10^8 *Expi293* cells were added with a mixture of DNA diluted with Opti-MEM™ Reduced Serum Medium and ExpiFectamine™ 293. The DNA mixture contained 0.2 g pTT5_{emST-rho} plasmid, 12 mL Opti-MEM™ Reduced Serum Medium and 640 µL ExpiFectamine™ 293. The mixture was incubated for 20 minutes at room temperature before being added to the cell culture. The cells cultures were grown at the above-mentioned conditions for 48 h. Centrifugation at 4000 g for 20 min at 4 °C was used to harvest the cultures. Cell pellets were stored at -80 °C.

2.5 emST purification

2.5.1 Cell lysis and membrane preparation.

In general, membrane protein purification includes cell lysis, separation of the membrane fraction from the soluble cytosolic fraction, solubilization of membrane integrated proteins using membrane mimicking agents (e.g. detergents, nanodisc, styrene maleic acid (SMA) or di-isobutylene maleic acid (DIBMA), etc.) and finally purifying the solubilized membrane proteins using affinity and/or size exclusion chromatography [152, 153]. The affinity chromatographic resin was determined by the purification-tag included in the construct. Two kinds of purification tags were used in this work: his-tag (Table 2.16), which was used only in bacterial expressed constructs, and rho-tag, which was used for all the four different kinds of protein expression systems (Table 2.16).

Cell lysis during all purifications was achieved by using either an EmulsiFlex C3 cell disruptor (for large scale i.e. 10 g cell pellets) or a sonicator (for small scale i.e. 0.5 g cell pellet). Cell pellets were resuspended in respective lysis buffers (Table 2.13) at 1 g cell pellet to 8 ml lysis buffer ratio. Protease inhibitors were added to the cell suspensions before cell lysis (Table 2.13). For bacterial cell pellets, 1 mg of DNaseI to 10 g cell pellet and 1 mg of lysozyme for 1ml of mixture were added to the cell suspension before cell lysis. Incubation of the bacterial cell suspensions in the cold room was carried out for 1 hour before opening the cells with the disruptor. Prior to the

cell lysis the periplasmic fraction of the bacteria cells were removed by the osmotic shock method (Appendix IV: Protocols). This step provides better binding of protein with his-tag to the Ni-NTA resin as the periplasmic space of *E.coli* contains the most metal chelators, which could interfere with the target protein binding to the Ni-NTA resin [154]. The final lysate was collected by centrifuging at 900×g for 30 minutes to remove unopened cells from the cell lysis after passing the cell suspension through the cell disruptor 3-8 times at a pressure of 14,000-18,000 psi. The lysate supernatant was centrifugated for 30 min at 4°C with 9,000×g to remove the inclusion bodies, after which the collected supernatant was ultracentrifugated for 1 hour at 4°C with 100,000×g for membrane harvesting.

Membrane pellets were resuspended in 1 ml of lysis or PBS buffer (Table 2.13) per gram cell pellet equivalent and homogenized to prepare a membrane stock. Stocks of membranes were flash-frozen with liquid nitrogen and stored in -80 °C until required. Membrane stocks from different expression systems were solubilized by using a detergent (FOS12 or DDM) or a polymer (DIBMA) in different buffers with variation in pH and NaCl concentrations as shown in Table 2.13. Membrane stocks from bacterial expression were solubilized by using 1 % Fos12 in buffers with different pH (6.5, 7.0 and 8.0) (Table 2.13). Membrane stocks from insect cell expression were solubilized using 1 % Fos12 in a buffer with pH 7.5 (Table 2.13). Mammalian cell membrane stocks were solubilized by using either 1 % Fos12 or 2% DDM or 7 % DIBMA, where the pH of the buffers with detergents was 7.5 and that with polymer was 7.0. (Table 2.13). Membrane stocks from mammalian cells were diluted into above mentioned solubilization buffers (Table 2.13) with a ratio of one gram cell pellets into 8 mL solubilization buffer and incubated with gentle agitation for 2 to 4 hrs at 4 °C. The mixture was then ultracentrifuged for 1 hr at 100,000 × g and the supernatant was used for affinity purification.

The detergent screening was performed for emST-his and emST-rho protein expressed in *E. coli* (RP) and *Expi293* cells, respectively, using respective constructs i.e. pET27b_{emST-his} and pTT5_{emST-rho}. A membrane equivalent to 0.25 g cell pellet was used for each detergent used during this screening (Table 2.21). The above procedures were applied for every expression test and these samples were directly used for SDS-PAGE and immunoblot analysis.

Table 2.21 Detergents used in solubilization.

Detergent used for solubilization	Type	Abbr.	Formula Weight (g/mol)
n-Octyl- β -D-glucopyranoside	Non-ionic	OG	292.4
n-Dodecyl- β -D-maltoside	Non-ionic	DDM	510.6
n-Decyl- β -D-maltopyranoside	Non-ionic	DM	482.6
n-Nonyl- β -D-glucopyranoside	Non-ionic	NG	306.40
6-Cyclohexyl-1-hexyl- β -D-maltoside	Non-ionic	Cy6	508.5
N,N-Dimethyl-dodecylamine-N-oxide	Zwitterionic	LDAO	229.4
FOS-choline-12	Zwitterionic	FOS-12	351.5

2.5.2 Affinity chromatography

The solubilized membrane fractions with variants of emST protein with either his-tag or rho-tag were purified using Ni-NTA/Ni-indigo and Rho1D4 resins, respectively.

2.5.2.1 His-tag based purification

Solubilized membrane fractions with his-tagged emST proteins were mixed with pre-equilibrated Ni-NTA or Ni indigo resin and incubated in the cold room for 4 hours in batch mode. The resin was washed with 20-30 CV (column volume) of different solutions as summarized (Table 2.13) to remove the unbound/weakly bound proteins/impurities. The bound proteins were eluted with at least 5 time 1 CV elution buffer containing 200-250 mM imidazole concentration.

2.5.2.2 Rho-tag based purification

Rho-tag based purification was performed for the respective solubilized membrane fractions containing rho-tagged emST variants with PureCube Rho1D4 Agarose resin [155]. Pre-equilibrated resin at 0.5 ml per solubilized membrane fraction equivalent of 1 gram cell pellet was incubated overnight in the cold room. The flow-through was collected on the second day by applying the mixture to a gravity flow column. The resin has been washed with ten times 1 CV of different wash buffers (Table 2.13). Protein was eluted using 200 μ M rho1D4 peptide: Resin with bound protein was incubated on a shaker for 1 hour with 1 CV of elution buffer containing the rho1D4 peptide at 4 °C. This elution step was repeated at least 5 times to achieve a sufficiently complete elution.

2.5.3 Ion exchange chromatography

Solubilize membrane fraction was loaded onto a manually packed 5 mL PureCube Q Agarose column and 5 mL PureCube SP Agarose column (Cube Biotech, Monheim) with a flow rate of 0.5 mL/min at a DuoFlow 10 (Bio-Rad, Munich) FPLC system at 4 °C. Flow through was further purified through IMAC (Ni-NTA) [156, 157].

2.5.4 Size exclusion chromatography

Size-exclusion chromatography was applied using either a Dualflow 10 FPLC or a ÄKTA explorer 100 system at 4 °C. Columns were equilibrated with two column volume of SEC buffer (Table 2.13). The samples from the affinity purification were filtrated through a membrane filter with pore size of 0.22 µm before applicaton to the column. From the SEC elution profile of the detergent-protein complexes' the apparent molecular weight was calculated using calibration curves of therespective column.

Samples were collected during every step of the purification for the analysis by SDS-PAGE and immunoblot. Each sample was added with SDS-sample loading dye (Table 2.12) and incubated for 10 min at 46 °C before loading to the SDS-PAGE. Each SDS-PAGE was either used directly to capture the TCE fluorescence image [158] or for blue-silver staining [159] or used for western blot. Each sample was prepared for SDS-PAGE immediately after the collection as described above then stored at -20 °C for further use. Sample was loaded to SDS-PAGE after normalizing to contain the yield of a specific cell pellet weight. For samples from SEC normalization was made only based on volume.

2.6 Deglycosalation assay

Samples of purified emST-rho, emST-mCherry-rho and emST-tm2-rho were analyzed by enzymatic removal of the glycosylation moiety and mass spectroscopy (at Mass Spectrometry and Proteomics core facility (Heidelberg)) to confirm their glycosylation status [160, 161].

Endoglycosidase H (Endo H) is a recombinant glycosidase, that cleaves the bond between two subunits of N-acetylglucosame (GlcNAc) specifically two N-acetylglucosamine (GlcNAc) subunits directly proximal to the asparagine of the N-linked glycoprotein [162]. Peptide-N-Glycosidase F (PNGase F) is an amidase, which

cleaves between the innermost GlcNAc and asparagine residues of high mannose, hybrid, and complex oligosaccharides from N-linked glycoproteins [162]: EndoH/PNGase F was added at 50 U/ μ L reaction volume for 2 μ g of emST-rho and its variants and incubated at 27°C overnight. Samples were further analyzed by coomassie blue silver stained SDS-PAGE and anti-rho western blot.

2.7 Protein Identification and Characterization

2.7.1 Mass spectrometry

Mass spectrometric analysis was performed at EBML SPC facility (Heidelberg) and Core Facility for Mass Spectrometry and Proteomics (CFMP, Heidelberg) to identify desired samples of interest and to confirm protein glycosylation and the sites of glycosylation. Protein bands were excised after coomassie blue silver stained SDS-PAGE and submitted for mass spectrometric analysis (LC-MS/MS).

2.7.1.1 LC-MS Analysis

Protein samples were analyzed by SDS PAGE. The Coomassie stained bands were excised and with minor modifications processed as described by Fecher-Trost [163]. In brief, the protein sample was digested with trypsin at 37°C. The trifluoroacetic acid (20 μ L of 0.1%TFA) was added to quench the trypsin digestion. Before LC-MS analysis the sample was dried in a vacuum concentrator [163]. An Ultimate 3000 liquid chromatography system coupled to a QExactive HF mass spectrometer was used for the nanoflow LC-MS/MS analysis. The protein samples were dissolved in 0.1% TFA, subsequently injected to a self-packed analytical reversed phase column and eluted with a flow rate of 300 nl / min in an acetonitrile-gradient (3% - 40%) [163]. The mass spectrometer was operated in data-dependent acquisition mode, automatically switching between MS and MS/MS [163]. Collision induced dissociation MS/MS spectra were generated for up to 20 precursors with a normalized collision energy of 29% [163].

2.7.1.2 Database search

To identify and quantify the peptides, the Proteome discoverer 2.2 (Thermo Scientific) was used for raw data processing [163]. MS/MS spectra were searched against the Uniprot *E. multilocularis* database (UniprotKB) and the contaminants database

(MaxQuant database; MPI Martinsried) (altogether 10689 entries) with the following parameters: Acetyl (Protein N-term), Oxidation (M), NEM (C) and NEM+H2O (C) variable modifications were required, and trypsin/P was used as the proteolytic enzyme, with up to two missing cleavages permitted. For proteins and peptides, the maximum false discovery rate was 0.01, and a minimum peptide length of 7 amino acids was needed. [164].

2.7.2 Circular dichroism spectroscopy

Traditionally, protein structure and folding properties have been assessed by measuring circular dichroism (CD), which is depended on the differential absorption of right-handed and left-handed circularly polarized light by chromophores [165]. As the basic structure in proteins, the peptide bonds, have strong absorption at 250nm to 180 nm, the secondary structure composition of proteins can be analyzed by CD spectroscopy. The signal from the near UV range (320 - 260 nm) is used for investigating tertiary structure in the proteins e.g. changes in the disulfide bonds.

A Zeba desalting column was used for exchanging the buffer of the purified protein samples (Table 2.22) to their CD buffers (Table 2.22). NanoDrop was used to determine the protein concentrations. Quartz cuvettes with a path-length of 0.1 cm were used for all the CD measurements at 4 °C employing an Aviv CD 425 spectrometer. CD data (200 - 250 nm) were analyzed using the BESTSEL analysis program for deconvolution.

Table 2.22 Protein sample and CD buffer

Protein	Conc. µg/mL	No.of residue s	M W	Protein buffer	CD buffer
emST-his (<i>E.coli</i> BI21(DE3))	188	658	74. 4	150 mM NaCl; 20 mM TRIS (pH 8); 10 % (w/v) Glycerol; 0.1 % (w/v) Fos12; 0.5 mM TCEP	10mM NaPi; 50mM NaF; 0.05% Fos- 12;0.5mM TCEP (pH 8)
emST-rho (<i>Expi293</i>)	200	644	73. 9	150 mM NaCl; 20 mM HEPES (pH 7.5);10 % (w/v) Glycerol; 0.5 mM TCEP; 0.1 % (w/v) Fos12	10mM NaPi; 50mM NaF; 0.05% Fos- 12;0.5mM TCEP (pH 7.5)
	200	644	73. 9	150 mM NaCl; 20 mM HEPES (pH 7.5);10 % (w/v) Glycerol; 0.1 % (w/v) Fos12; 0.5 mM TCEP	10mM NaPi; 50mM NaF; 0.05% Fos- 12;0.5mM TCEP; 0.01% CHS (pH 7.5)

	240	644	73. 9	150 mM NaCl; 20 mM HEPES (pH 7.5); 10 % (w/v) Glycerol; 0.1 % (w/v) Fos12; 0.5 mM TCEP	10mM NaPi; 50mM NaF; 0.05% Fos-12; 0.5mM TCEP; 1mM CIT (3:1) 6.09 μ M (pH 7.5)
	114	644	73. 9	150 mM NaCl; 20 mM HEPES (pH 7.5); 10 % (w/v) Glycerol; 0.1 % (w/v) DDM; 0.5 mM TCEP;	10mM NaPi; 50mM NaF; 0.05% DDM; 0.5mM TCEP (pH 7.5)
emST-tm2-rho (<i>Expi293</i>)	147	644	73. 9	150 mM NaCl; 20 mM HEPES (pH 7.5); 10 % (w/v) Glycerol; 0.1 % (w/v) DDM; 0.5 mM TCEP	10mM NaPi; 50mM NaF; 0.05% DDM; 0.5mM TCEP (pH 7.5)
	148	644	73. 9	150 mM NaCl; 20 mM HEPES (pH 7.5); 10 % (w/v) Glycerol; 0.1 % (w/v) DDM; 0.5 mM TCEP;	10mM NaPi; 50mM NaF; 0.05% DDM; 0.5mM TCEP (pH 7.5)
emST-mCherry-rho (<i>Expi293</i>)	189	898	101	150 mM NaCl; 20 mM HEPES (pH 7); 10 % (w/v) Glycerol; 0.1 % (w/v) DDM; 0.5 mM TCEP;	10mM NaPi; 50mM NaF; 0.05% DDM; 0.5mM TCEP (pH 7)
	180	898	101	150 mM NaCl; 20 mM HEPES (pH 7); 10 % (w/v) Glycerol; 0.1 % (w/v) DDM; 0.5 mM TCEP	10mM NaPi; 50mM NaF; 0.05% DDM; 0.5mM TCEP (pH 7)
emST-his (MSP1D1)	100	658	74. 4	150 mM NaCl; 20 mM TRIS pH 7.5	10mM NaPi; 50mM NaF (pH 7.5)

2.8 Subcellular localization

The localization of emST was investigated by protein confocal microscopy and subcellular fractionation. In confocal microscopy experiments the pTT5_{emST-mCherry-rho} construct was used. In the subcellular fractionation assays pTT5_{emST-rho} and pTT5_{emST-mCherry-rho} were used to monitor possible effects of the mCherry tag.

2.8.1 Confocal microscopy

Immunofluorescence assays were performed using *Expi293* cells with transiently transfected pTT5_{emST-mCherry-rho} and different sub-cellular specific labeled antibodies. For protein identification the mCherry fusion protein was used. The sample preparation conditions for the use of the different microscopes (Table 2.23) are summarized below (Table 2.23).

Table 2.23 Microscope

Microscope	Leica SP8	Spinning Disk Perkin Elmer Nikon Ti Eclipse	Axiovert 135TV Carl Zeiss Microscopy
Objective	Plan Apo 63x/1.40 oil	Plan Apo 60x/1.4 oil	Plan Apo 63x/1.4 oil
Camera	Leica APD	Orca R2 EM-CCD	Coolsnap HQ2
Software	LAS X	Volocity	Visi View

2.8.1.1 Preparation of coverslips

10 mm Coverslips (Thermo Fisher Scientific) were washed with 60% (v/v) ethanol and 40% (v/v) HCl solution for 30 min on a shaker. The washing solution was removed and the coverslips were rinsed extensively (at least 5 times) with distilled water. Coverslips were spread separately on Whatman filter paper, dried under a clean bench and subsequently sterilized by autoclaving (121°C, 30 min).

2.8.1.1 Coating of coverslips

The autoclaved coverslips were coated with fibronectin, which is an extracellular matrix protein that improves cell adhesion on the glass surface, using 25 µg/mL fibronectin (Roche) in PBS at room temperature for 1 h. The coverslips were cleaned three times with PBS after the coating solution was removed.

2.8.1.1 Fixation and staining

Fibronectin coated coverslips were placed in the wells of a 24 well plate, and 2×10^3 *Expi293* cells per well were added from a culture in the logarithmic growth phase, which was obtained from a culture with (or diluted to) 0.5×10^6 cells/mL. These cultures were allowed to grow for 24 h before adding 4 µg pTT5_{emST-mCherry-rho} and ExpiFectamine™ 293 reagent (section 2.4.3), and then allowed to grow overnight at 37 °C with 5 % CO₂. After washing the cells two times with PBS buffer, they were treated for 15 min at room temperature with pre-warmed (37 °C) 4% (w/v) PFA in PBS to turn into the adherent state on a cover slide. Cells were washed thrice with PBS and permeabilized for 30 min at room temperature with 0.2% (v/v) Saposin in PBS, which allowed larger structures like antibodies to enter the cells. Cells were washed three times with PBS. To avoid nonspecific binding of the antibody, cells were incubated in blocking solution

(1% (w/v) BSA in PBS) for 1 h at room temperature facing downwards in a humid chamber. Cells were then stained with the primary antibody (Table 2.24) diluted in the blocking solution. The prepared cover slide with the cells was placed upside down in a humidification chamber. Afterward, cells were washed three times in PBS and incubated as described above with the secondary antibody (Table 2.25) diluted in the blocking solution for 1 h at room temperature. Cells were washed two times with PBS and one time with deionized water to remove all the salts. Coverslips were overturned on a microscope slide covered with ProLong™ Diamond Antifade Mountant with DAPI, a nuclear dye, (Thermo Fisher Scientific) and stored in the dark at room temperature, ready for imaging.

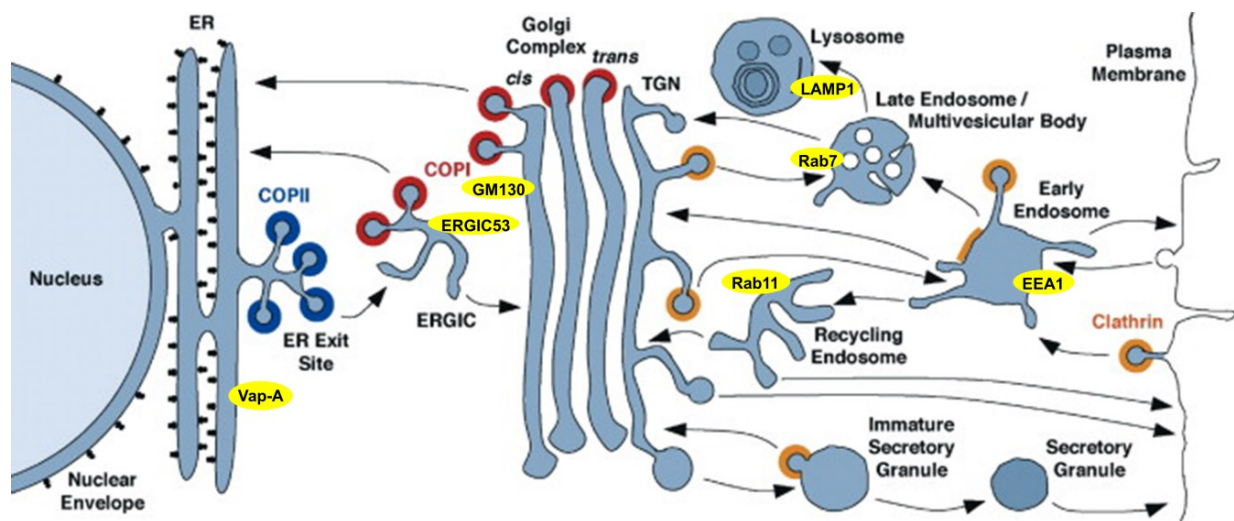


Figure 2.3 Intracellular Transport Pathways (adapt from [166])

The compartments of the lysosomal/vacuolar, secretory and endocytic pathways are shown in this diagram. Arrows signify the phases in the transportation process. COPI (red), COPII (blue) and clathrin (green) are seen in different colors to signify their locations (orange). Clathrin coats are heterogeneous, containing a variety of accessory and adaptor proteins at various membranes.

Seven different antibodies for seven different organelle specific marker proteins were used: Anti-Vap-A, anti-ERGIC-53, anti-GM130, anti-LAMP1, anti-EEA1, anti-Rab6, and anti-Rab11. These target ER, intermediate region between the endoplasmic reticulum and the Golgi, cisternae near the endoplasmic reticulum Golgi (cis Golgi) membrane, lysosome, early endosome, recycle endosome, and late endosome, respectively [167-173]. Six different antibodies were used with two fluorochromes i.e. Alexa Fluor™ 647, Alexa Fluor™ 488 (Table 2.25).

Table 2.24 Primary antibodies

Targetted organelle	Marker protein	Clone	Species	Application	Source
Early endosome	EEA1	monoclonal	rabbit	IF 1:100	Cell Signaling, C45B10
Recycle endosome	Rab7	monoclonal	rabbit	IF 1:100	Cell Signaling, D95F2
Late endosome	Rab11	monoclonal	rabbit	IF 1:50	Cell Signaling, D4F5
Endoplasmic reticulum–Golgi intermediate compartment	ERGIC53	polyclonal	rabbit	IF 1:50	Sigma, E1031
cis Golgi	GM130	monoclonal	rat	IF 1:50	BD, 610823
Lysosome	LAMP1	monoclonal	rat	IF 1:200	Abcam, 25245
Endoplasmic reticulum	Vap-A	monoclonal	Goat	IF 1:50	Santa Cruz, 48698

Table 2.25 Secondary antibodies

Name	Description	Marker protein	Coupled to	Application
A19C	goat anti-mouse IgG	GM130, LAMP1	Alexa Fluor™ 647	IF 1:400
B19C	goat anti-rabbit IgG	EEA1, Rab7, Rab11, ERGIC53	Alexa Fluor™ 647	IF 1:400
G19C	donkey anti-goat IgG	VAP-A	Alexa Fluor™ 647	IF 1:400
A12C	goat anti-mouse IgG	GM130, LAMP1	Alexa Fluor™ 488	IF 1:400
B12C	goat anti-rabbit IgG	EEA1, Rab7, Rab11, ERGIC53	Alexa Fluor™ 488	IF 1:400
G12C	donkey anti-goat IgG	VAP-A	Alexa Fluor™ 488	IF 1:400

2.8.2 Cell fractionation and organelle isolation

Cell fractionation is a method to isolate subcellular components and separate organelles and other subcellular components from one another [174]. To investigate the localization of emST-rho and emST-mCherry-rho plasma membrane and endoplasmic reticulum were isolated from the same homogenate of *Expi293* cells

expressing the respective protein, and analyzed by anti-rho western blot.

Cellular fractions were isolated from Expi293 cells using the process previously described for yeast. [175].

The Expi293 cells were washed with PBS, resuspended in cold homogenization buffers (4 °C) with 75 mM sucrose, 225 mM mannitol, protease inhibitor cocktail, 0.1 mM EGTA and 5 mM Tris-HCl at pH 7.4, and homogenized with a teflon stroke by utilizing 8-10 strokes at 1500 rpm in the ice cold bottle of a 50 ml Potter-Elvehjem homogenizer. The homogenate was centrifuged twice for 3 minutes at 600 g, and the supernatant was centrifuged for 20 minutes at 20,000 g. The supernatant (25 ml/ tube) comprising microsomes and cytosolic proteins was centrifuged at 100,000 g for 1 hour to sediment the microsomes, then at 100,000 g for 2 hours to extract the pellet and separate the ER fraction and the supernatant (Cytosol (C) fraction). The homogenous supernatant was twice centrifuged for 3 minutes at 600 × g then the supernatant was centrifuged for 20 minutes at 20 000 × g. The supernatant containing cytosolic and microsomal proteins was centrifuged for 1 hour at 100,000 × g to sediment microsomes. Finally, the supernatant centrifuged at 100,000 × g for 2 hours to separate supernatant (Cytosol (C) fraction) and the pellet (ER fraction).

The above sedimented microsome pellet containing plasma membrane (PM), plasma membrane associated membranes (PAM) fraction and mitochondria were resuspended in 0.2 mM EDTA, pH 6.0, 5 mM Bis-Tris and subjected to further separation on a discontinuous sucrose gradient i.e. 53%, 43% and 38% in base buffer: 0.2 mM EDTA, pH 6.0, 5 mM Bis-Tris, at 100,000 × g for 2 h. This centrifugation should yield three thick bands: a visible PAM band above 38% sucrose gradient, a band composing of mitochondria tightly associated with PM at the 43/38% sucrose gradient interface and a purified PM band at the 43/53% sucrose gradient interface. Of these three subcellular fractions only PM and PAM related band fractions have been collected and diluted threefold with 75 mM sucrose, 225 mM mannitol, 0.1 mM EGTA, pH 7.4, 5 mM Tris–HCl. The PAM fraction was sedimented for 45 min at 100,000 × g. Apart of the PAM pellet was resuspended and was first centrifuged at 10,000 g for 10 minutes to extract contaminating mitochondria, and then the PM fraction was isolated by sedimentation at 48,000 × g for 20 min. All the above-mentioned pellets corresponding to ER, PAM and PM fractions were suspended in 250 µL of 75 mM

sucrose, 225 mM mannitol, 0.1 mM EGTA, pH 7.4, 5 mM Tris–HCl using a loose-fitting Dounce homogenizer. The total protein concentration of each fraction was determined by the Bradford assay. Each fraction sample was separated on a SERVA Tris-Glycine 4-12% (wt / vol) precast gel (SERVA) and analyzed by western blot using anti-rho and other antibodies specific for the subcellular localization (Table 2.26).

Table 2.26 Antibodies of subcellular marker proteins

Antibody	Target subcellular fraction	Dilution used
Syntaxin	trans-Golgi network	1:2000
ATP2A2/SERCA2	ER	1:1000

3 Results

3.1 Bacterial system

Bacterial expression of emST-his and emST-rho were performed using in vivo and in vitro expression systems.

3.1.1 In vitro expression and purification of emST by CECF

Six different constructs, pQE2_{emST-his}, pQE2_{ΔN-emST-his}, pQE2_{ΔNL-emST-his}, pQE2_{ΔNL-emST-tm2-his}, pET27b_{emST-his} and pET20a_{emST-rho} were used for the expression of emST and its variants by CECF (Table 3.1).

Table 3.1 Constructs of emST

Constructs	M.W.
pQE2 _{emST-his}	74.4kDa
pQE2 _{ΔN-emST-his}	70.8kDa
pQE2 _{ΔNL-emST-his}	69.8kDa
pQE2 _{ΔNL-emST-tm2-his}	69.8kDa
pET27b _{emST-his}	74.4kDa
pET20a _{emST-rho}	73.9kDa

3.1.1.1 CECF expression without a solubilizer

In a preliminary experiment to optimize the amount of plasmid to use in the CECF expression system different amounts of plasmid from 0.75 - 1.5 μg were tested. Out of four pQE2 constructs used only pQE2_{emST-his} showed bands corresponding to a monomeric emST-his with a 68 kDa apparent molecular weight when anti-his western blot was used to analyze the pellet fractions. It should be noted that these images were taken with long exposure times (180 s). In these experiments a very intense signal for emST-his could be observed when 1.25 μg of plasmid was used (Figure 3.1A). The other three pQE2 constructs using the ΔN, ΔNL and ΔNL-tm2 variants of emST-his showed the protein only as a degraded product (Figure 3.1 B, C and D). The other two constructs i.e. pET27b_{emST-his} and pET20a_{emST-rho} were also screened for optimal

plasmid amount (Figure 3.2). Figure 3.2 A clearly indicates that the pET27b vector showed higher expression levels than pQE2_{emST-his} which did not have any signal while pET27b_{emST-his} samples showed bands, with only 15 s exposure time, corresponding to monomeric protein. Finally, 1.25 µg plasmid per 50 µL reaction was used as a standard for further experiments.

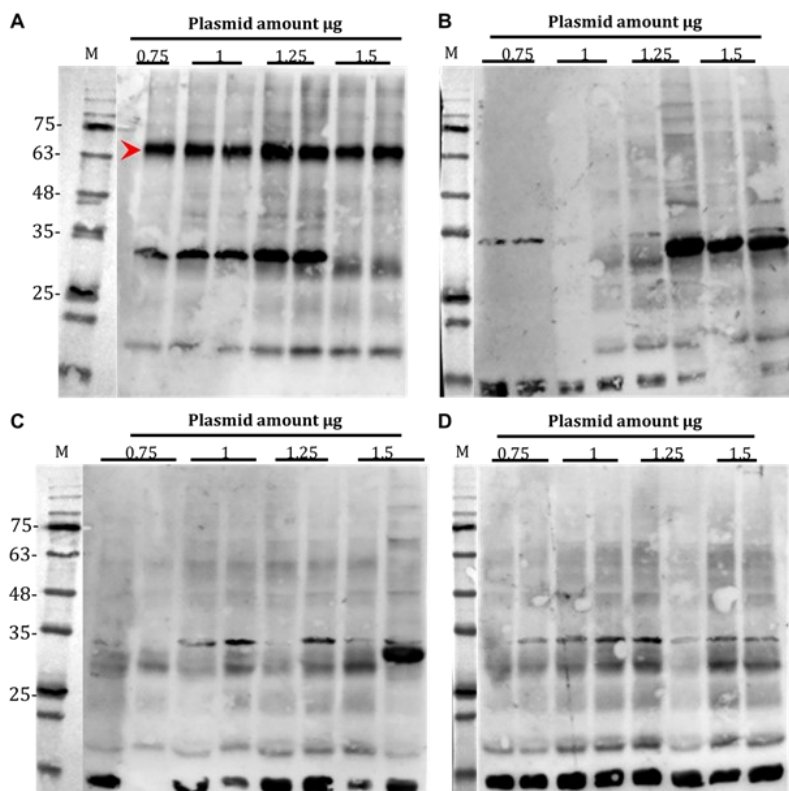


Figure 3.1 Without a solubilizer, anti-His western blot of cell-free expressed emST

A: pQE2_{emST-his}. B: pQE2_{ΔN-emST-his}. C: pQE2_{ΔNL-emST-his}. D: pQE2_{ΔNL-emST-tm2-his}. Red arrow indicates the expected molecular weight of emST. Just the pQE2_{emST-his} shows 70kDa full-length band, while others did not indicate high degradation of these constructs.

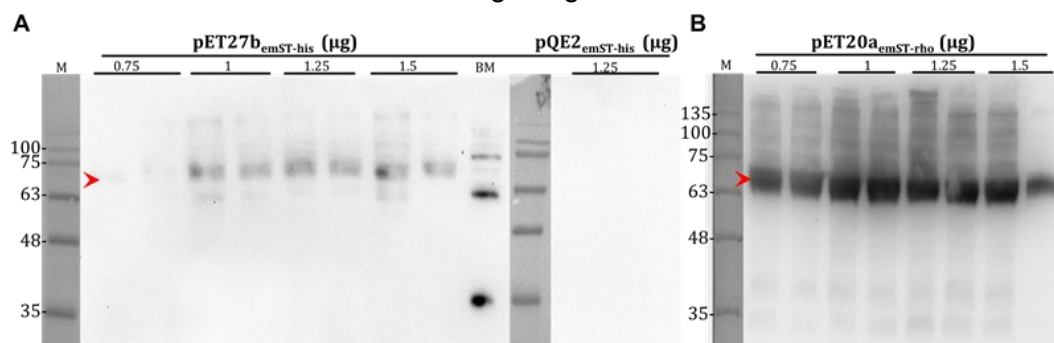


Figure 3.2 Western blot of cell-free expressed emST without a solubilizer

A: Anti-His blot of pET27b_{emST-his} expression and pQE2_{emST-his} as a positive control. B: Anti-Rho blot of pET20a_{emST-rho} expression.

3.1.1.1 CECF expression with nanodisc

Nanodiscs were included in the cell-free reactions to introduce a membrane mimicking environment expecting that the protein being expressed will be integrated into them. The amount of nanodisc used in CECF was optimized by a concentrations screening. All the pQE2 constructs and pET20a construct (Table 2.16) were used for the CECF expression where nanodisc concentrations of 40 μ M and 60 μ M were tested. Figure 3.3. shows the nanodisc concentration screening for pQE2 constructs where monomeric protein signal could be detected in the supernatant fraction. Also, at 25 kDa a band corresponding to MSP protein indicated the presence of nanodisc. All the emST-his variants with the pQE2 vector showed monomeric protein bands without any degradation. Clearly, higher amounts of nanodisc yielded a higher protein specific signal in the soluble fractions.

The influence of the size of nanodiscs on emST integration were analyzed by supplying two different sizes i.e., 9-10 nm (MSP1D1) and 12-14 nm (MSPE3D1) with the pET20a_{emST-rho} construct and his-tagged nanodiscs in the CECF. Anti-rho1D4 western blot analysis indicated that both MSP1D1 and MSPE3D1 allow solubilization of emST-rho. MSP1D1 showed a monomeric protein band at \approx 68 kDa in the supernatant fractions with both nanodiscs in the CECF at 40 μ M and 60 μ M. At the higher nanodisc concentration (60 μ M) a higher intensity of the band corresponding to emST-rho was be observed (Figure 3.3). MSPE3D1 showed emST-rho only in the soluble supernatant fractions in the reactions with a nanodisc concentration of 60 μ M and higher but not with 40 μ M. Overall emST-rho displayed a weaker nanodisc integration when MSPE3D1 was used (Figure 3.3) but the nanodisc concentration dependent solubilization was similar to the MSP1D1 experiment.

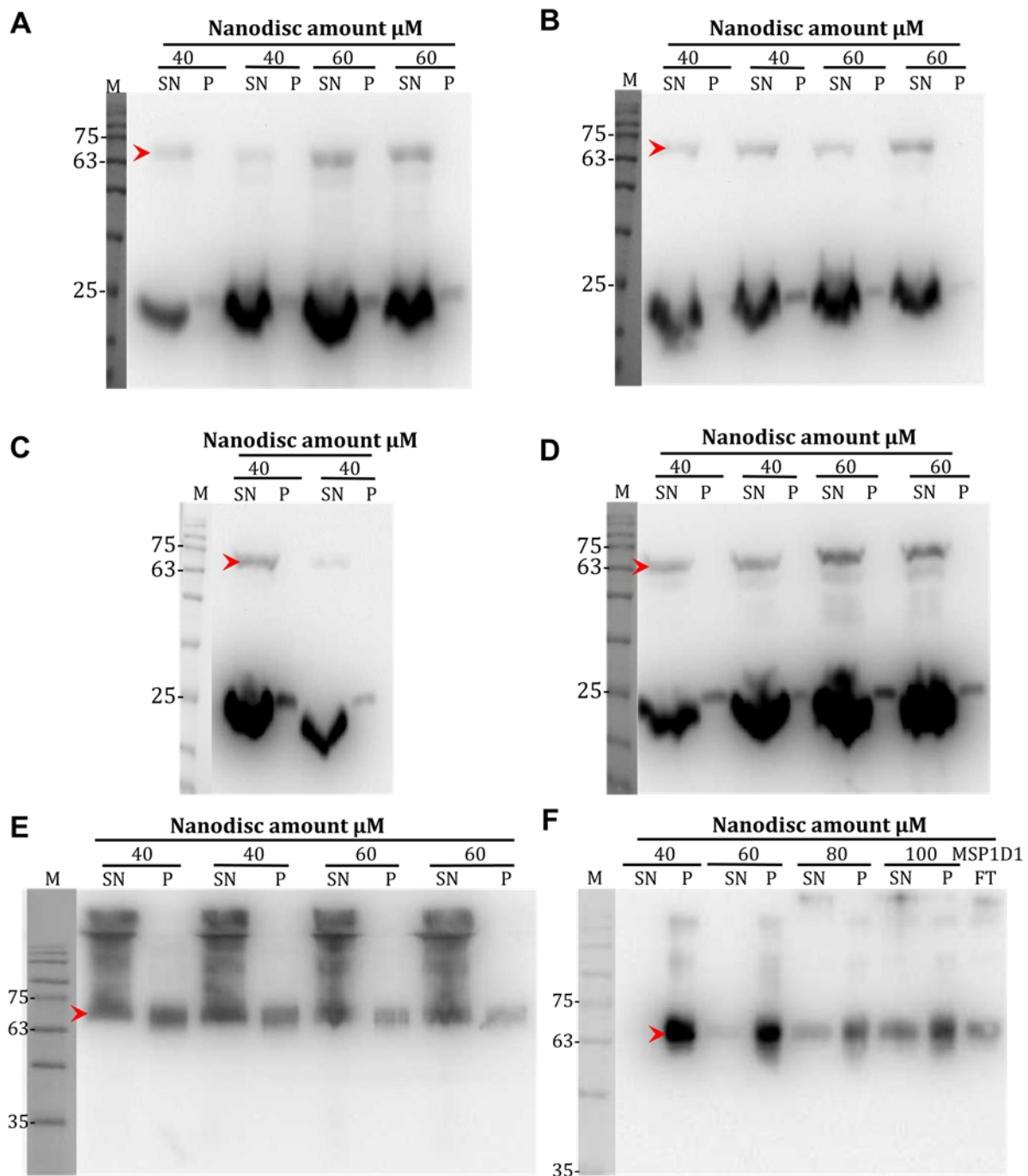


Figure 3.3 emST expressed into nanodiscs anti-his western blot

SN: supernatant; P: Pellet; A: expression of pQE2_{emST-his} in MSP1D1 nanodiscs. B: expression of pQE2_{ΔN-emST-his} in MSP1D1 nanodiscs. C: expression of pQE2_{ΔNL-emST-his} in MSP1D1 nanodiscs. D: expression of pQE2_{ΔNL-emST-tm2-his} in MSP1D1 nanodiscs. E: expression of pET20a_{emST-rho} in MSP1D1 nanodiscs. F: expression of pET20a_{emST-rho} in MSP1DE3 nanodiscs.

3.1.1.2 Purification cell-free expressed emST

A 100 μL CECF reaction with 100μM MSP1D1/MSP1DE3-POPC nanodisc was setup

to investigate the purification of the expressed emST-nanodisc complex (section 2.3.3). After 16 hours incubation the sample was centrifuged for 15 min at 20000 × g and wash buffer (Table 2.13) was used to dilute the supernatant ten times. before incubating with rho1D4 resins overnight at 4°C for binding and subsequent rho1D4 resin based purification (section 2.5.2.2).

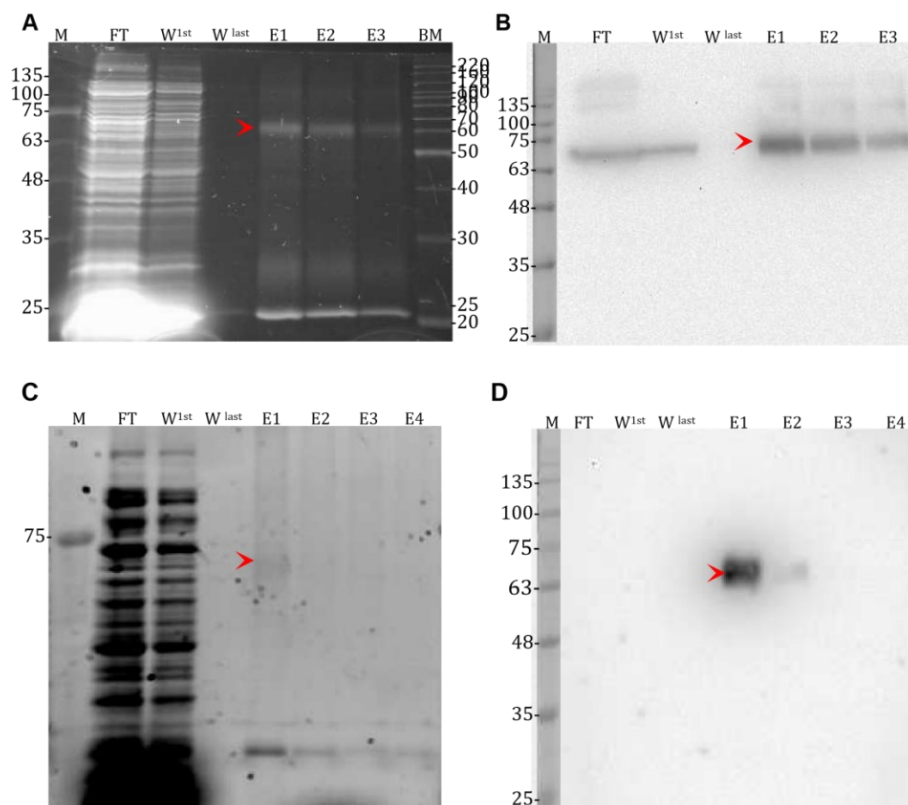


Figure 3.4 Expression and purification of emST-nanodisc in in-vitro system

FT: Flow through; W: Wash fraction; E: Elution fraction; A: TCE stain of pET20 α _{emST-rho} in MSP1D1 nanodiscs rho purification. B: Anti-rho blot of expressed pET20 α _{emST-rho} in MSP1D1 nanodiscs rho purification. C: TCE stain of pET20 α _{emST-rho} in MSP1DE3 nanodiscs rho purification. D: Anti-rho blot of expressed pET20 α _{emST-rho} in MSP1DE3 nanodiscs rho purification.

The emST-rho was immobilized by the rho resin, whereas the empty nanodiscs went to the flow through. Figure 3.4A shows both emST-rho and MSP-his were eluted with 200 μ M rho1D4 peptide elution buffer and subsequently identified by western blot (Figure 3.4B). The positive correlation between the signal intensity from nanodiscs (his-tagged) and emST (rho-tagged) indicated successful incorporation of emST in nanodiscs. The yield of 15 μ g / mL (for MSP1D1 sample) of emST-nanodisc sample was achieved by rho affinity chromatography. It should be noted that samples with MSP1D1 and MSP1DE3 were purified with pH 7 and pH 8, respectively. Protein

showed a better binding at pH 8 than pH 7 with no unbound protein in the flow-through fractions (Figure 3.4). Finally, size exclusion chromatography (SEC) was performed to allow subsequent biophysical analysis of the proteins.

3.1.2 In vivo expression and purification of emST

Three different constructs were used to express emST in bacterial strains (Table 2.3). Two different modes of induction for protein expression were used: IPTG and lactose induction (auto-induction). IPTG induction was used with TB media as the nutrient source. In the auto-induction experiments either ZY-CAIM or TB-CAIM (Composition Table 2.7 and Table 2.7) was employed.

When pET27b_{emST-his} was expressed using BL21(DE3)_{TB-CAIM} only a nominal anti-his western positive band could be observed with a 50 kDa apparent molecular weight for the samples starting from 4-22 h. Even after 24 h samples did not show a significant yield for the protein (Figure 3.5).

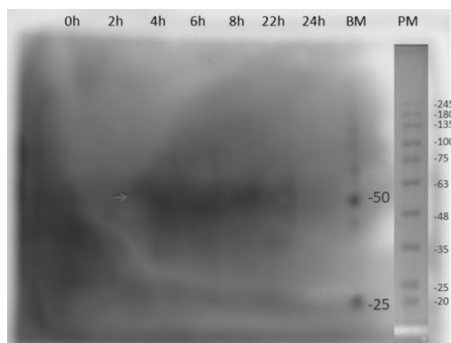


Figure 3.5 emST in BL21(DE3) strains with pET27b_{emST-his} expression

Immunodetection with his antibody of total cell lysate. pET27b_{emST-his} expressed in BL21(DE3) cells.

Similarly, when pET27b_{emST-his} was expressed using C43_{TB-CAIM}, C41_{TB-CAIM} and Lemo21_{TB-CAIM} no significant differences in expression were observed compared to that with BL21(DE3)_{TB-CAIM}. C43 samples showed only nominal anti-his western positive bands at 80 kDa, 70 kDa, 50 kDa, 35 kDa and 22 kDa. for the samples starting from 0-22 h (Figure 3.6). IMAC purification fractions of emST-his expressed using C41_{TB-CAIM} showed weak anti-his western positive bands at ≈75 kDa and ≈160 kDa only for the samples from 0-6 h but no protein signal could be observed for samples with 8 h, 22 h and 24 h time point (Figure 3.6B). Lemo21_{TB-CAIM} with expression emST-his also had anti-his western positive bands at 70kDa and 48kDa.for the samples starting from 0-24 h (Figure 3.6C).

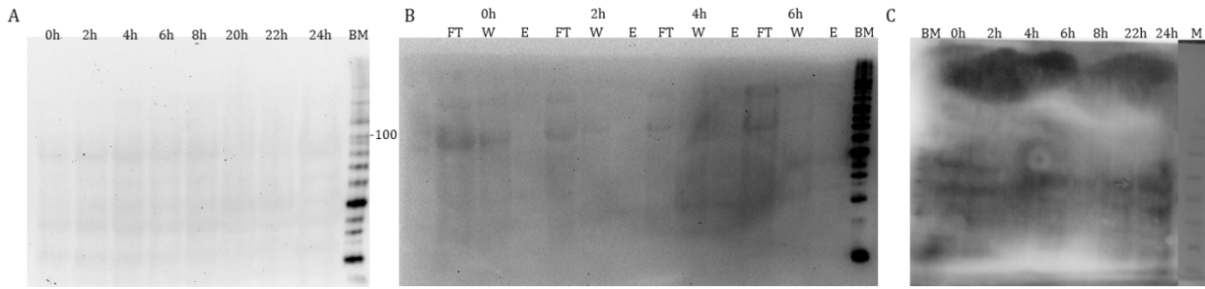


Figure 3.6 Expression analysis of emST in different strains with pET27b_{emST-his}

A: Immunodetection with his antibody using total cell lysate. pET27b_{emST-his} expressed in C43 cells. B: Immunodetection with his antibody. pET27b_{emST-his} expressed in C41 cells. C: Immunodetection with his antibody of total cell lysate. pET27b_{emST-his} expressed in Lemo21 cells.

The membrane fraction of RP_{ZY-CAIM} cells pellet after 100 000x g centrifugation with expressed emST-his showed two anti-his western positive bands with apparent molecular weight \approx 50 kDa and the other above 135kDa (Figure 3.7). The same fraction was used for screening detergents for optimal solubilization (Table 2.21). Out of eight detergents used in the screening three were zwitterionic (LDAO, FOS10 and FOS12) and five were nonionic (OG, DM, DDM, NG and Cy6) detergents. Samples where OG, NG or Cy6 was used showed hardly any solubilization. Best results were obtained after overnight solubilization and subsequent centrifugation at 100k \times g (Figure 3.7). Only samples with DM and DDM showed an anti-his western positive band at \approx 63 kDa corresponding to monomeric emST-his. However, there was also a considerable amount of protein in the insoluble (pellet) fraction. The samples containing zwitterionic detergent showed signal for the protein neither in soluble fraction nor in insoluble fraction (Figure 3.7).

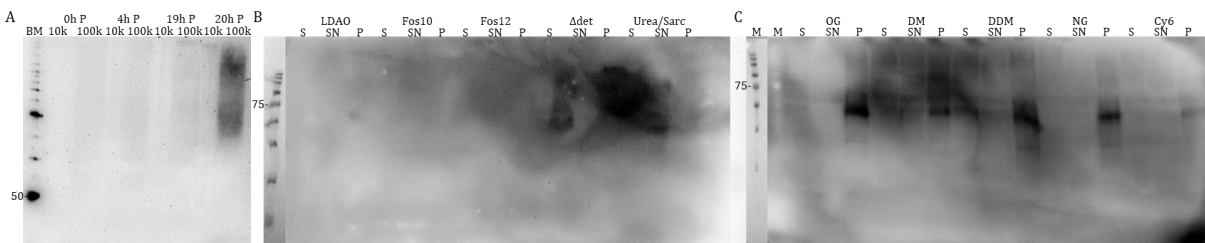


Figure 3.7 emST expressed in RP cells with pET27b_{emST-his}(ZY-CAIM)

Auto-induction in ZY medium. A: Immunodetection with his antibody of total cell lysate. pET27b_{emST-his} expressed at different duration. B and C: Immunodetection with his antibody of membrane solubilization. pET27b_{emST-his} expressed 20h in RP cells.

Samples of RP_{TB-CAIM}, where TB buffer was used as a base buffer in auto-induction experiments, also showed a very weak anti-his western signal between 50-160 kDa for emST-his. But for RP_{ZY-CAIM} samples the emST-his was detected in the inclusion body fraction (Figure 3.8). Furthermore, it was observed that the intensity of the signal decreased for the samples between 4h and 19h. When analyzing total cell lysate samples no signal could be detected. Therefore, in later stages samples were analyzed only after fractionation e.g. 10 000 × g fraction (inclusion body), 100 000 × g fraction (membrane fraction), etc. Furthermore, when emST-his was expressed in RP cells using IPTG induction (RP_{TB-IPTG}), protein could be detected in the inclusion body fraction when sonicated samples were analyzed. Samples obtained using the cell disruptor for protein release showed the targeted protein in both the fractions i.e. inclusion body as well as the membrane fractions (Figure 3.8).In both cases, the protein expression level was very marginal.

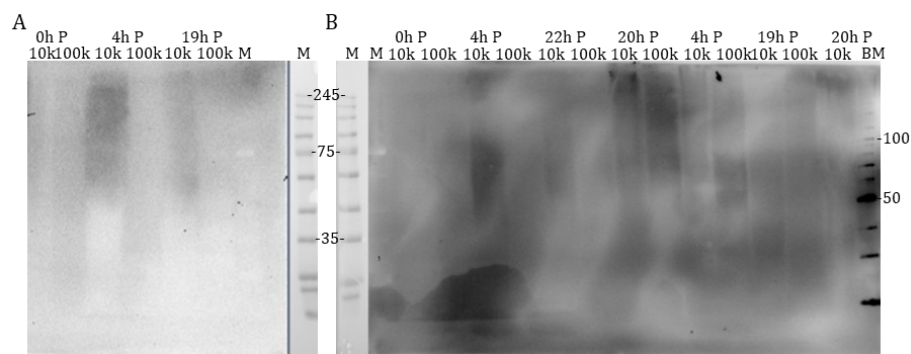


Figure 3.8 emST expressed in RP cells with pET27b_{emST-his}(TB-CAIM)

A and B: Immunodetection with his antibody of total cell lysate. pET27b_{emST-his} expressed with auto-induction and IPTG induction in TB medium.

The membrane fraction of RILTB-CAIM cell samples with expressed emST-his were solubilized using Fos12 (Table 2.21) and purified using IMAC (Section 2.5.2.1) by elution with 250 mM imidazole. Protein could be observed by western positive bands at ≈60 kDa, and other molecular weights which indicated either oligomerization or degradation. SEC, SDS-PAGE, and anti-his western blot analysis indicated that the protein was eluted in different peaks but in very low amounts, while the impurities were present in large amounts and could be detected by blue silver staining (Figure 3.9).

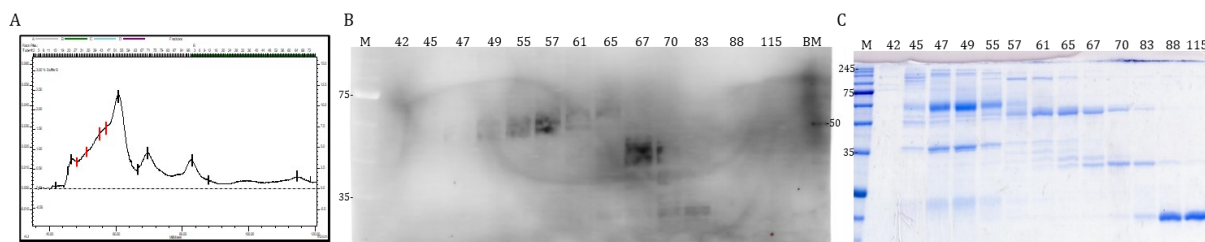


Figure 3.9 Expression analysis of emST in RIL cells with pET27b_{emST-his}

pET27b_{emST-his} expressed with auto-induction in TB medium. A: SEC profile. B: Immunodetection with his antibody of elution fraction from SEC. C: Blue silver stain of elution fraction from SEC.

The emST-his was also expressed using RIL_{ZY-CAIM} and RP_{ZY-CAIM}. The emST-his construct used here is based on the pQE2 vector (Table 3.1). FOS12 solubilized membranes from RIL_{ZY-CAIM} and RP_{ZY-CAIM} samples were used for IMAC purification (Section 2.5.2.1). Anti-his western blot analysis indicates that the protein was present only in the elution fractions from RIL_{ZY-CAIM} (Figure 3.10A) but not in RP_{ZY-CAIM} isolates (Figure 3.10C). Protein with an apparent molecular weight \approx 90 kDa could be detected in elution fractions where 60 mM, 90 mM and 250 mM imidazole was used (Figure 3.10A). On SEC emST-his from RIL_{ZY-CAIM} was eluted at 60 mL corresponding to an estimated molecular weight of \approx 287 kDa (Figure 3.10B). Samples from the 60 mL peak showed an anti-his western positive band at 73 kDa corresponding to a monomeric emST-his (Figure 3.10B), but the protein yield was very marginal.

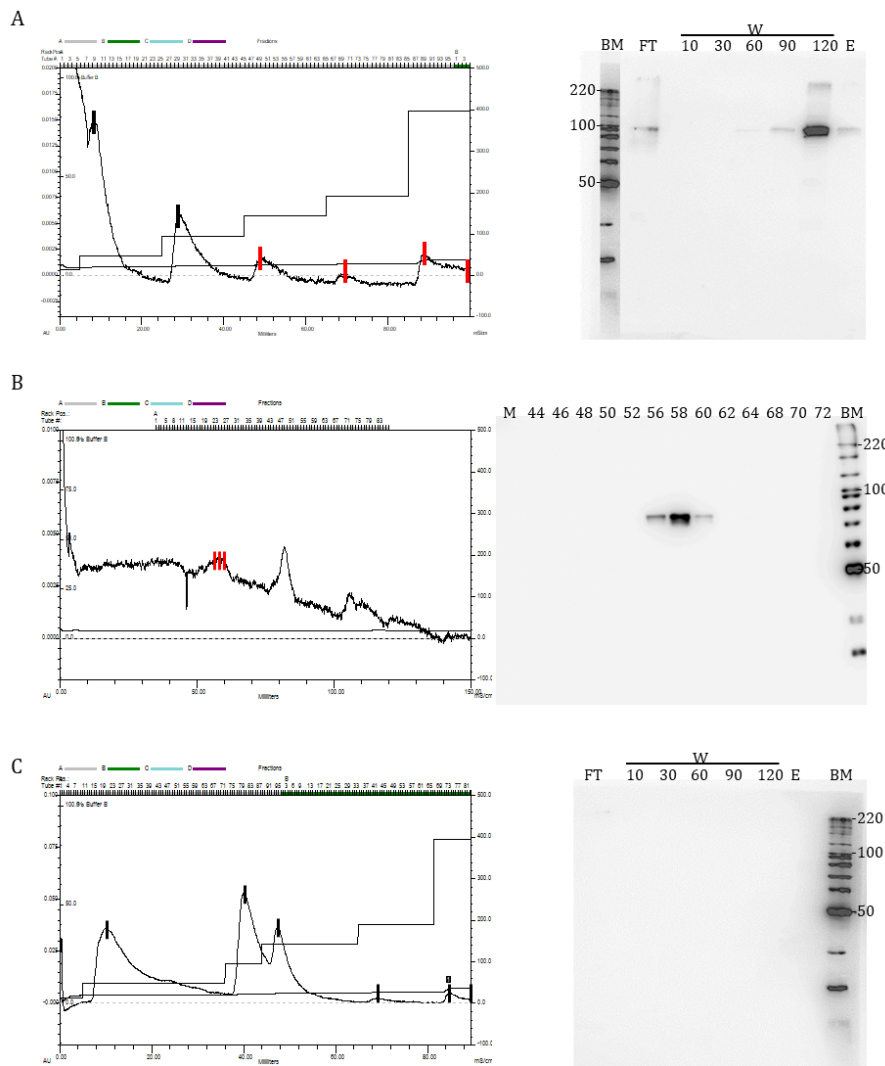


Figure 3.10 Expression analysis of emST in RIL and RP cells with pQE2_{emST-his}

pQE2_{emST-his} expressed with auto-induction in ZY medium. A: emST expressed in RIL cells. Left: IMAC profile. Right: anti-his western blot of IMAC. B: emST expressed in RIL cells. Left: SEC profile. Right: anti-his western blot of SEC. C: emST expressed in RP cells. Left: IMAC profile. Right: anti-his western blot of IMAC.

Samples from BL21(DE3)_{TB-IPTG} cells with pQE2 based emST-his were purified by IMAC (Section 2.5.2.1). Protein was eluted with 30 mM, 60 mM, 90 mM and 250 mM imidazole (Figure 3.11A). The elution fractions with 30 mM, 60 mM and 90 mM imidazole were pooled and analyzed by SEC (Figure 3.11B). The IMAC elution fraction with 250 mM imidazole was also analyzed separately (Figure 3.11C). Samples from both pool fractions did not show any difference either on the SEC profile or with the anti-his western blot (Figure 3.11B and C). The samples from the 60 mL SEC peak showed an anti-his western positive band at 63 kDa corresponding to a monomeric emST-his (Figure 3.11B and C). Blue silver staining indicated the presence of many

impurities and the yield to be very low. A scale up of 1.4L expression and purification was made where the Fos12 solubilized membrane fraction was passed through 5 ml (manually packed) Q-Sepharose and SP-Sepharose columns. The flow through was used for IMAC purification (Section 2.5.2.1) (Figure 3.12), and further purified by SEC (Figure 3.13). As expected from the test purification described above (Figure 3.11B and C) the BL21(DE3)_{TB}-IPTG expressed and Fos-12 purified emST-his was also eluted on SEC at ≈ 60.5 mL corresponding to an estimated molecular weight of 254 kDa (Figure 3.13). Samples from this peak showed a monomeric protein band at a 68 kDa apparent molecular weight on anti-his western blot (Figure 3.13). One of the post peak samples with elution volume 64 mL showed a band at ≈ 48 kDa, which was also anti-his western positive. The yield of purified emST-his_{BL21(DE3)-TB-IPTG} from the fractions corresponding to lanes 9-12 (Figure 3.13) was about 1.2 μg / g cell pellet.

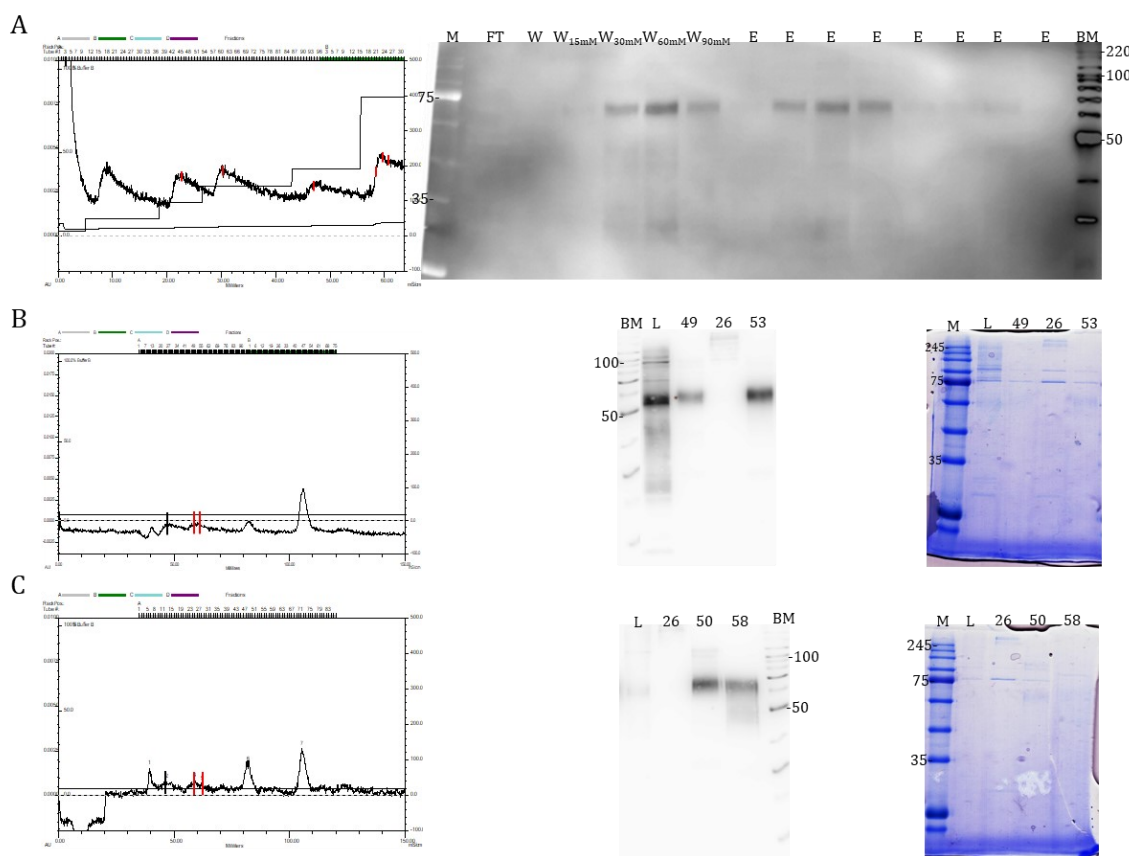


Figure 3.11 Expression analysis of emST in BL21(DE3) cells with pQE2_{emST-his}

pQE2_{emST-his} expressed with IPTG induction in TB medium. A: left: IMAC profile; Right: immunodetection with his antibody of IMAC. B: elution fraction with 30-90mM imidazole. left: SEC profile; cental: anti-his western blot; Right: blue stain. C: elution fraction with 250mM imidazole. left: SEC profile; cental: anti-his western blot; Right: blue stain.

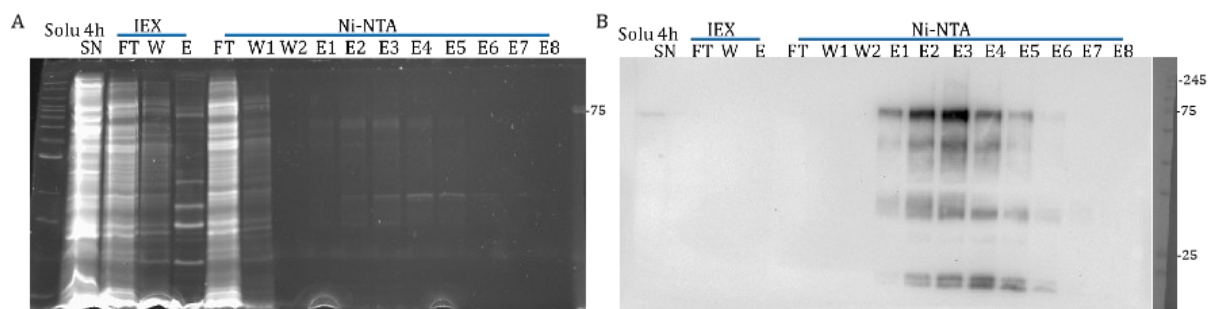


Figure 3.12 Purification analysis of emST in BL21(DE3) cells with pQE2_{emST-his}

pQE2_{emST-his} expressed with IPTG induction in TB medium. IEX: ion-exchange chromatography. Ni-NTA: immobilized metal affinity chromatography with nickel NTA matrix; Solu 4h SN: the supernatant sample after fos-12 solubilized for 4 hours; FT: flow through from Rho resin; W1-2: wash fractions; E1-8: elution with 300 mM imidazole. A: TCE stained SDS-PAGE; B: anti-His western blot.

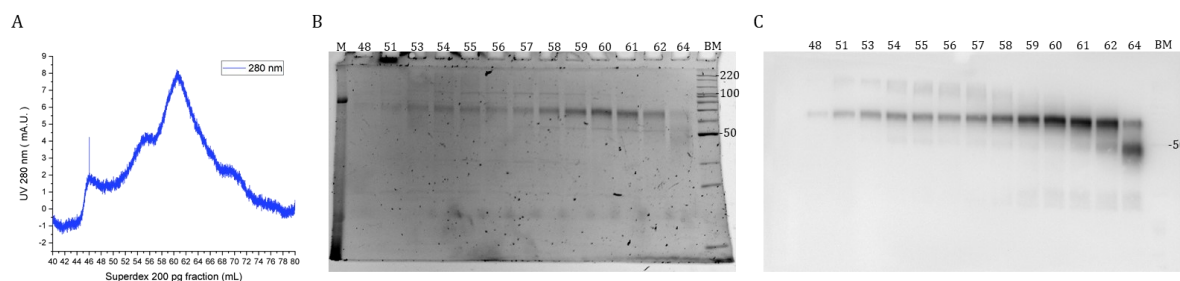


Figure 3.13 SEC analysis of emST in BL21(DE3) cells with pQE2_{emST-his}

Superdex 200 pg column with SEC buffer: 20 mM Tris pH 6.5, 0.1% (W/V) Fos-12, 150 mM NaCl, 0.5 mM TCEP, 10% Glycerol. A: SEC profile of emST. B: TCE stained gel. C: anti-his western blot.

A pET20a vector-based construct (Table 3.1) was used to express emST-rho using BL21DE3_{TB-IPTG}. The protein was isolated using rhoID4 resin (Section 2.5.2.2). Fos12 and DIBMA were employed for membrane solubilization before the purification. SDS-PAGE and anti-his western blot analysis indicated that the protein migrated at a 68.8 kDa apparent molecular weight (Figure 3.14). Furthermore, the results indicated that 2.5 % DIBMA was not able to extract the protein from the bacterial membrane.

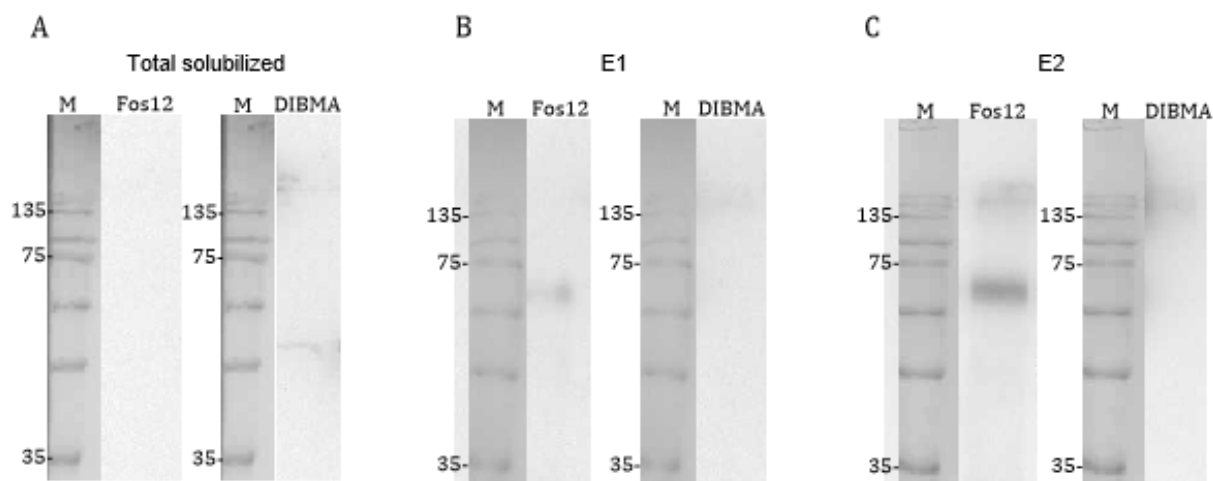


Figure 3.14 Expression analysis of emST in BL21(DE3) cells with pET20a_{emST-rho}

Aliquots of membrane fractions were solubilized with DIBMA and analyzed via SDS-PAGE and western blot. Total solubilized; E: Elution fraction; A: anti-rho blot of Total solubilized emST. B: anti-Rho blot of first elution fraction of emST. C: anti-rho blot of second elution fraction of emST.

3.1.3 Mass spectrometric analysis of emST

Mass spectrometric (MS) analysis for the purification samples of emST-his (BL21(DE3) with Fos12), emST-rho (*Expi293* with DDM), emST-mCherry-rho (*Expi293* with DDM) and emST-tm2-rho (*Expi293* with DDM) was performed at EBML(Heidelberg) SPC facility and CFMP facility.

Purification samples of emST-his expressed in BL21(DE3) (Figure 3.13) showed two bands i.e. at 68 kDa and 48 kDa, which were also anti-his western positive (Figure 3.15 from purification section 3.1.1). MS analysis of these two bands confirmed that the protein as emST-his with a sequence coverage of 12.4-16.5 %. The graphical sequence representation below depicts the sequence identified by MS (Figure 3.15). The peptides of emST-his that were identified belonged to the cytoplasmic C-terminus loop and extra membrane loops.

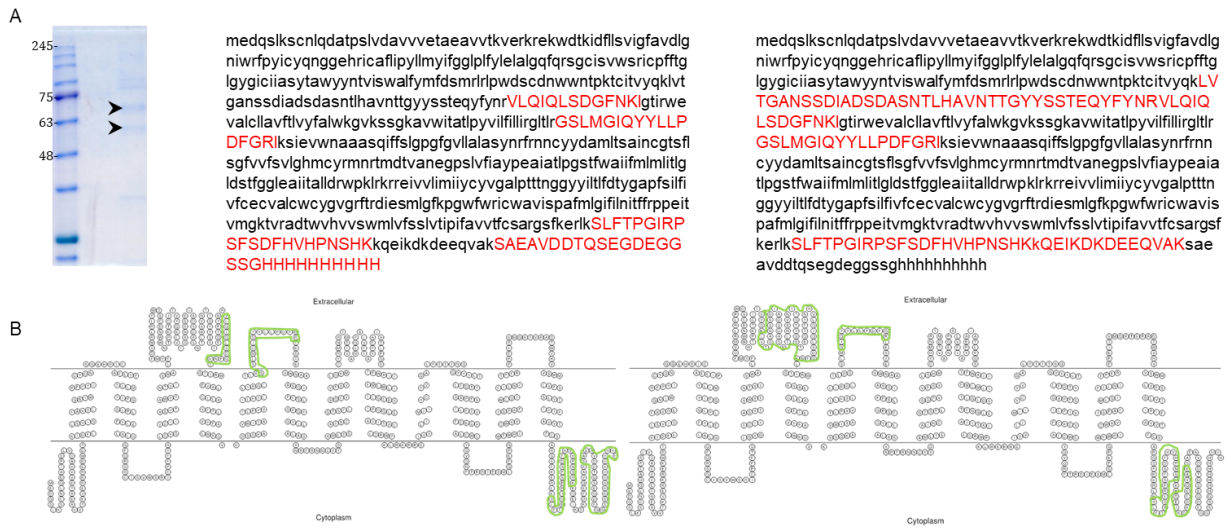


Figure 3.15 Peptides identification of emST by LC-MS/MS analysis

A: left: blue silver stained SDS-PAGE. Center: Identified peptides of 68 kDa emST band are shown in bold red. Right: Identified peptides of 50 kDa emST band are shown in bold red. B: left: predicted secondary structure and membrane organization of the emST. Identified peptides of 68 kDa emST band are shown in the green circle. Right: predicted secondary structure and membrane organization of the emST. Identified peptides of 50 kDa emST band are shown in the green circle. Figure generated using MEMSAT2 software.

3.1.4 CD spectroscopic analysis

CD spectra of emST-his expressed and purified from bacterial (BL21(DE3)) and CECF system are shown below (Figure 3.16). Deconvolution of CD spectrum of purified sample of BL21(DE3) derived emST-his showed that it was typical for random coiled protein with a low intense negative peak at around 200 nm (Figure 3.13).

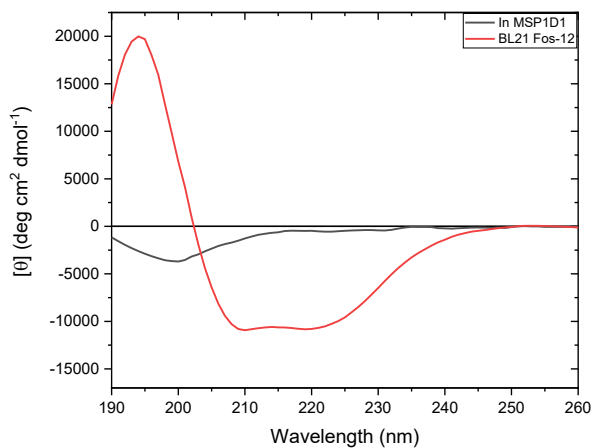


Figure 3.16 CD spectra of emST-his

Red line: Fos-12 purified emST-his in BL21(DE3). Black line: Far UV circular dichroism was recorded for emST-his in MSP1D1 from CECF. the CD spectra minima (208nm and 222nm)

Table 3.2 Secondary structure contents of BL21(DE3) derived emST-his.

Protein	Source	Helical (%)	β -sheet (%)	Other (%)	NRMSD
emST-his	Sequence based prediction	37.1 (aa)	10.8 (aa)	52.1 (a)	
	Structure based prediction	63	0	36	
	Fos-12 BL21	22.4	2.9	74.7	0.02148

3.2 Insect cell expression system

Insect cell expression of emST-rho and its variants was performed using Sf9 and High5 cells. In Sf9 cells only emST-rho was expressed via flashBAC ULTRA and in High5 cells emST-rho, emST-I273A-rho and emST-tm2-rho were expressed using the via TGE system (Section 2.4.2).

3.2.1 Expression of emST-rho in Sf9 cells

Preliminary insect cell expression analysis using *Sf9* cell for the construct pOET2_{emST-rho} was performed at the laboratories of Cube-Biotech, Monheim. At different time points, the pOET2-emSET construct at MOI 0.5 and 2.0 showed only a degradation band at a molecular weight of about 20 kDa (Figure 3.17).

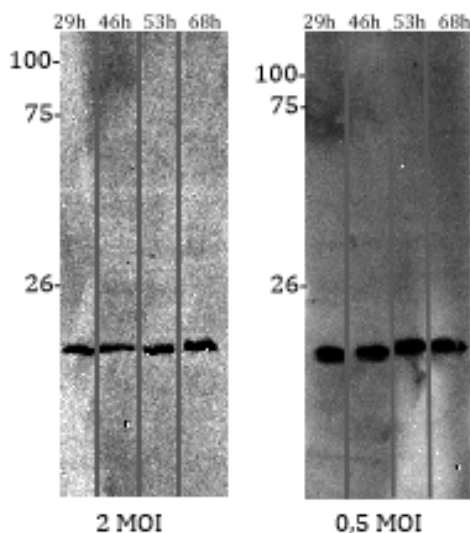


Figure 3.17 Anti-Rho western blot of Sf9 cell expressed emST

The expression of pOET2_{emST-rho} in Sf9 cells was analyzed at different time points after 29, 46, 53 and 68 hours. The insect cell culture was grown at 27 °C. Samples were prepared as described in section 2.4.2. A: 2 MOI. B: 0.5 MOI. At 29 hours to 68 hours, the same intense bands with molecular weight less than 26 kDa were observed.

3.2.2 Expression of emST in High 5 cells

Three different constructs (pOpiE2_{emST-rho}, pOpiE2_{emST-I273A-rho} and pOpiE2_{emST-tm2-rho}) were used for expression analysis in High5 cells using the virus free system (section 2.5.2). 40 mL and 48 h culture harvests of each construct (s.a.) were used for the purification of emST-rho and its variants using their FOS12 solubilized membranes. Anti-rho western blot analysis indicated no expression for pOpiE2_{emST-rho}, while the samples of the other construct showed western positive bands at a 68 kDa apparent molecular weight in the elution fractions (Figure 3.18). However, the signal was only detected by western blot which indicated both constructs have a poor expression in the High 5 cells.

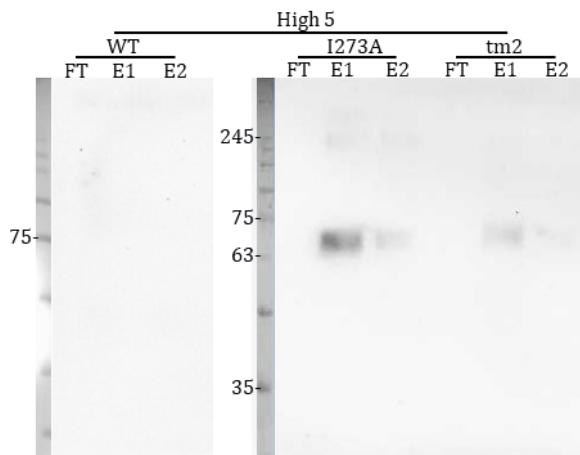


Figure 3.18 Anti-Rho western blot of High 5 cell expressed emST

The expression of pOpiE2_{emST-I273A-rho} and pOpiE2_{emST-tm2-rho} in High 5 cells were analyzed with rho-tag western blot. The insect cell culture was grown at 27 °C. Samples were prepared as described in section 2.5.2. FT: Flow through; E: Elution fraction; I273A: I273A mutation (isoleucine of native protein replaced with alanine); Y69A: Y69A mutation (tyrosine of native protein replaced with alanine). Both mutations showed a molecular weight of 68 kDa

3.3 Mammalian expression system

Both bacteria and insect cell expression systems were not able to produce a sufficient amount of protein for analytical experiments. Therefore, the emST was expressed with the mammalian expression system.

Five constructs: pTT5_{emST-rho}, pTT5_{emST-Y69A-rho}, pTT5_{emST-I273A-rho}, pTT5_{emST-tm2-rho} and pTT5_{emST-mCherry-rho} were expressed in mammalian cell lines. Two different mammalian cell lines were used for expression i.e *HEK293* and *Expi293*.

3.3.1 Expression analysis of emST

Expi293 and *HEK293* cell samples from the expression of emST-rho, emST-I273A-rho, and emST-tm2-rho were analyzed by anti-rho western to confirm expression Figure 3.19. This analysis confirmed the expression of all the three proteins in *Expi293* and

HEK293 cell lines with some variation in expression levels. Overall *Expi293* cell samples showed higher intensity western signal indicating higher expression levels. When there is a reasonably strong expression and membrane integration protein signal is expected in the samples containing unopened cells (SN, Figure 3.19) and in the samples containing membrane fraction (P1, Figure 3.19), which was the case throughout the samples. The samples from *Expi293* cells showed consistently anti-rho western signal also in the supernatant after 100 000 × g (SN1, Figure 3.19).

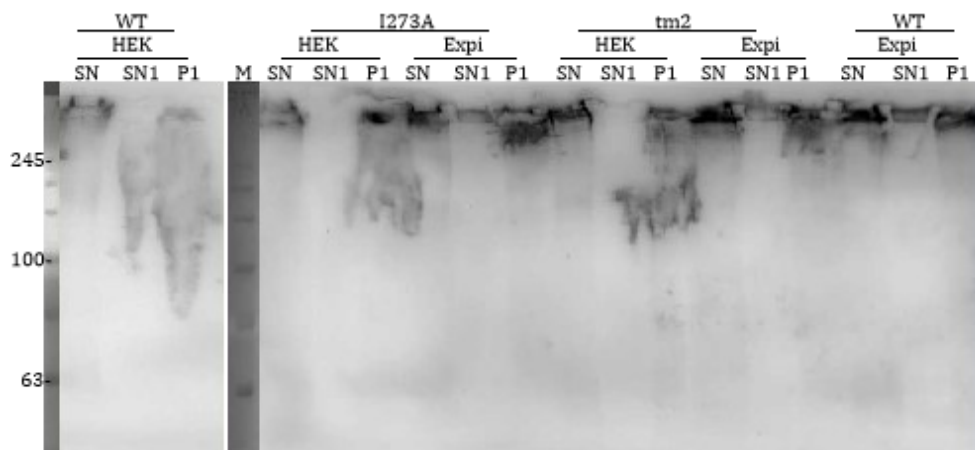


Figure 3.19 Mammalian expressions for different construct of emST

The samples were normalized to the weight of the used cell pellet. SN: the supernatant of 8 000 x g centrifugation; SN1: the supernatant of 100 000 x g centrifugation; P1: the pellet of 100 000 x g centrifugation. WT: wild type; Δ L: Residues 182-192 (EL2) deletion; I273A: I273A mutation (isoleucine of native protein replaced with alanine); Y69A: Y69A mutation (tyrosine of native protein replaced with alanine). HEK: *HEK293* cell. Expi: *Expi 293* cell.

Figure 3.20 shows the anti-rho western blot analysis of the Fos12 solubilized purification samples from *Expi293* cells and *HEK293* cells expressing emST-rho, emST-I273A-rho, and emST-tm2-rho. All the cells with all the three constructs displayed expression as the elution fractions (rho1D4 resin) showed anti-rho western positive bands corresponding to a monomeric emST and its variants at a 68.8 kDa apparent molecular weight. Oligomers or aggregate signals were observed at molecular weights of 199.5 kDa, above 254 kDa and in the pockets.

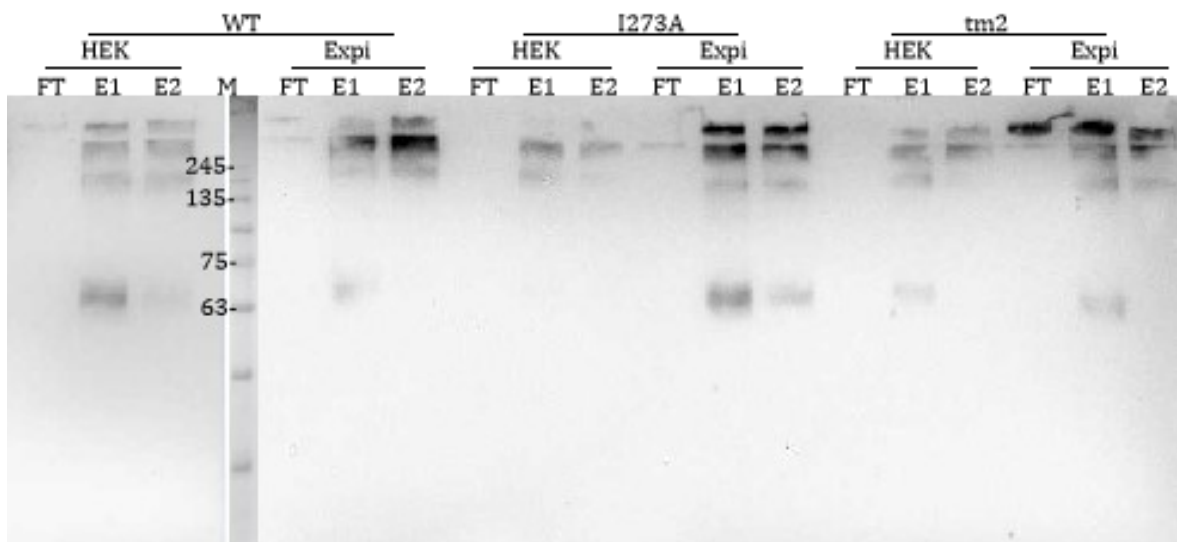


Figure 3.20 Anti-Rho western blot of mammalian cell expressed emST mutants

The expression of emST in mammalian cells was analyzed for different mutants and vectors. The mammalian cell culture was performed at 37 °C. Samples were prepared as described in section 2.4.3. FT: Flow-through; E: Elution fraction; WT: wild type; I273A I273A mutation (isoleucine of native protein replaced with alanine); The arrows indicate the molecular weights of emST at 68.8 kDa and 199.5 kDa.

3.3.2 Detergent screening for solubilization of emST

For membrane proteins after expression analysis and before purification determination of a protein stabilizing detergent is required. In such a screening procedure (Section 2.5.1) six different detergents were analyzed (Table 2.21). The membrane fraction of *Expi293* cells containing emST-rho was solubilized with different detergents overnight. In the case of Fos12 solubilization, 2 h was sufficient; Samples were centrifuged at $100,000 \times g$ to collect supernatant and pellet, which represent the solubilized protein fraction and the insolubilized protein fraction, respectively. These samples were analyzed by anti-rho western blot (Figure 3.21). The detergent depending variation in the extent of solubilization was analyzed by anti-rho western blot of the SN fractions (Figure 3.21). This detergent screening indicated that OG and NG were the least solubilizing detergents, Fos-12 and LDAO were reasonably better with 50 % solubilized protein in the supernatant compared to DM and DDM, where less than 50 % of the protein could be solubilized (Figure 3.21).

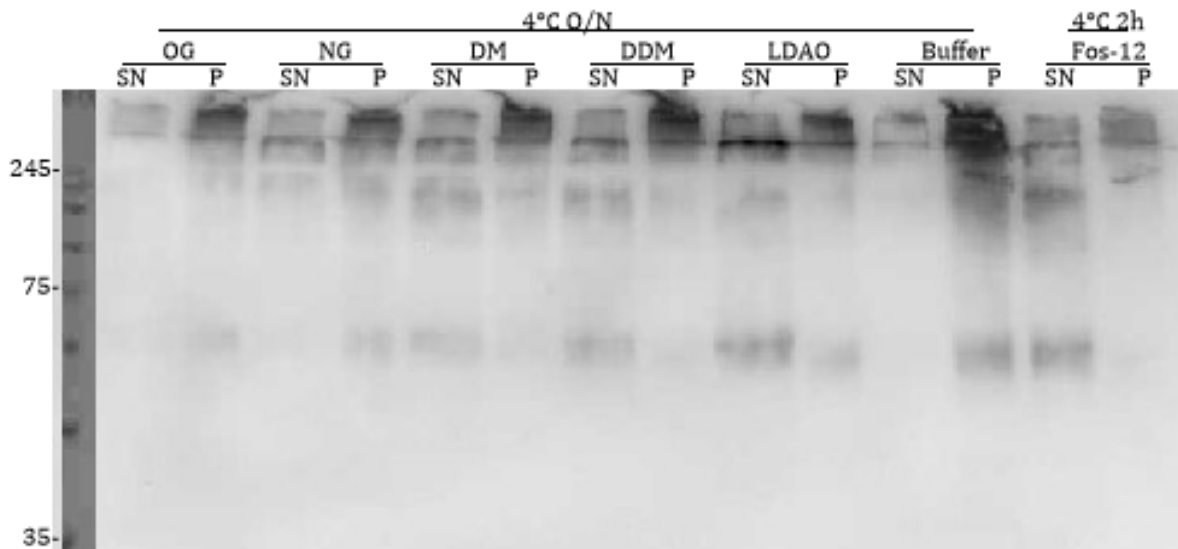


Figure 3.21 Detergent screening of mammalian expressed emST

The 6 different detergents were used in the solubilization buffer (2% OG, NG, DM, DDM, LDAO, and Fos-12). SN: soluble fraction; P: insoluble fraction.

Membrane fractions of *Expi293* cells with emST-rho, emST-Y69A-rho and emST-I273A-rho were solubilized overnight with 1 % (w/v) Fos12 and 7 % (w/v) DIBMA (section 2.5.1). Solubilized membrane samples were centrifuged and the supernatant was used for affinity purification and the total solubilized membrane fractions, Elution fractions were analyzed by anti-rho western blot (Figure 3.22). Anti-rho analysis indicated that the DIBMA at 7 % did not display efficient solubilization compared to Fos12 at 1 %. Another observation is that the Fos12 solubilized samples showed a monomeric protein band at a 68.8 kDa apparent molecular weight while that from DIBMA solubilized samples showed only high molecular weight bands (Figure 3.22).

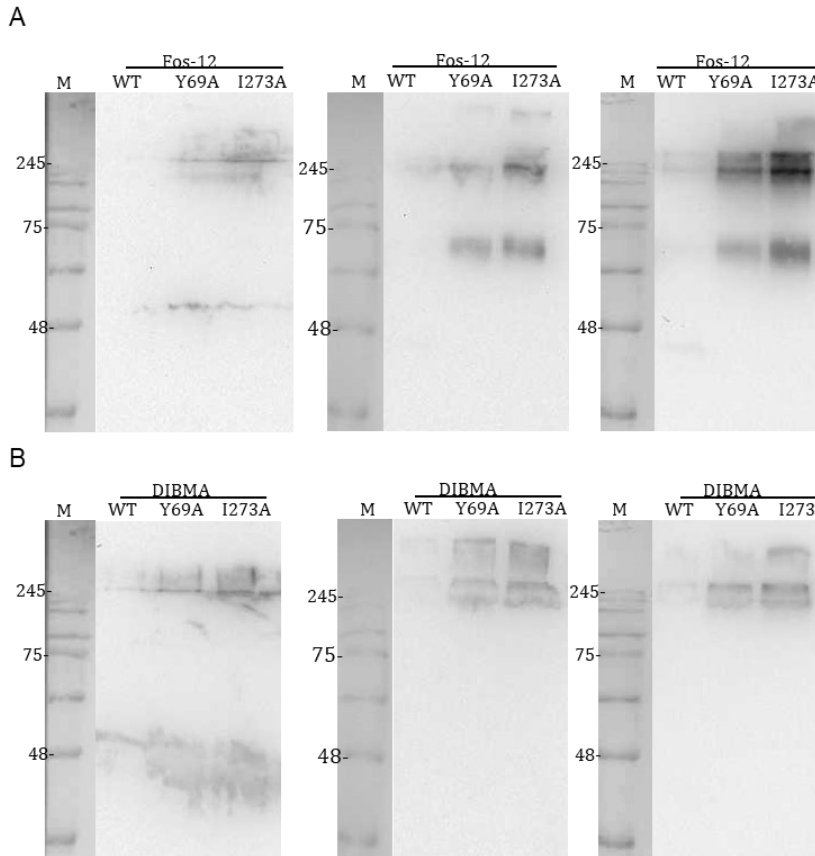


Figure 3.22 Fos-12 and DIBMA

solubilization of emST

A: Western blot. Fos-12 detergents was used with 1% concentration (w/v). B: Western blot. DIBMA used with 7% concentration (w/v). Aliquots of membrane fractions were solubilized and analyzed via SDS-PAGE and FT: Flow though; W: Wash fraction; E: Elution fraction; Left: Anti-rho blot of Total solubilized emST. Center: Anti-Rho blot of first elution fraction of emST. Right: Anti-rho blot of second elution fraction of emST.

3.3.3 Purification of emST-rho and its variants

Three constructs: pTT5_{emST-rho}, pTT5_{emST-tm2-rho} and pTT5_{emST-mCherry-rho} were expressed and purified in *Expi293* cells.

3.3.3.1 Purification of DDM solubilized emST-rho

Membrane prepared from 10 g of *Expi293* cells expressing emST-rho was solubilized using DDM (section 2.5.1) and subjected to affinity purification (section 2.5.2.2). Samples from the purification were analyzed by TCE fluorescence and anti-rho western blot analysis (Figure 3.23). Rho-1D4 purification sample analysis indicated that the elution fractions contained the protein (anti-rho positive Figure 3.23A) and were sufficiently pure (TCE fluorescence image, Figure 3.23A).

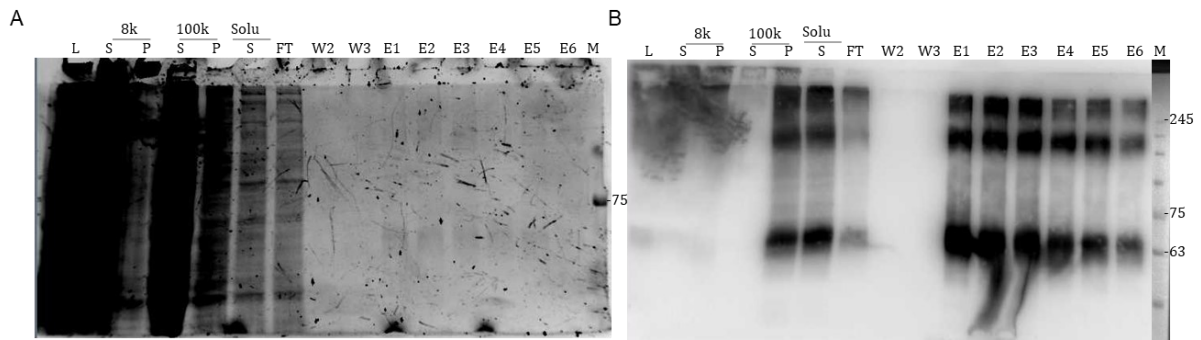


Figure 3.23 Rho-tag Purification of *Expi 293* expressed emST

A: TCE stained SDS-PAGE; B: anti-rho western blot. L: total cell lysate of *Expi 293* expressed emST. 8k: 8 000 g centrifugation; 100k: 100 000 g centrifugation; S: the supernatant; P: the pellet; Solu S: the supernatant sample after DDM solubilized for 4 hours; FT: Flow through from Rho resin; W2 and W3: wash fractions; E1-6: Elution with 400 μ M of rho1D4 peptide.

SEC analysis of the emST-rho sample after affinity purification showed a major peak at a \approx 53 mL elution volume (superdex 200 pg) a small peak at 62 mL corresponding to the estimated molecular weight of 632 kDa and 301 kDa, respectively. Analysis of SEC elution fractions by SDS-PAGE showed a monomeric protein band at a 68 kDa apparent molecular weight and two high molecular weight western positive bands at 162.8 kDa and slightly above 245 kDa. The total yield of the DDM solubilized and purified emST-rho protein from fraction 48-68 was calculated to be 6.2 μ g / g cell pellet. TCE fluorescence image of the SEC elution fractions showed a dual band, between 91 kDa and 97 kDa, which was western negative (Figure 3.24).

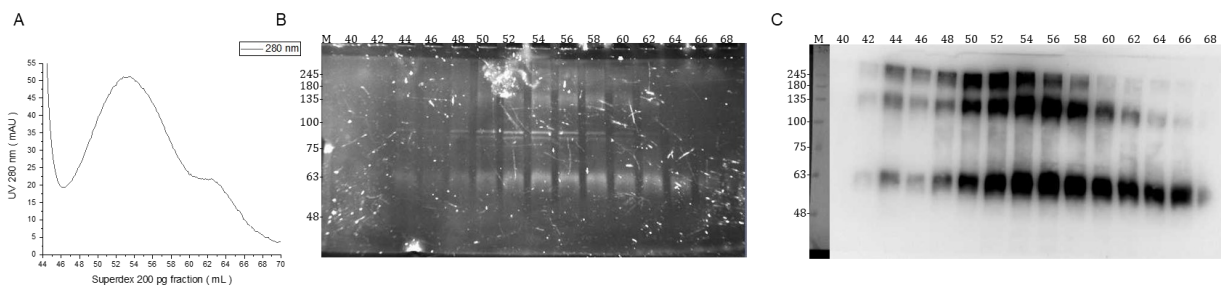


Figure 3.24 SEC Purification of *Expi 293* expressed emST

A: SEC profile of pTT5emST-rho. B: TCE stained SDS-PAGE; C: anti-rho western blot;

3.3.3.2 Purification of DIBMA solubilized emST-rho

DIBMA solubilized membrane from 10 g of *Expi293* cells expressing emST-rho (section 2.4.3) was used for affinity purification (Section 2.5.2.2). The insoluble membrane fraction after 100 000 × g centrifugation still contained emST-rho protein (Figure 3.25). Samples were analyzed by TCE fluorescence and anti-rho western blot analysis (Figure 3.25). Analysis of sample after affinity purification indicated that the protein could be seen in the elution fractions (anti-rho positive Figure 3.25) and the protein was already pure (TCE fluorescence image, Figure 3.25).

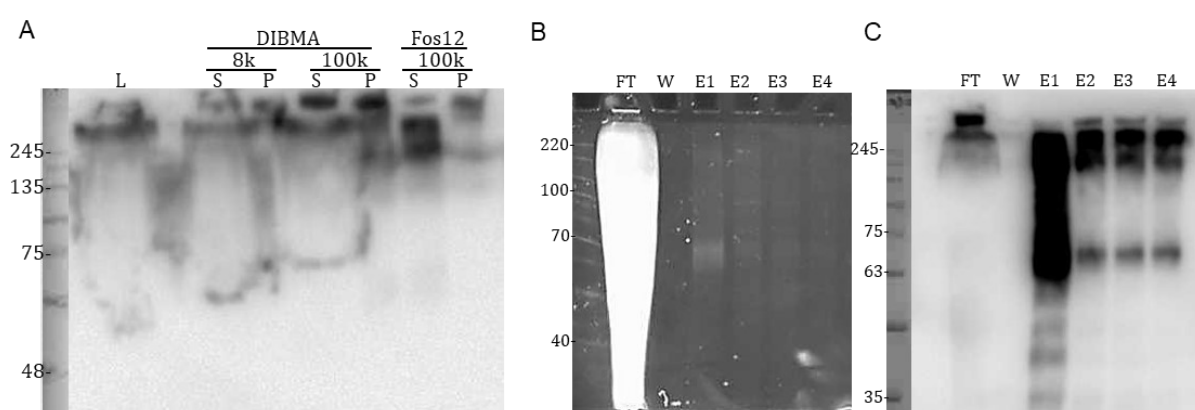


Figure 3.25 DIBMA Purification of *Expi 293* expressed wild type emST

A: anti-rho western blot of cell lysate sample; B: TCE stained SDS-PAGE; C: anti-rho western blot. FT: Flow through from Rho resin; W2 and W3: wash fractions; E1-4: Elution with 400 μ M of rho-1D4 peptide.

SEC analysis of the DIBMA solubilized emST-rho sample after affinity purification resulted in a peak at a \approx 50 mL elution volume corresponding to an estimated molecular weight of 791 kDa. On SDS-PAGE SEC elution fractions showed a monomeric protein band at a 64.8 kDa apparent molecular weight (Figure 3.26). Also two more high molecular weight western positive bands could be detected at 162.8 kDa and at slightly above 245 kDa. The total yield of the DIBMA solubilized and purified emST-rho protein from fraction 47-65 was calculated to be 3 μ g / g cell pellet. TCE fluorescence image of the SEC elution fractions showed a dual band, between 81 kDa and 97 kDa, which was western negative.

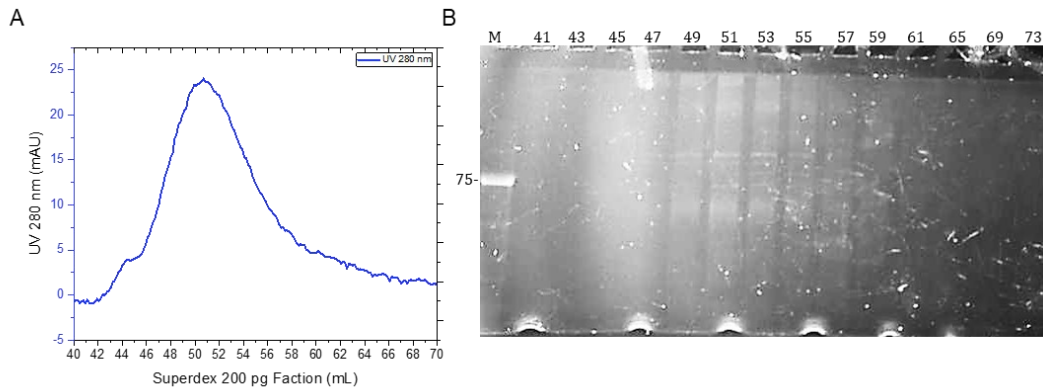


Figure 3.26 DIBMA SEC Purification of *Expi 293* expressed wild type emST

A: SEC profile of pTT5emST-rho. B: TCE stained SDS-PAGE; with SEC buffer: 20 mM HEPES pH 7, 150 mM NaCl, 0.5 mM TCEP, in Superdex 200pg column

3.3.3.3 Purification of Fos12 solubilized emST-rho

Insolubilized membrane after DIBMA solubilization (Figure 3.25) was solubilized using Fos12 (Section 2.5.1) and used for affinity purification (Section 2.5.2.2). Purification samples were analyzed by TCE fluorescence and anti-rho western blot (Figure 3.27). Analysis of purification sample indicated that the elution fractions contained the protein (anti-rho positive Figure 3.27A) and the protein was pure (TCE fluorescence image, Figure 3.27).

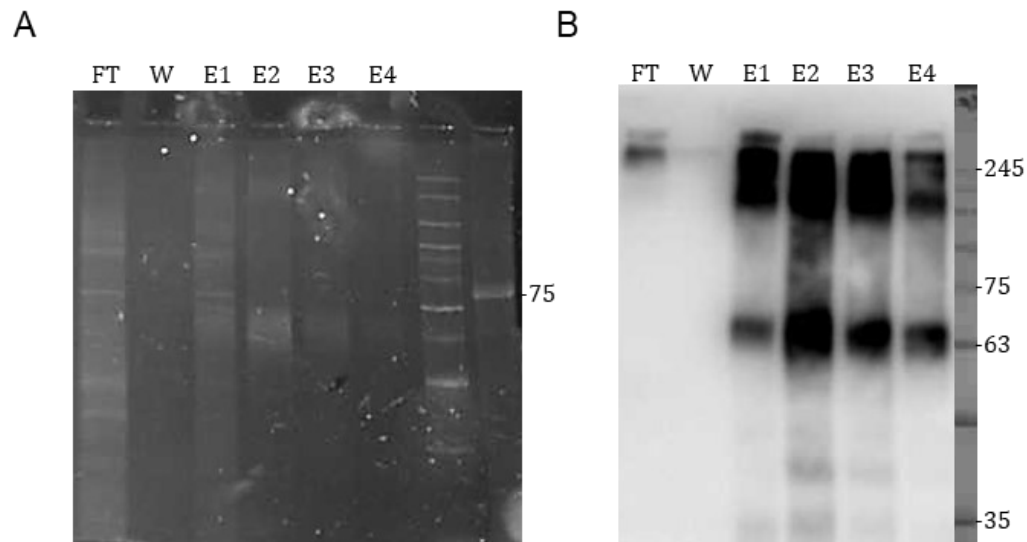


Figure 3.27 Fos12 Purification of *Expi 293* expressed wild type emST

A: TCE stained SDS-PAGE; B: anti-rho western blot. L: total cell lysate of *Expi 293* expressed emST. 8k: 8 000 g centrifugation; 100k: 100 000 g centrifugation; FT: flow through from Rho resin; W2 and W3: wash fractions; E1-4: Elution with 400 μ M of rho-1D4 peptide.

Subsequent SEC analysis resulted in a peak at a ≈ 51 mL elution volume with a shoulder at 55 mL corresponding to an estimated molecular weight of 760 kDa and 532 kDa, respectively. SEC elution fractions showed a monomeric protein band at a 64.8 kDa apparent molecular weight with two more high molecular weight western positive bands at 162.8 kDa and the other at slightly above 245 kDa. The total yield of the Fos12 solubilized and purified emST-rho protein from fraction 48-68 was calculated to be 5.2 μg / g cell pellet. SEC elution fractions on denaturing-PAGE indicated separable monomeric and higher oligomeric forms of emST-rho (Figure 3.28).

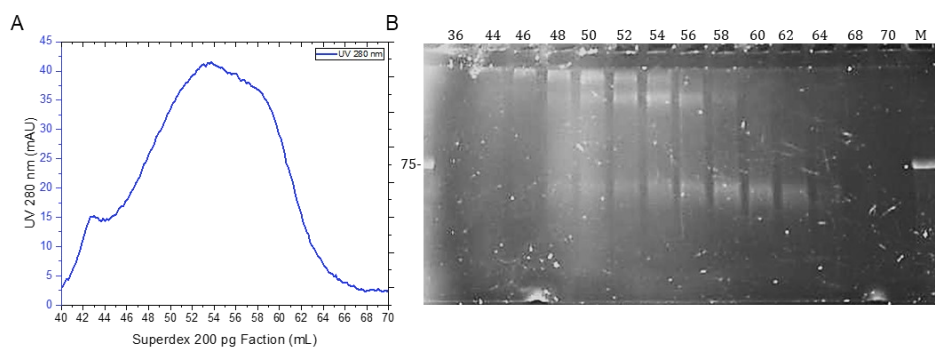


Figure 3.28 Fos12 SEC Purification of *Expi 293* expressed wild type emST

A: SEC profile of pTT5_{emST-rho}. B: TCE stained SDS-PAGE; Superdex 200 pg column with SEC buffer: 0.1% (W/V) Fos12, 150 mM NaCl, 0.5 mM TCEP, 5% Glycerol, 20 mM HEPES pH 7.5.

3.3.3.4 Purification of DDM solubilized emST-tm2-rho

DDM solubilized membrane prepared from 10 g *Expi293* cells expressing with emST-tm2-rho (section 2.4.3) was isolated by affinity purification (Section 2.5.2.2) and subsequently subjected to SEC. Purification samples contained the protein along with some impurities (anti-rho positive and TCE fluorescence image Figure 3.29).

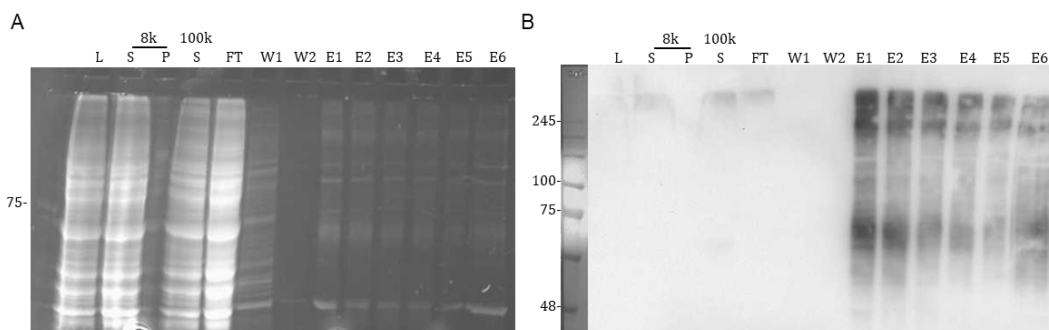


Figure 3.29 DDM Purification of *Expi 293* expressed emST-tm2 emST

A: left: TCE stained SDS-PAGE; B: anti-rho western blot. L: total cell lysate of *Expi 293* expressed emST. 8k: 8 000 g centrifugation; 100k: 100 000 g centrifugation; FT: Flow through from Rho resin; W2 and W3: wash fractions; E1-6: Elution with 400 μM of rho-1D4 peptide.

SEC profiles showed a peak at a ≈ 53 mL elution volume of with a small shoulder peak at 59 mL corresponding to estimated molecular weights of 632 kDa and 397 kDa, respectively. SEC elution fractions showed a monomeric protein band at a 64.8 kDa apparent molecular weight and two more high molecular weight western positive bands at 162.8 kDa and at slightly above 245 kDa. The total yield of emST-tm2-rho protein from fraction 48-66 was calculated to be 8.7 μg / g cell pellet. TCE fluorescence image of the SEC elution fractions showed a dual band similar to other purifications(s,a.) (Figure 3.23, Figure 3.25 and Figure 3.27), between 81.9kDa and 97.7 kDa, which was western negative and could be separated on SEC (Figure 3.30). This bands had not been observed in other purifications (Table 3.3).

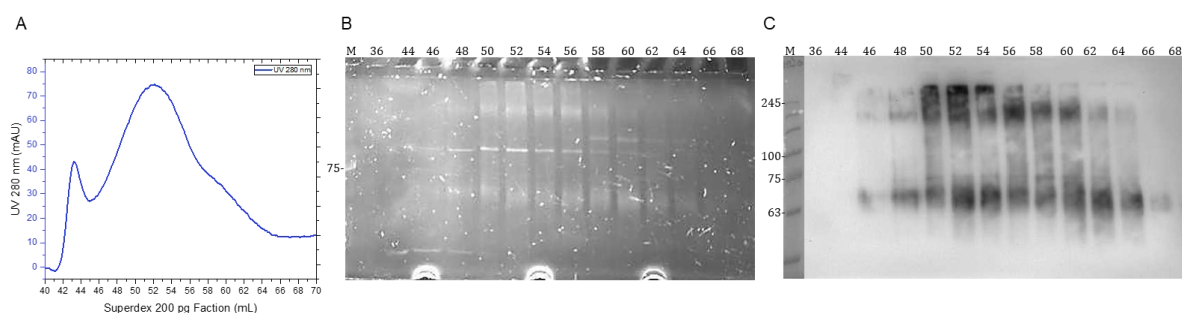


Figure 3.30 DDM SEC Purification of *Expi 293* expressed emST-tm2 emST

A: SEC profile of pTT5_{emST-rho}. B: TCE stained SDS-PAGE; C: anti-rho western blot.

3.3.3.5 Purification of DDM solubilized emST-mCherry-rho

Membrane from 10 g of *Expi293* cells expressed with emST-mCherry-rho was solubilized using DDM (section 2.5.1). The solubilized membrane was used for affinity purification (Section 2.5.2.2) and later purified by SEC. Samples from affinity purification contained emST-mCherry-rho (anti-rho positive and TCE fluorescence image Figure 3.31A). SEC analysis showed a peak at a ≈ 52 mL elution volume and a small peak at 63 mL corresponding to estimated molecular weights of 701 kDa and 267 kDa, respectively (Figure 3.31). SEC elution fractions showed a monomeric protein band at a 91 kDa apparent molecular weight along with two more high molecular weight western positive bands at 184.3 kDa and at slightly above 245 kDa (Figure 3.31). The total yield of the emST-mCherry-rho protein from fraction 53-69 was calculated to be 5.8 μg / g cell pellet. SEC elution fractions showed two western negative bands at 76

kDa and 99 kDa (Figure 3.32).

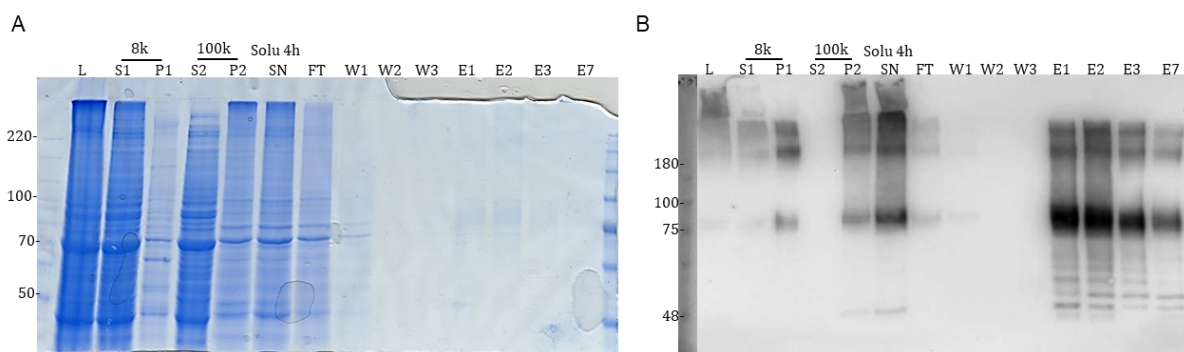


Figure 3.31 Rho-tag Purification of *Expi 293* expressed emST-mCherry

A: the blue-silver stain; B: anti-rho western blot. 8k: 8 000 g centrifugation; 100k: 100 000 g centrifugation; S: the supernatant; P: the pellet; Solu 4h SN: the supernatant sample after DDM solubilized for 4 hours; FT: Flow through from Rho resin; W1, W2 and W3: wash fractions; E1-7: Elution with 400 μ M of rho-1D4 peptide.

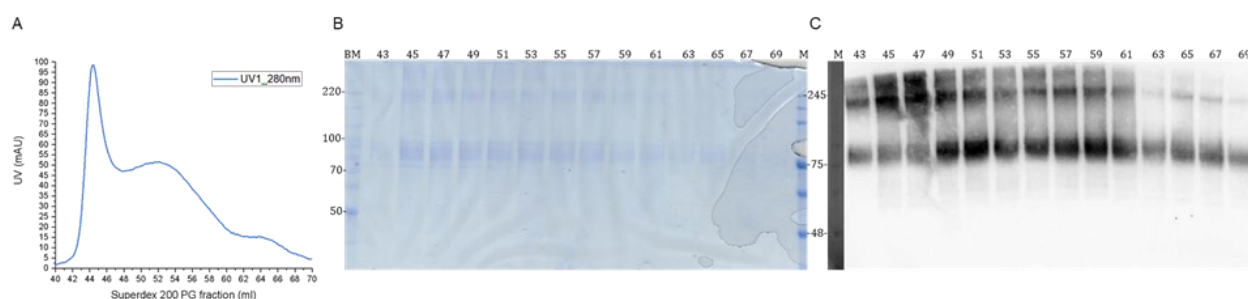


Figure 3.32 SEC Purification of *Expi 293* expressed emST-mCherry

A: SEC profile of emST-mCherry. B: the blue-silver stained SDS-PAGE; C: anti-rho western blot.

Table 3.3 The molecular weight of emST variants and HSPs

	HSP70-1B	emST variants	HSP90 β
emST-rho (DDM)	91 (Figure 3.24)	68	97
emST-rho (DIBMA)	81 (Figure 3.26)	64.8	97
emST-tm2-rho (DDM)	81.9 (Figure 3.30)	64.8 (MS confirmed)	97.7 (MS confirmed)
emST-mCherry-rho (DDM)	97 (Figure 3.32)	91	99-112

Among different purifications in the SEC profile overlay only the sample purified with DIBMA showed a peak with no shoulders while the other samples purified with Fos12 and DDM showed shoulders (Figure 3.33).

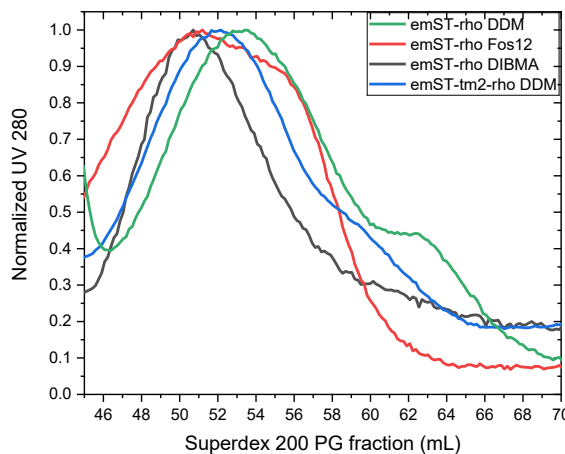


Figure 3.33 SEC profile of Superdex 200pg

An overlay of elution fraction from superdex 200 pg, include emST-rho purified with DDM, fos-12 and DIBMA, emST-tm2-rho purified with DDM.

3.3.4 Analysis of emST glycosylation

Three variants of *Expi293* expressed and purified emST protein i.e. emST-rho, emST-tm2-rho and emST-mCherry-rho were treated with EndoH and PNGaseF to confirm the presence of N-Glycosylation. Samples treated with EndoH did not show any difference in the band pattern on SDS-PAGE and anti-rho western blot (Figure 3.34A), while the samples treated with PNGaseF showed a difference in the molecular weight ranging between 2.9 - 8.2 kDa compared to untreated sample considering only monomeric protein bands (Figure 3.34B) Table 3.4. Interestingly the differences in the molecular weights of the three variants of emST after PNGaseF treatment are different (Table 3.4).

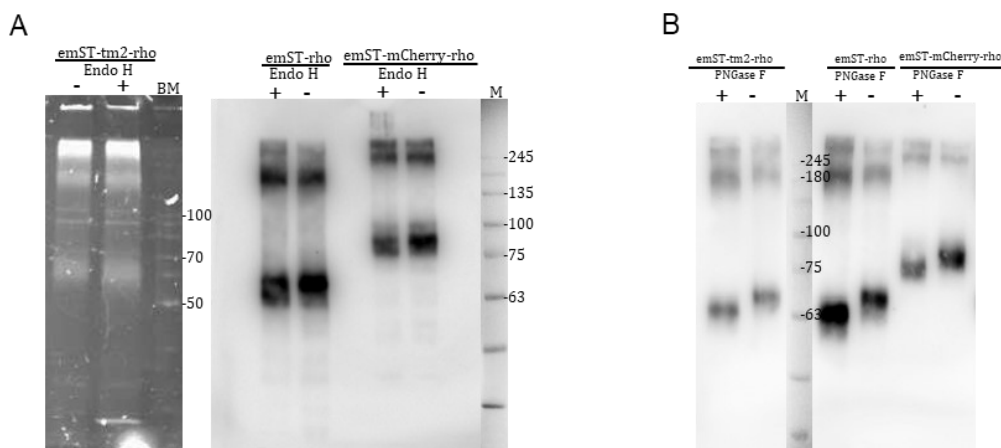


Figure 3.34 SDS-PAGE analysis of emST digested with endo H or PNGase F

A: TCE stain SDS-PAGE and anti-rho western blot of DDM purified emST-tm2-rho, emST-rho and emST-mCherry-rho digested with endo H. B: anti-rho western blot of emST-tm2-rho, emST-rho and emST-mCherry-rho digested with PNGase F. All the protein samples were purified with DDM. Samples were analyzed on a 10 % polyacrylamide gel.

Table 3.4 Molecular weights of the three variants of emST after PNGaseF treatment

PNGase F	Untreated samples (lane number)	Treated sample (lane number)	Difference
emST-rho	68.1 kDa (lane 4)	64.6 kDa (lane3)	3.5 kDa
emST-tm2-rho	68.4 kDa (lane 2)	65.5 kDa (lane 1)	2.9 kDa
emST-mCherry-rho	85 kDa (lane 6)	76.6 kDa (lane 5)	8.4 kDa

3.3.5 Mass spectrometric analysis of emST

The 68 kDa band that was observed in the purified sample of emST-rho expressed in *Expi293* cells (Figure 3.35, Figure 3.23) allowed a sequence coverage of 26 % of emST-rho by MS-analysis (Figure 3.35).



Figure 3.35 Peptides identified of emST by LC-MS/MS

Left: blue silver stained SDS-PAGE. Right: LC-MS/MS analysis. Bold red: identified peptides; Underlined: transmembrane region.

When emST-tm2-rho expressed in *Expi293* cells was purified using respective DDM solubilized membrane two anti-rho negative bands at molecular weight 81.9 kDa and 97.7 kDa were observed (Figure 3.36 and Figure 3.29). MS analysis of these two bands (at 70 kDa and 90 kDa) confirmed that they belong to HSP70-1B (Uniprot: P0DMV9) and HSP90 β (Uniprot: P08238) with a sequence coverage of 35 % and 65 %, respectively (Figure 3.36).



Figure 3.36 Peptides identified of HSP by LC-MS/MS

Left: TCE stained SDS-PAGE. Red arrow: HSP 90. Green arrow: HSP 70; Center: Identified peptides of HSP 90 band are shown in bold red. Right: Identified peptides of HSP 70 band are shown in bold red.

Samples of emST-rho and its variant (emST-mCherry-rho) with and without PNGaseF treatment were analyzed by MS. The emST-rho protein was identified by at least 10 different peptides depending on the sample (2µg), for both samples - with and without PNGaseF treatment. The emST-mCherry-Rho was also identified, but with lower coverage because of the 6 times lower concentration compared to the emST-rho. As it is extremely difficult to detect glycosylated peptides by MS, treatment with PNGaseF was used to hydrolyze the glycosidic bond between asparagine and the first glycan moiety converting asparagine to aspartic acid, which leads to an addition of +0.984 Da. From the PNGaseF treated emST-rho sample the peptide L₁₈₀VT GANSSDIADSDASNTLHAVNTTGYYSSTEQYFYN-R₂₁₇ containing two glycosylation sites following the consensus N-x-S/T-x (N₁₈₅-S-S-D₁₈₈ and N₂₀₂-T-T-G₂₀₅) was detected with high signal intensity. Manual inspection of the fragment spectra revealed that both asparagines, N185 and N202 were converted to aspartic acid, which means that both sides were N-glycosylated (Figure 3.37A). In addition, the unmodified peptide was also identified, but with less than 10% of the signal intensity of the deamidated counterpart. It is important to note that no peptide with a single deamidation was detected, which means that either both the sites were glycosylated or none of them were glycosylated. In samples of emST-rho without PNGase F treatment no aspartic acid was detected in small amounts. Interestingly for the sample of emST-mCherry-rho, treated with PNGaseF, the double deamidated peptide was detected (Figure 3.37B). The signal intensity was, however, 20 times less than the emST-rho sample treated with PNGaseF.

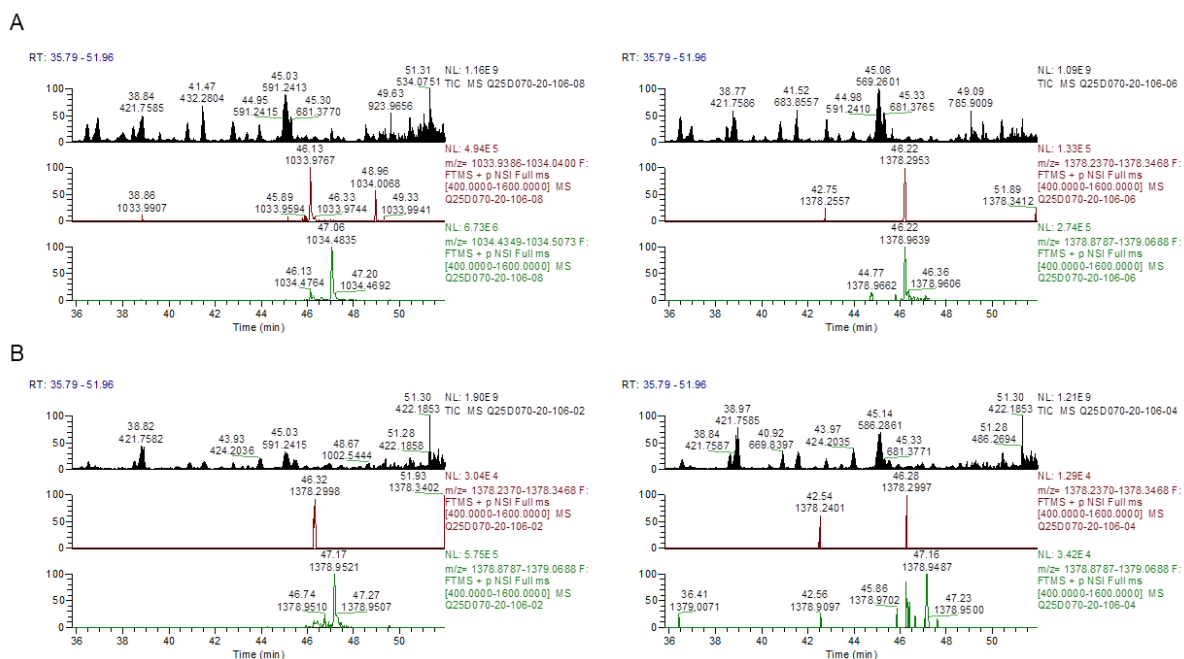


Figure 3.37 Sequence and extracted ion chromatogram (XIC) diagram

A: Left: XIC obtained by LC-MS/MS for PNGase F treated emST-rho sample. Right: XIC obtained by LC-MS/MS for emST-rho sample Unmodified XIC diagram at $m/z = 1033.98$ and from time = 46.13 min. Deamidated XIC diagram at $m/z = 1034.48$ and from time = 47.06 min;
 B: Left: XIC obtained by LC-MS/MS for PNGase F treated emST-mCherry-rho sample. Right: XIC obtained by LC-MS/MS for emST-mCherry-rho sample Unmodified XIC diagram at $m/z = 1378.30$ and from time = 46.32 min. Deamidated XIC diagram at $m/z = 1078.95$ and from time = 47.17 min.

3.3.6 CD spectroscopic analysis

Rho tagged emST (emST-rho) expressed in *Exp1293* cells was purified using two different detergents i.e Fos12 (Figure 3.27) and DDM (Figure 3.23). CD spectrometric analysis of both the samples resulted in spectra that showed variation only at wavelengths below ≈ 215 nm (Figure 3.38). The emST-rho purified using Fos12 was also analyzed by CD spectroscopy in the presence of CHS (Cholesteryl-hemisuccinate Tris Salt) and CIT (Citalopram hydrobromide). The CD spectrum of the sample in the presence of CIT showed no significant difference from the spectrum of the sample without CIT (Figure 3.38). Whereas the CD spectrum of emST-rho purified using Fos12 in the presence of CHS was significantly different from others by having a higher helical content (Figure 3.38, Table 3.5), but still was lower than the value expected from the predictions (Table 3.5)

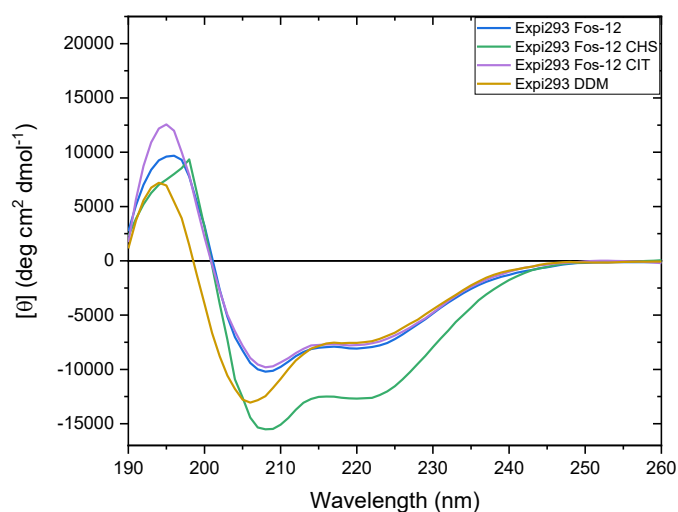


Figure 3.38 CD spectra of emST-rho

The fos-12 and ddm purified emST from *Expi293* cells

Table 3.5 Secondary structure contents of *Expi293* derived emST-rho

Sample	Detergent used	Helical (%)	β -sheet (%)	Other (%)	NRMSD
emST-rho	Sequence based	--	37.1	10.8	52.1
predicted value	Structure based	--	61.0	1.0	36.0
emST-rho	Fos-12	20.0	21.4	58.6	0.01158
emST-rho + CHS	Fos-12	29.4	10.4	60.2	0.02053
emST-rho + CIT	Fos-12	20.1	19.1	60.8	0.01394
emST-rho	DDM	21.9	19.1	59.0	0.01742

Samples of two other variants of emST-rho i.e. emST-tm2-rho and emST-mCherry-rho were also analyzed by CD spectroscopy. Samples of emST-tm2-rho were co-purified with HSP70-1B and HSP90 β (Figure 3.29). SEC fraction containing emST-tm2-rho-HSP70-1B and emST-tm2-rho-HSP90 β were analyzed separately by CD spectroscopy (Figure 3.39A). As these sample contained emST-tm2-rho and either of the HSPs, sample concentrations and the MRW were calculated considering sequences of both the proteins of respective complex i.e. emST-tm2-rho + HSP70 (644aa + 641aa =

1285aa) and emST-tm2-rho + HSP90 β (644aa + 724aa = 1368aa). These two samples in their CD spectra showed significant differences at a wavelength lower than 215 nm (Figure 3.39A). For both the emST-tm2-rho samples the experimentally determined secondary structural contents are in good agreement with sequence based predicted values except for emST-tm2-rho + HSP70-1B which were slightly low (Table 3.6).

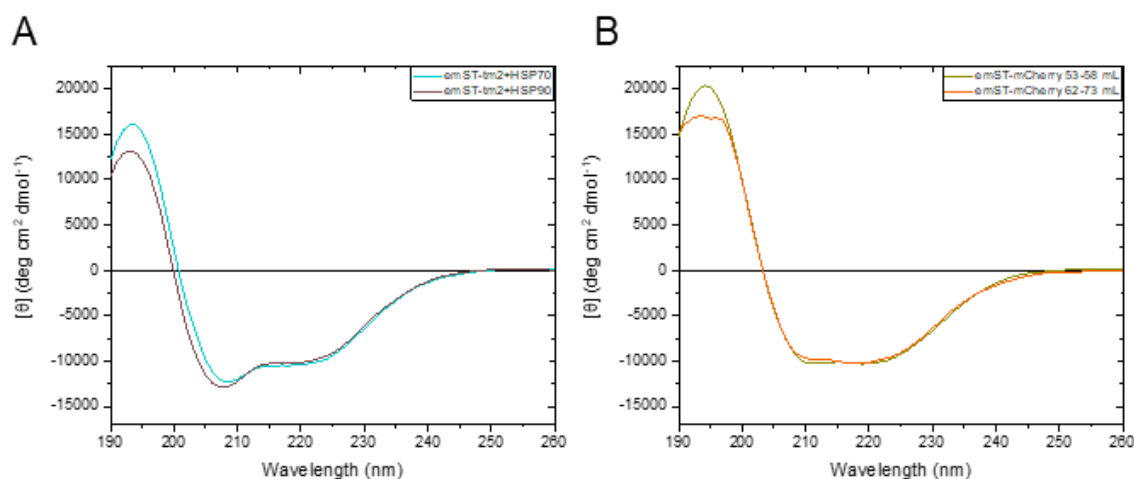


Figure 3.39 CD spectra of emST-tm2-rho and emST-mCherry-rho

Far UV circular dichroism was recorded for DDM purified A: emST-tm2-rho and B: emST-mCherry-rho in *Expi293*.

Also, emST-mCherry-rho was co-purified with HSP70-1B and HSP90 β (Figure 3.31). SEC fractions containing emST-mCherry-rho + HSP90 β were analyzed by CD spectroscopy, where samples from fractions 53-58 and 62-73 were analyzed separately (Figure 3.39B). The CD spectra of these two samples (Figure 3.39B) showed helical content similar to the sequence-based predictions (Table 3.6)

Table 3.6 Secondary structure contents of *Expi293* derived emST-tm2-rho

Samples		Helical (%)	β -sheet (%)	Other (%)	NRMSD
emST-tm2-rho + HSP90 (prediction)	Sequence based	26.6	11.6	61.8	
	Structure based	46.1	8.4	43.3	
emST-tm2-rho + HSP90 (SEC: 64-68 mL)		26.2	10.8	63.0	0.01151
emST-tm2-rho + HSP70 (prediction)	Sequence based	29.7	13.9	56.4	
	Structure based	50.9	8.03	38.3	
emST-tm2-rho + HSP70 (SEC: 52-56 mL)		26.6	10.8	62.6	0.01203
emST-mCherry-rho + HSP90 (prediction)	Sequence based	22.2	18.9	58.9	
	Structure based	41.0	14.0	44.0	
emST-mCherry-rho + HSP90 (SEC: 53-58 mL) (SEC: 62-73 mL)		23.9	13.9	62.2	0.01233
		21.3	25.2	53.5	0.00141

3.3.7 Subcellular localization of emST

The subcellular localization of emST was investigated by protein confocal microscopy and subcellular fractionation.

3.3.7.1 Immunofluorescence

Imaging cells immuno-stained specifically for ER and ERGIC resulted in the co-localization signal for ER specific marker and emST-mCherry-rho (Figure 3.40). the colocalization signal for the ERGIC specific marker and emST-mCherry-rho is very weak.

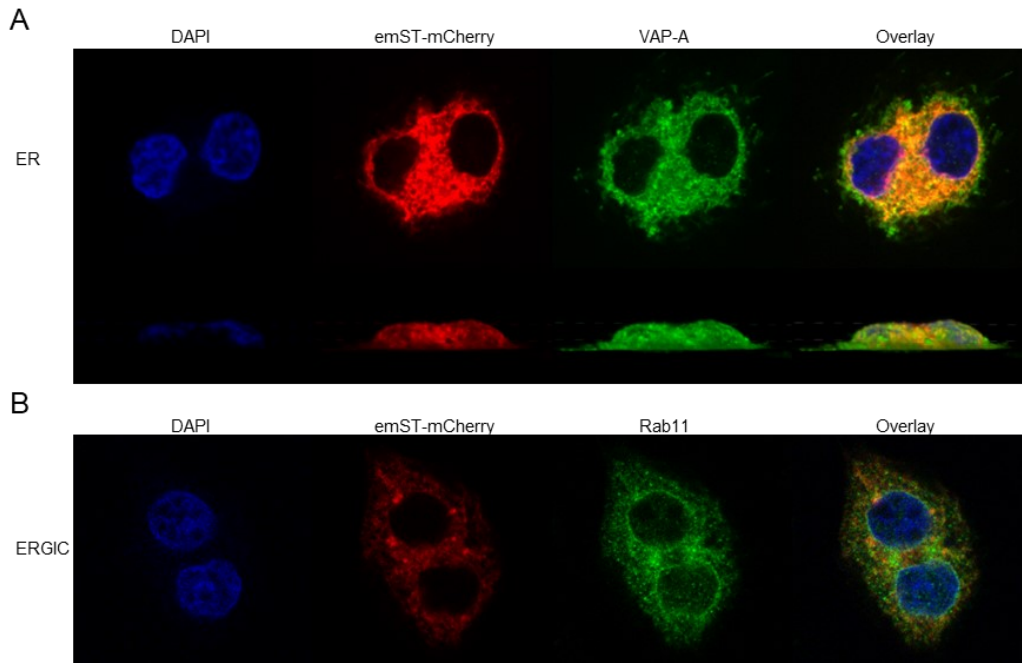


Figure 3.40 Co-localization of VAP-A, ERGIC-53 and emST-mCherry in transfected *Expi293* cells.

emST-mCherry was transiently transfected into Expi293 cells. Confocal laser scanning microscopy was used to investigate the co-localization pattern, as defined in Materials and Methods (Section 2.4.3). A: top: X-Y cross-sections of double staining of DAPI and VAP-P of emST-mCherry transfected into Expi293 cells. Blow: Y-Z cross-sections of double staining of DAPI and VAP-P of emST-mCherry transfected into Expi293 cells. B: X-Y cross-sections of double staining of DAPI and ERGIC-53 of emST-mCherry transfected into Expi293 cells

No colocalization signal could be observed while imaging cells immuno-stained specifically for cisGolgi (Figure 3.41 A), early endosome (EE, Figure 3.41 B), late endosome (LE, Figure 3.41 C), recycle endosome (RE, Figure 3.41 D) and lysosome (Figure 3.41 E).

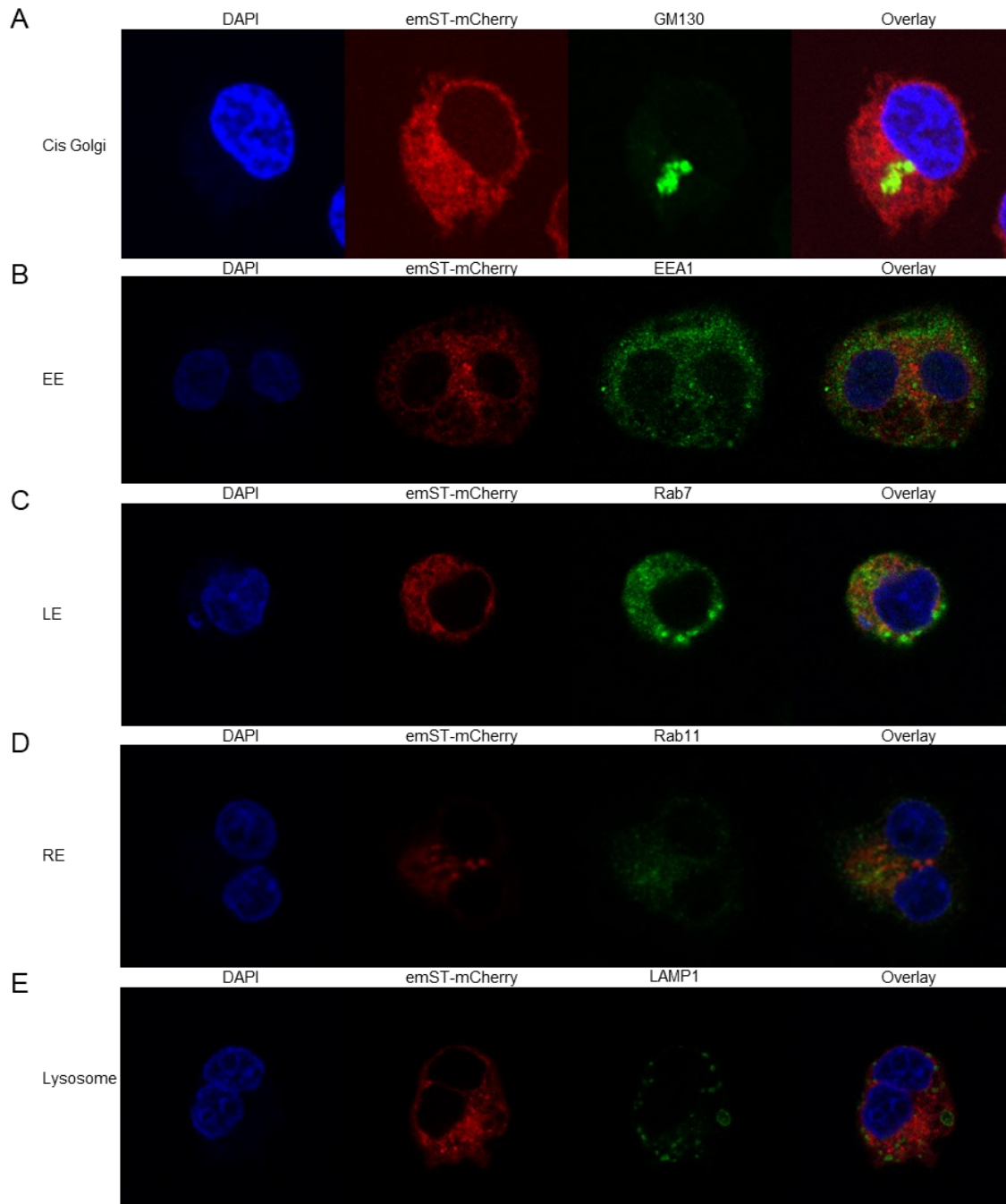


Figure 3.41 Co-localization of GM130, EEA1 Rab7 Rab11 LAMP1, and emST-mCherry in transfected *Expi293* cells.

A: double staining of DAPI and GM130 of emST-mCherry transfected into Expi293 cells.
 B: double staining of DAPI and EER1 of emST-mCherry transfected into Expi293 cells.
 C: double staining of DAPI and Rab7 of emST-mCherry transfected into Expi293 cells.
 D: double staining of DAPI and Rab11 of emST-mCherry transfected into Expi293 cells.
 E: double staining of DAPI and LAMP1 of emST-mCherry transfected into Expi293 cells.

3.3.7.2 Subcellular fractionation

Three different subcellular fractions from *Expi293* cells expressed with emST-rho and

emST-mCherry-rho, i.e. ER, PAM and PM fractions, were isolated and analyzed (Section 2.8.2). Samples prepared from the sedimented microsome pellet was loaded onto a sucrose gradient (Figure 3.42A) and subjected to the respectively required centrifugal force (Section 2.8.2) to isolate and collect PAM and PM fractions (Figure 3.42B).

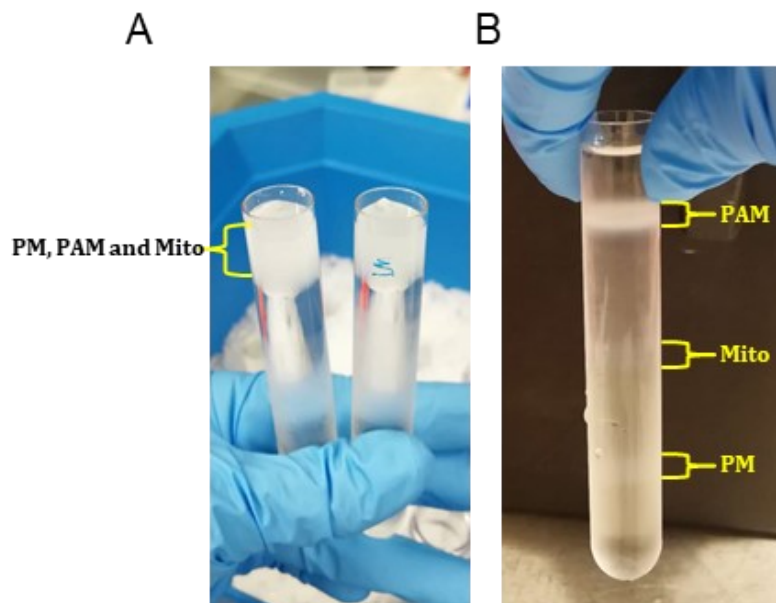


Figure 3.42 Fractional image acquired during isolation

A standard result of mammalian cell fractionation is presented in the figure. A: Crude PM laid on the gradient of sucrose. Containing mainly PM: Plasma membrane, PAM: Plasma associate membrane, and Mito: mitochondrial contamination. B: Result of sucrose gradient centrifugation. From the top to the bottom bands represents plasma associate membrane, mitochondrial contamination, and plasma membrane.

For western blot analysis the samples corresponding to total cell lysate, PAM, PM ER and Cytosol fraction were analyzed by anti-Syntaxin (Figure 3.43A), anti-SERCA2 (Figure 3.43B) and anti-rho western blots (Figure 3.43C). Anti-Syntaxin blot resulted in positive bands only for the fractions H, PAM, ER and C (Figure 3.43A). Anti-SERCA2 blot resulted in positive bands for all the fractions except that the PM fraction showed only a very weak signal. The 114kDa band corresponded to unglycosylated SERCA-2, while its glycosylated form is detected at 140kDa. This indicated that the PM fractions also contain ER to some extent. Only deglycosylated SERCA 2 was observed in PAM fraction and the PM fraction showed this band but relatively with less intensity (Figure 3.43B). Anti-Rho blot indicated the presence of emST protein in all the fractions (Figure 3.43C). These blots showed a pattern similar to the anti-SERCA2 blots, but with high intensities of positive signal for emST and its mCherry variant in H, PAM, PM and ER

fraction. For the ER fraction the signal was very weak.

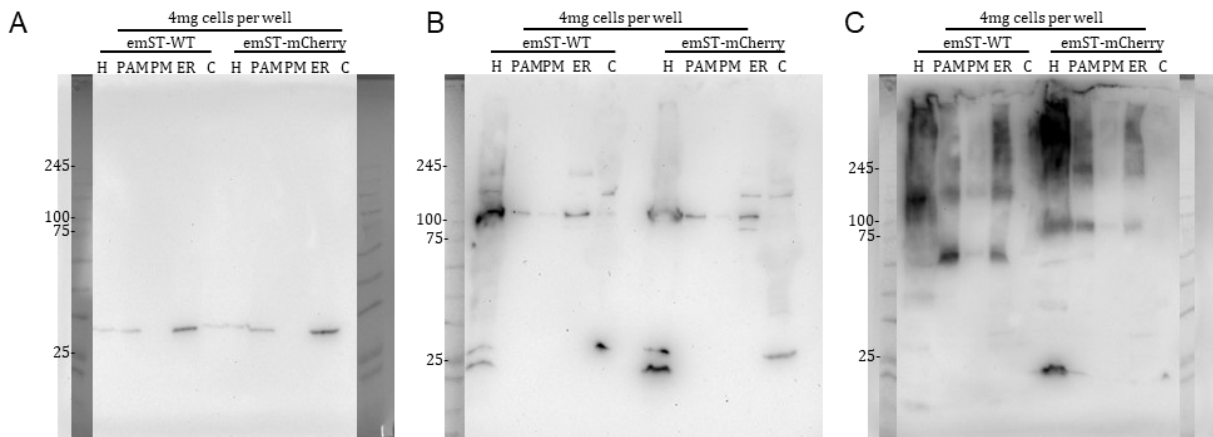


Figure 3.43 Intracellular distribution of emST and other markers.

All the samples analyzed are equivalent to 4mg of cell pellet. Proteins were detected with anti-Syntaxin, anti-SERCA2 and anti-Rho1D4, each of which was followed by secondary anti-rabbit IgG-horseradish peroxidase (HRP)-linked antibody. H: homogenate; PAM: Plasma membrane associated membrane fraction; ER: Endoplasmic reticulum fraction; PM: Plasma membrane fraction; C: Cytosol.

4 Discussion

So far the only *E. multilocularis* protein successfully expressed was an 8kDa subunit of antigen B that was expressed in BL21 (DE3) cells (EmAgB8) [176]. On the other hand hST could be obtained by expression in *E. coli* [177]. Therefore wild-type emST-his/rho protein was expressed with three different vectors (pET27b_{emSET-his}, pQE2_{emST-his} and pET20a_{emST-rho}) in different bacterial strains (BL21 RP RIL Lemo21 C41 and C43) in different combinations as these plasmids were previously found to allow expression of hST. But the analogous experiments for emST-his failed due to low yield and degradation. The sequence alignment of hST and emST showed emST differences at the N-terminus and a longer extracellular loop 2 (EL2) than hST. These differences might have been the cause for the lower stability of emST. Therefore mutants with a shortened N-terminus(Δ N) and EL2(Δ L) were constructed for the following expression experiments in the in-vitro system.

Furthermore the tm2 mutants were adopted from hST [179]. This mutant had been proved to improve hST stability and allowed solving the first hST X-ray structure [86, 87].

4.1 Unfolded emST from *E.coli* and in-vitro expression

In the in-vitro expression analysis emST-his and emST-rho constructs showed a stable expression with a full-length monomeric band in western blot analysis (Figure 3.1, Figure 3.2, Figure 3.3 and Figure 3.4). The screening of constructs of the wild-type protein with three different vectors showed distinct differences in their expression levels: pQE2_{emST-his} < pET27b_{emST-his} < pET20a_{emST-rho} (Figure 3.2). Probably the cause for these differences were the different copy numbers for these vectors [180-182]. The emST-his variants Δ N-emST-his, Δ NL-emST-his, Δ NL-emST-tm2-his appeared as degraded protein (Figure 3.1). Interestingly, the same in-vitro expression analysis in the presence of nanodiscs (MSP1D1) resulted in a stable expression of full-length protein without any degradation for any construct. With MSP1D1 more than 50 % of the protein expressed was solubilized, whereas with MSP1DE3 surprisingly less than 30% could be isolated (Figure 3.3 E, F) indicating substantial difference in solubilization by a change of the nanodisc size from 9-10 nm to 12-14 nm. The protein was detected only

as a monomeric band on western blot in all cases (Figure 3.3). These results indicated that membrane mimicking nanodiscs provided a stable membrane environment for these proteins allowing their stable presence in the soluble fraction, either being protected directly against protease activity by the nanodiscs or stabilized in a structure that was inherently more resistant to proteolysis [183-185].

The observation that the wild-type protein i.e. emST-rho/his was expressed emST as a full-length protein in the absence of nanodiscs, while the variants (ΔN , ΔNL , ΔNL -tm2) were degraded, indicated that the wild-type protein was more stable than the variants. Therefore it had to be concluded that the ΔNL deletions destabilized the structure more than the tm2 stabilized.

The analysis of the purified emST-nanodisc complex (Figure 3.16) by far UV CD showed an unfolded state for emST (Figure 3.16). This proved that the nanodiscs can integrate unfolded protein. Furthermore, this result indicated that the lipidic environment as provided by the nanodisc was not sufficient to allow or maintain a folded state of the proteins.

Table 4.1 Strain and medium used for bacteria expression

Construct	Strain	Expression medium	Scale Expression level	Degradation
pET27b _{emST-his}	BL21(DE3)	TB-CAIM	hardly detectable*	--
	RP	TB-CAIM	hardly detectable	no
		ZY-CAIM	hardly detectable	--
	RIL	TB-CAIM	low*	50kDa
		ZY-CAIM	low	no
	Lemo21	TB-CAIM	hardly detectable	--
	C41	TB-CAIM	hardly detectable	--
	C43	TB-CAIM	hardly detectable	--
pQE2 _{emST-his}	BL21(DE3)	TB-IPTG	yield: 1.2 μ g / g cells	~45kDa ~30kDa blow 20kDa
	RP	ZY-CAIM	hardly detectable	--
	RIL	ZY-CAIM	low	no
pET20a _{emST-rho}	BL21(DE3)	TB-IPTG	low	no

* hardly detectable: only a patterned signal (not form a proper band) was observed on western blot.
* low: the protein only can be detected with western blot, not blue silver staining.

As expected the emST-his/rho protein could be expressed in all the bacterial strains (*E.coli*) used (section 2.4.1), but typically at a very low level and accompanied by degradation, which indicated the instability of emST and possible folding issues that made the proteins more susceptible to the comparatively increased levels of proteases in *E.coli* (Table 4.1). As shown in Figure 3.16 Fos12 yielded a helix signal (22.4%) which was significantly different from the predicted value (sequence-based: 37.1% and structure base: 63%) (Table 3.2).

It was concluded that the lacking folding of the isolated emST proteins was most likely caused by the missing glycosylation in the in-vitro system and *E.coli*. Sequence analysis indicated that emST had three potential N-glycosylation sites (section 3.3.4 and section 3.3.5) (NetNGlyc 1.0 Server).

The hypothesis that posttranslational modification may be required for protein stability was investigated by expression in insect cells. Unfortunately, the yields obtained were only marginally better than those from *E. coli* expression. Upon expression using the BEVS system (section 2.4.2) in sf9 cells only a degradation band with a molecular weight lower than 26 kDa could be detected, whereas with the virus free TGE (section 2.4.2) system in High5 cells western positive bands for the full-length protein for the variants of emST-rho could be detected (section 1.1.1 - Figure 3.18). It could be possible that the degradation occurs in both cell lines. But as a higher protein production cell line, the high5 cells provide an opportunity to detect the full-length emST-rho which had not proceeded toward degradation yet [186]. The thermal-stability mutants adapted from the human analogue hST [178]. showed expression in contrast to the wild-type i.e. emST-rho (Figure 3.18) suggesting that the wild-type protein lacked in stability and also proving the effectivity of the thermo-stability mutations against unfolding. It is important to note that these mutations are internally located while protease tolerance typically requires surface stabilization, which implied that emST was inherently prone to major unfolding. The expectation of relatively easy unfolding was based on the dynamic nature of these transporters which adopt at least three states, namely the open, closed and occluded state [73, 187].

4.2 EmST was isolated in form of HSP complexes

The HSP complexes were found for the tm2 variant of emST-rho purified using DDM.

EmST and its variants expressed in mammalian cells co-purified with two anti-rho negative proteins which were subsequently identified to be HSP70-1B and HSP90 β (Figure 3.29 and Figure 3.30) by MS analysis (Section 2.7.1.1). Using size exclusion chromatography two different HSP complexes could be isolated: emST-tm2-rho+HSP70-1B complex (at 53mL -632 kDa) and emST-tm2-rho+HSP90 β complex (at 59mL - 398 kDa) (Figure 3.30). The calculated apparent molecular weights for these complexes suggested a dimer of the heterodimeric emST-rho-HSP70-1B complex and a heterodimeric emST-rho-HSP90 β complex, respectively. It should be noted that the estimates of the oligomerization states were calculated using the molecular weights of protein-free micelles.

Table 4.2 The oligomer state of DDM purified emST and its variants.

Peak No.	Protein detected	Elution vol (mL)	M.W.* (expected) (kDa)	Oligomer state
1	emST-rho, HSP70-1B, HSP90 β	53	632 (606)	heterodimer of the heterodimeric complex
2	emST-rho	62	301 (288)	dimer
1	emST-tm2-rho, HSP70-1B	53	632 (580)	dimer of the heterodimeric complex
2	emST-tm2-rho, HSP90 β	59	398 (303)	Heterodimer
1	emST-mCherry -rho, HSP70-1B, HSP90 β	52	702 (656)	dimer of the heterodimeric complex
2	emST-mCherry-rho	64	267 (269)	dimer

* The molecular weight was calculated based on column calibration.

Based on the extended chaperone exchange model, the obtained complexes of emST and its variants suggested that the major amount of the emST was located in the ER membrane (Figure 3.40) [57]. Therefore, an emST-mCherry construct (pTT5_{emST}-

mCherry-rho) was used for expression in *Expi293* cells and subsequent analysis of the subcellular localization of the protein by fluorescence microscopy. As expected, the mCherry fused emST-rho protein was also found to co-purify (Table 3.3) with the two HSPs proteins (Figure 3.31). In contrast to other expression methods the mammalian system allowed for comparatively high yields of the emST in form of HSP complexes. It is to be noted that the yields obtained from insect cells and bacterial expression were too low to allow conclusions on possible complex formations. Therefore the mammalian expression system appeared to be the most suitable for production and analysis of emST.

How finely tuned the organization of the HSP complexes were could be seen from the protein variant based differences of the affect of emST with respect to HSPs on SEC: emST-rho and emST-mCherry-rho showed no separation between HSPs (Figure 3.23, Figure 3.25 and Figure 3.31), whereas in emST-tm2-rho purification these HSPs could be separated on SEC (Figure 3.29). Both emST-HSPs complexes exhibited typical helical structure and expected tertiary structure as analyzed with far UV CD (Figure 3.39).

The complexes emST-tm2-rho-HSP90 β and emST-tm2-rho-HSP70-1B displayed helical contents of about 26% (emST: 37.8%) which was in agreement with the predicted values within the error margins for complexes with a 1:1 ratio of emST to the respective HSP (Table 3.6). The agreement in secondary structure suggested that the mutation in emST-tm2 provided increased integrity of the structure in HSP- complexes (Figure 4.1).

Experimentally hST-HSP70 and hST-HSP90 complexes allowed monitoring progress in the folding trajectory (Figure 4.1) [103]. Many scholars hold the view that according to the HSP/COPII exchange model that inhibition of HSPs are able to synergize with pharmacochaperones, and the HSP-relay also important for rescue the structure of folding-deficient mutants [57, 105]. Nevertheless, the folding trajectory of ST is poorly understood, and a better understanding of the conformations selected by pharmacochaperones is required [106, 189, 190]. The expression of emST in mammalian cells ST allowed the isolation of the relevant complexes in yields of 3-8.7 μg / g cell pellet which will allow further studies on pharmacon interaction of these complexes.

For further confirmation the cellular localization of emST was analyzed by subfractioning (organelles) of the cellular content. The comparative subcellular distribution analysis for the wildtype emST and emST-mCherry has been performed employing density gradient centrifugation, SDS-PAGE and western blot (Figure 3.43). For investigation of the cellular transport process the localization of fluorescence-labeled emST (emST-mCherry-rho) was investigated by confocal microscopy. Both methods indicated the ER localization of emST. No protein was detected in the plasma membrane which meant that there was no effective protein transport from the ER.

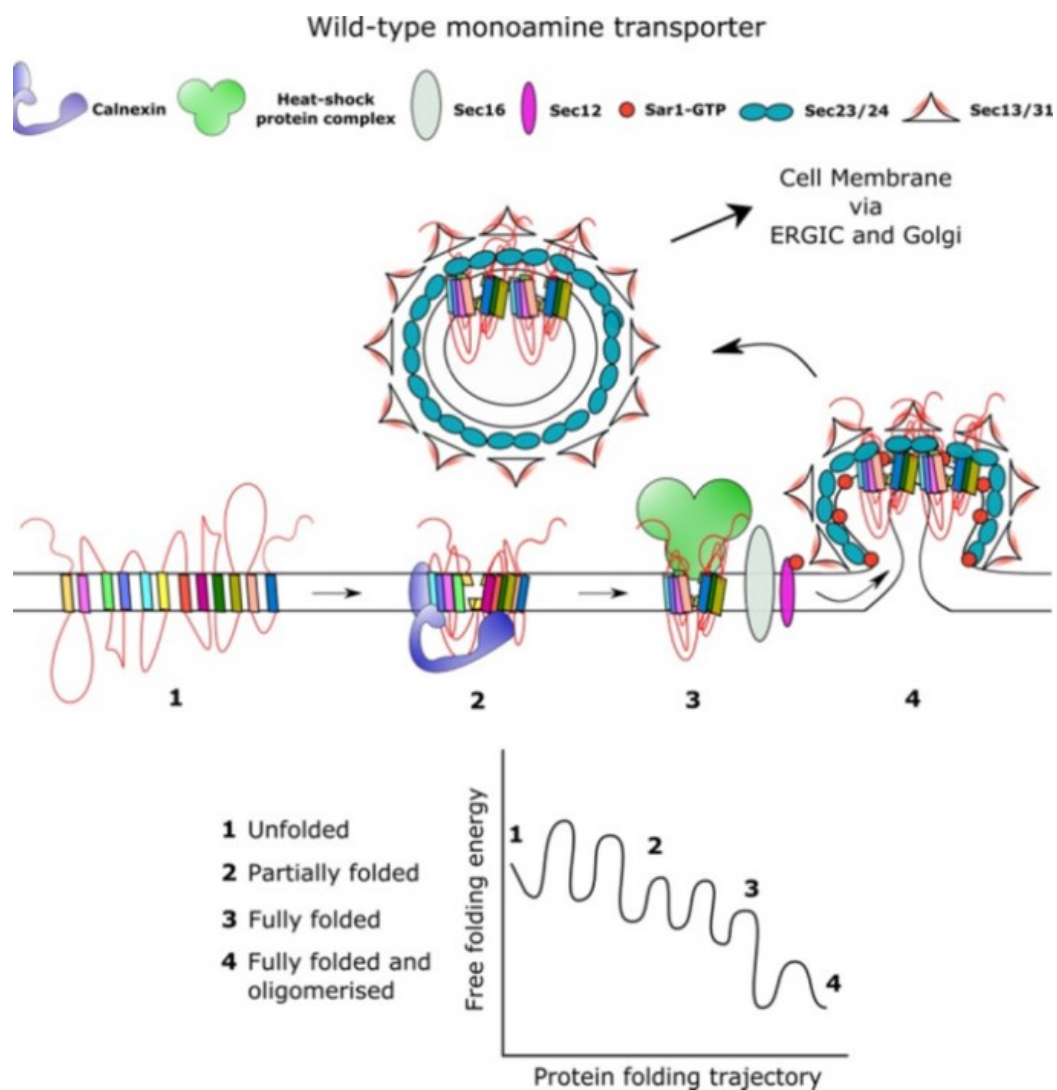


**Figure 4.1 Native folding and trafficking from ER to the plasma membrane.
(adopted from [106])**

4.3 The conformation of the emST-HSP complexes

The hypothesis on the role of posttranslational modifications for emST stability was investigated by expression analysis of four different constructs (pTT5_{emST-rho}, pTT5_{emST-Y69A-rho}, pTT5_{emST-I273A-rho} and pTT5_{emST-tm2-rho}) in mammalian expression systems, namely *Expi293* and *HEK293* cells, using the virus-free TGE system (section 2.4.3) *Expi293* displayed a higher expression level than *HEK293* cells (Figure 3.20). In contrast to the insect cell expression, in mammalian cells the wild-type protein emST-rho could be expressed which indicated that mammalian cells provided more suitable conditions for the expression of the *Echinococcus* protein than insect cells.

Fos12, DDM and DIBMA purified wild-type emST-rho protein expressed in *Expi293* cells allowed the isolation of full-length protein with no evidence for degradation. It was therefore concluded that the major issue with expression in insect cells compared to mammalian cells was the direction of emST towards degradation in the former expression system.

When analyzing solubilization conditions it was found that with the detergent Fos12 pure protein samples could be obtained from mammalian cells (Figure 3.27), whereas solubilization with DDM or DIBMA led to samples containing HSP. This indicated that Fos12, a very stringent detergent, had broken up the emST-rho-HSPs complex, while DDM, a relatively moderate detergent, could not. In agreement with this hypothesis detergent-free solubilization by DIBMA also contained the HSPs. DIBMA is supposed to solubilize protein-lipid complexes and thereby extract the native complexes from membranes [191]. Overall, this analysis indicated that the emST protein in its native form exists in complex with HSPs in an *Expi293* membrane.

For *Expi293* expressed emST-rho, DDM solubilization yielded a slightly higher helical content (21.9%) than Fos12 (20%) (Table 3.5). But both these structural compositions were significantly different from the predicted values (emST sequence-based: 37.1%, homology modeling hST-structure based: 61%) (Table 3.5). In the presence of the inhibitor citalopram no significant change of helical structure was observed in Fos12 purified emST-rho (helical content: 20.1%, respectively 20%) (Figure 3.38) which showed that ligand-based structure stabilization failed. In the case of hST it had been shown that citalopram and paroxetine stabilized ST in the presence of Na⁺ ions in the outward-facing conformations [192].

For the circumstance without stabilization, a rapid interchange of inward and outward-facing conformations was suggested

For the situation without stabilization a fast conformational interchange of the inward and outward-facing conformations was suggested [193]. There is no appreciable concentration of Na⁺ in ER, which means those inhibitors are not able to stabilize the inward-facing conformation state of hST [107, 194]. Therefore, the lacking affect of citalopram agreed with the localisation of emST in ER in inward-facing conformation (Figure 1.7).

4.4 Differences of hST and emST with regard to the extended chaperone/COPII exchange model

The finding of emST-HSP complexes suggested that the isolated protein was not located in the plasma membrane. In order to understand the formation of emST-HSPs complexes, the model of the human serotonin transporter (hST) folding trajectory and exporting process (section 1.4, Figure 1.10) was considered as a reference model. Comparing this model with the results for emST indicated that both CNX, HSPs and SECs had a role with regard to protein folding and vesicle trafficking (Table 4.3). But the E3-ligase was found to be remarkably different in *E. multilocularis* (Identity: 11.4%). Most likely the mammalian expressed emST-rho was recognized as a misfolded hST (Identity: 43%, Figure II.0.1). Then it should be targeted for degradation by the ERAD proteasome after labeling by E3-ligase, but no degradation was detected. The significant dissimilarity of E-ligase in human and *E. multilocularis* cells might prevent proper labeling of emST and consequently disallow digestion.

Table 4.3 Protein similarity

Protein (<i>E. multilocularis</i>)	Protein (Human)	Identical positions	Identity
emCNX	hCNX	282	46.8%
emHSP40	hHSP40	205	51.4%
emHSP70	hHSP70	309	47.1%
emHSP90	hHSP90	342	45.6%
emSAR1	hSAR1	124	62.6%

emSEC23	hSEC23	445	57.6%
emSEC24	hSEC24	403	30.4%
emE3-ligase	hE3-ligase	54	11.4%

Similar to the situation of hST in human cells where the interaction with HSPs was identified by cell biological methods (Figure 1.10), the emST proteins also form complexes with HSP proteins (HSP70-1B and HSP90 β (Figure 3.30)). In contrast to the case of hST for emST it was possible to isolate these complexes for further studies. There must have been a very stable interaction between these proteins to be able to carry them through the purification, which included solubilization, rho1D4 affinity purification and SEC. Interestingly, by the model, HSP70 was supposed to appear in an HSP40-HSP70-ST complex which was not observed. This implies that this complex either could not be formed with emST or that the model is incomplete in its description of the subsequent steps of protein transport. Anyhow, the cell biological analysis of the hST transport led to a model of ST-HSP interaction with a stoichiometry of complexes (s.b.) that was partially contradicted for emST. The higher degree of oligomerization in the case of emST than proposed in the model could be a reason for increased stability. It should be noted that the cell biological experiment did not provide clear evidence for the oligomerization state of the ST-HSP complexes [105, 195].

An alternative explanation could be given by a requirement for specific interactions. In the case of hST, the protein was not transported for discrete C-terminal mutants, and mutants at the SEC24 binding site (Figure 4.5) [196]. This implied that protein, that progressed that far in the transport process, could not revert to the degradation pathway. In difference to this work no complexes were isolated.

4.5 Ex-vivo reconstitution of the PM state of emST

Among the lipids, cholesterol had been best characterized as a lipid that affected the structure of membrane proteins. Indeed, in the crystal structures of hST (Figure 1.8) several potential cholesterol sites were identified [86]. Though cholesterol is essential for mammalian cellular membranes, it may be especially important in the transport related folding of membrane proteins as the human ER content of cholesterol is low (5

mol %), and it increases through the trans-Golgi network to reach the highest content in the plasma membrane (29 mol %) [197-200].

When cholesteryl-hemisuccinate was added to Fos12 purified emST-rho the far UV CD exhibited a significant increase of the helical signal (29.4%). This clearly showed that cholesterol binding induced structure formation in emST. As discussed above the emST was purified from ER where it should be inward-facing with respect to the curvature of the membrane in the inward-facing open conformation i.e. open to the ER lumen. Therefore, strictly, this implies only that cholesterol could induce structural induction in the inward-facing conformation of emST if this conformation is different from conformations in the PM. The difference in structural composition of this state and the expected PM-state indicated that the adoption of this outward-facing state of ST with respect to the PM would require further involvement of the cellular machinery.

For hST molecular dynamics simulation showed cholesterol molecules located between TM1a, TM5 and TM7, which indicated a strong binding in a membrane bilayer environment and supposedly was important for the conformation of hST (Figure 4.2).

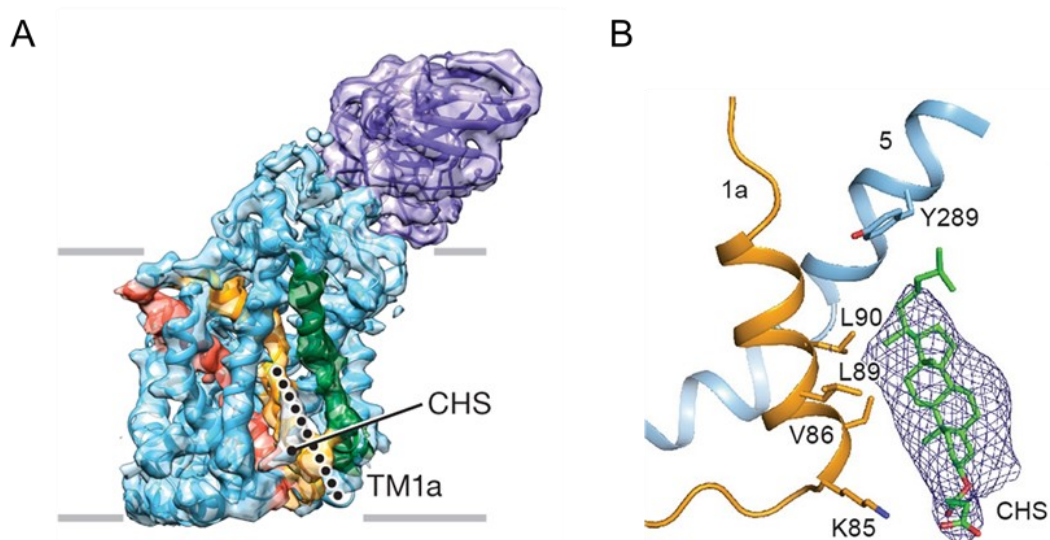


**Figure 4.2 Cryo-EM reconstructions of occluded hST conformations
(adopted from [88])**

A: Occluded conformation in 100 mM NaCl of Δ N72/C13 hST with 15B8 Fab, (4.2-Å resolution).
B: Cholesteryl hemisuccinate was located near TM1a and TM5.

In this occluded conformation of hST found using EM, the CHS has been observed as TM1a's distinct density characteristic [88]. This resulted in TM1a being 'splayed' away from the transporter center, allowing a route from the central binding site to the intracellular space (Figure 4.2 B) [88]. In the inward-open conformation, the density characteristic of the CHS close TM1a was not observed, which suggests that conformation is CHS-binding dependent [88]. Therefore the hypothesis was that cholesterol binding pushes the conformational equilibrium of detergent solubilized emST towards the outward-open conformation which is important for functional modulation. This suggested that transport activity of ST might be detrimental at locations apart from the PM.

4.6 The role of glycosylation

When emST-his was expressed in the BL21 (DE3) strain using the pQE2_{emST-his} construct a major degradation band at 50 kDa was observed (Figure 3.12). This band being anti-his immuno-blot positive indicated that the fragment that contained the C-terminus was isolated. Based on the molecular weight of the 50 kDa fragment the cleavage had occurred within the second extracellular loop (EL2), which is the largest loop in emST according to the homology model (Figure 4.3) [86]. Two of the three predicted N-glycosylation sites i.e., N₁₈₅SSD and N₂₀₂TTG (NetNGlyc 1.0 Server), were also located in this loop while the third site i.e., N₅₃₆ITF resides in the fourth extracellular loop (EL4). Therefore, it was concluded that the lack of glycosylation on bacterial expression may have been a major determinant of the instability of the emST protein, possibly due to lacking shielding against protease activity. The question raised as a result of the in-vitro experiments, if emST would have to be isolated as a proper protein-lipid complex, remained undecided because the protein could be isolated only with Fos12, a strongly delipidating detergent.

The comparison of bacterial and in-vitro expression of wild type emST with mammalian expression had clarified the secondary hypothesis that emST required certain glycosylation for proper folding, stability and possibly functionality i.e. transport.

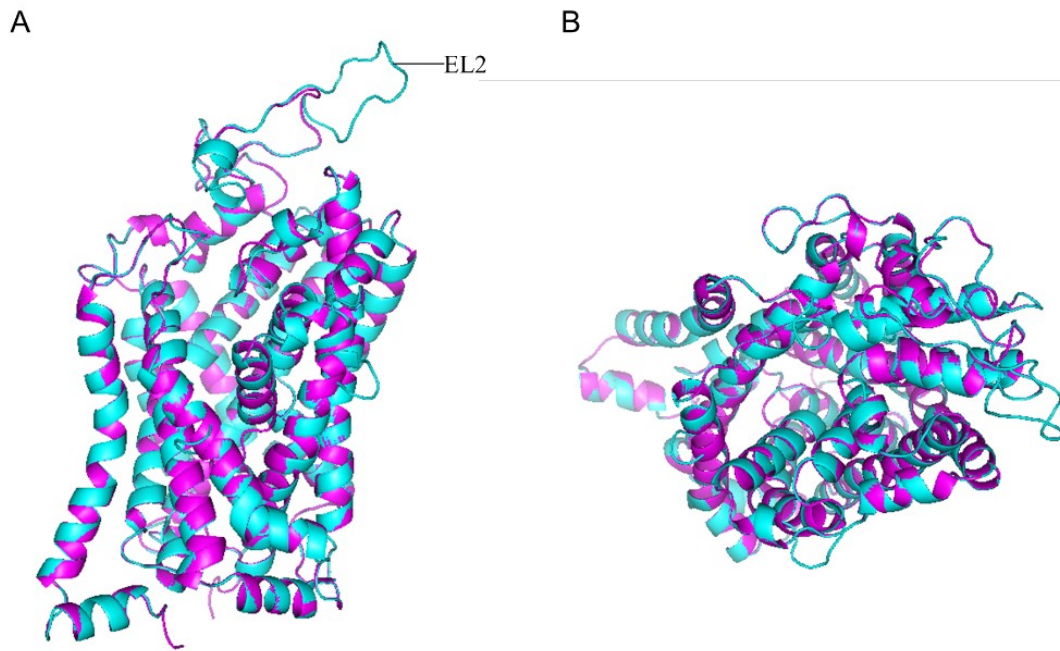


Figure 4.3 emST model and hST structure

The emST(cyan) model was predicted based on the hST (magenta) x-ray structure (PDB code: 5I6Z) [86]. SWISS-MODEL was used for emST structure prediction. A: side view; B: top view. Images were rendered using PyMOL and colored according to the spectrum coloring option [201-203].

The potential N-glycosylation sites predicted based on the emST sequence were N₂₀₂-T-T-G₂₀₅, N₃₇₃-R-T-N₃₇₆, and N₅₃₆-I-T-F₅₃₉. Experimentally sites found were: N₁₈₅-S-S-D₁₈₈ and N₂₀₂-T-T-G₂₀₅. Three proteins (emST-rho, emST-tm2-rho, emST-mCherry-rho) purified from mammalian system were analyzed to confirm the presence of N-glycosylation. These proteins were resistant to EndoH while the treatment with PNGaseF caused molecular weight differences (Figure 3.34). As N-glycosylation is susceptible to EndoH until being converted from high mannose to the hybrid or complex form in the medial- and trans-Golgi cisterna compartments, this result suggested that these EndoH resistant proteins must have surpassed already the ER [204]. This was contradicted by the cellular localization experiments. Therefore, it had to be concluded that emST carried EndoH resistant glycosylation. The secondary and tertiary structure of proteins often prevented endoglycosidases from reaching the mannose-asparagine bond, which probably caused the ER located emST not to be processed by EndoH [205].

Interestingly, the different emST variants showed different molecular weight

differences upon PNGaseF treatment (Table 3.2). This indicated that the glycan-moieties present on these three proteins were different. The molecular weight difference between the treated and untreated samples for emST-mCherry-rho (8.4 kDa) was significantly higher than the other two (2.9-3.5 kDa) (Figure 3.43 and Table 3.4). Processing of glycosylation in the mammalian ER is well described (Figure 4.4) for the precursor $\text{Glc}_3\text{Man}_9\text{GlcNAc}_2$ [205]. Especially for the constructs with a C-terminal mCherry tag, this tag might have been the cause for the formation of less processed complexes with the observed variation of the glycan composition (Figure 4.4). The glycan-moieties present on these three proteins were obviously of different accessibility for processing, the mCherry construct being the least processed. The major difference between the mCherry construct and the other two was the 25kDa-mCherry. This large tag by itself could not modulate the activity of the glucosidases physically because the tag and the glycosylation, respectively EL2, are located at different sides of the membrane. Therefore, a subtler affect of the tag on the folding of emST was expected.

The emST-mCherry-rho construct was chosen as part of the ERIC project, (the EU-funded Project Instruct-Ultra), which focuses on the development of a new method to express membrane proteins with high throughput. The result with emST-mCherry-rho indicated the C-terminus mCherry tag was not suitable at least in the case of expression of PM localized emST.

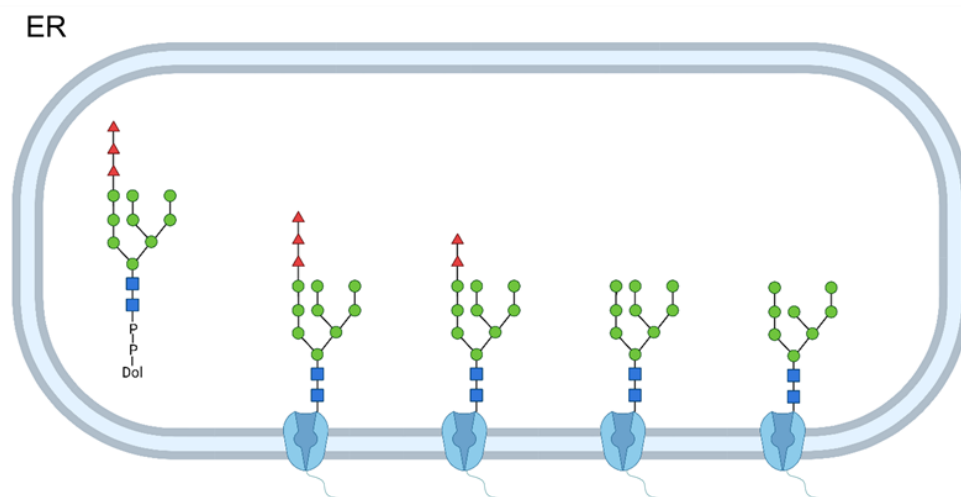


Figure 4.4 Oligosaccharide synthesis of synthesized glycoproteins in ER.

The symbols represent Green circle: mannose; Red isosceles triangle: glucose; Blue square: N-acetylglucosamine. During its vectorial transport through the ER membrane, the precursor $\text{Glc}_3\text{Man}_9\text{GlcNAc}_2$ is passed from the lipid donor to asparagine in a nascent polypeptide [205].

4.7 Transport process and degradation pathway

Only for the EmST-tm2-rho construct the two different of the HSP complexes were observed (Figure 3.23, Figure 3.25 and Figure 3.31, as compared to Figure 3.29. For the other constructs mixture of complexes were observed. In both cases the proteins were not transported from the ER. This was in agreement with the previous finding that the transport process was very sensitive to the C-terminal structure of the proteins where the HSPs bind to ST [103]. By the human transport model, the proper interaction of HSPs with ST is required for translocation into COP II vesicles and subsequent transport to the plasma membrane. The emST was supposed to either form COP II vesicles and then be exported from ER or proceed to the ERAD-proteasome to be degraded (Figure 1.10). Obviously, neither of these pathways were taken by emST in mammalian cells, as the emST-HSPs complexes could be isolated. Apparently, the binding to HSP90 was stronger for emST than in the case of hST such that neither SEC23/24 nor HSP70 were able to exchange/replace HSP90 for the tm2 variant, this suggests that between emST and HSP90 strong interactions existed that were not present for hST. In the case of the other constructs mixed HSP complexes were observed which indicates that in this case the binding of the HSPs were of comparable strength. Also no HSP40 or mixed HSP40/70 complexes were observed which might have been due to lower stability of these complexes. The appearance of the emST-HSP70 complex, which was observed not for hST also indicates that the interaction of this HSP with emST was stronger than that for hST. This stronger interaction might have also prevented the ubiquitination and the targeting towards degradation (Figure 1.10).

The emST and hST had 46% sequence similarity (Appendix II), therefore the changed strength of the HSP interaction was quite possible if these interactions were not entirely located at the C-terminus of emST.

The HSPs binding sites of hST P₆₀₁G and R₆₀₇I of hST were semi-conserved in emST (R₅₈₅G and R₅₉₁L, see Figure 4.5), therefore it appeared likely that heterologously expressed emST in mammalian cells is subjected to normal cellular transport. But in fact, the protein was isolated as HSP complexes which indicated that at least a substantial part of emST was not transported regularly. A similar observation had been made upon overexpression of hST in mammalian cells [103, 206]. Therefore, the transport process appeared to be negatively affected by increasing ST concentration.

This might be a functional feature to limit the amount or delivery speed of ST transported to the PM. The most likely mechanism for hST appeared to be a change in oligomerization to higher oligomers as observed for emST. It is noteworthy that the oligomerization states in the transport model are mostly conjecture.

```

hSERT  SIILGYCIGTSSFICIPITYIAYRLIITPGTFKERI IKSITPETPTEIPCGDIRLNAV--- 630
emSERT VHVVSWMMLVFSSSLVTIPIFAVVTFC SARGSFKERL KSLFTPGIRPSFSDFHVPNSHKKQ 617
      :.: : : **.: : ** : . : : : M:****: . :** .: .: : *:
                                     ^ ^
hSERT  -----
emSERT EIKDKDEEQVAKSAEAVDDTQSEGDEG 644

```

Figure 4.5 Sequences alignment of C-terminal hST and emST

emSERT (Fox tapeworm), A0A068XWX1; hSERT (Human), P31645; Figure generated alignment in CLUSTAL software. The green arrow indicates the HSPs binding site.

Confirmation of the cellular localization of emST was sought by localization analysis through subfractioning (organelles) of the cellular content. A comparative subcellular distribution analysis for the wildtype emST and emST-mCherry was performed by density gradient centrifugation, SDS-PAGE and western blot (Figure 3.43). For further investigation of the cellular transport process the localization of fluorescence-labeled emST (emST-mCherry-rho) was investigated by confocal microscopy. Both methods indicated the ER localization of emST. No protein was detected in the plasma membrane which means that there was no effective protein transport from the ER. In this situation the protein should be directed to degradation (Figure 1.10), which did not occur for emST as the complexes could be isolated. Indeed, the isolated complexes appeared to differ from the complexes in the hST case in composition (s.a). But though the changed composition may be the cause, it can not be excluded that another hidden, sequence encoded signal in the protein is required for directing the protein towards degradation. Another possible cause could have been post-translational modification of the protein: Processing of the glycosylation moiety happens throughout the transport from ER to the plasma membrane via the Golgi complex. Such transported protein would not be subjected to ubiquitination and degradation by E3-ligase in the ER [207], but emST was clearly localized at the ER

4.8 Perspectives

EmST is the first membrane protein of *E. multilocularis* that had been expressed.

This will allow further studies on emST as a possible target protein for the treatment of alveolar hydatid disease by finding a specific drug that only inhibits the *E. multilocularis* emST but does not affect the human serotonergic pathway.

The expression in human cells was found to be useful to isolate the intermediate state of emST, respectively its HSP complexes. Further studies of these complexes will for the first time provide structural insight and clarify the HSP-protein interactions.

In human cells it should be possible to express chimeric protein that will be transported to the PM, but as there appears to be a role of the C-terminus in folding the protein may not adopt the proper PM conformation. Therefore overexpression of emST into the plasma membrane possibly requires an expression host that is closer to *E. multilocularis*.

The utility of the mCherry-tag in a general approach to monitoring expression and transport of heterologously expressed protein in human cells as investigated in an Eric-Ultra project appears to be limited, at least for proteins that require tight control of their functionality or have specific folding requirements. But these results indicated that it was worthwhile to monitor the localization of the target protein.

Summary

This study set out to achieve the overexpression and isolation of serotonin transporter from *E. multilocularis*. Being the first membrane protein of *E. multilocularis* that was heterologously expressed, the overexpression of emST was carried out in three different expression systems i.e. bacteria, insect and mammalian systems.

In the bacterial system, a 50kDa degradation product was observed. By CD spectroscopy the full-length protein was shown to be significantly different from the prediction, probably because of missing glycosylation in the bacterial system. Indeed, folded full-length protein was obtained in the mammalian expression system. Even for the in vitro expressed emST-MSP1D1 complex the CD spectra showed a random coil structure, which indicated unfolded state. In this case, the nanodisc environment was not sufficient to maintain a folded state of the protein.

In mammalian cells, the emST was isolated as emST-HSPs complexes. This provided the insight that the isolated protein was in an intermediary state in ER. The ER localization was confirmed by both confocal microscopy-based localization analysis using a mCherry-construct and subcellular fractionation analysis. The investigation of glycosylation has shown that the glycan-moieties present on emST and its variants were obviously of different accessibility for processing, the mCherry construct being the least processed. The CD analysis of both complexes showed secondary structure close to the predicted values, which indicated that the HSP, as a co-chaperone, was able to keep the emST in a properly folded state. The helical content was significantly increased when CHS was added to detergent purified emST, which had a low helical content after detergent solubilization. The hypothesized relevance of CHS for maintaining folding was thereby shown. But the reconstitution of the secondary structure of emST was found to be incomplete which indicated that deviation from the proper intracellular processing of emST caused irreversible changes in the protein structure.

In this work, for the first time the HSP complexes of a target protein were isolated. The isolated complexes have not been described previously and provide an extension to the COPII/exchange model of membrane protein transport.

The yield of about 5-7 μg / g cell pellet allowed characterizing the biochemical and biophysical properties, especially wrt the folding trajectory of the protein. These

complexes will allow further studies relevant to the transport and folding process and present a suitable target for pharmaceutical intervention in AHD.

Zusammenfassung

Diese Studie zielte darauf ab, die Überexpression und Isolierung des Serotonintransporters aus *E. multilocularis* zu erreichen. Als erstes Membranprotein von *E. multilocularis*, welches heterolog exprimiert wurde, wurde die Überexpression von emST in drei verschiedenen Expressionssystemen, d. H. in Bakterien-, Insekten- und Säugetiersystemen, durchgeführt.

Im bakteriellen System wurde ein Abbauprodukt von 50 kDa beobachtet. Durch CD-Spektroskopie wurde gezeigt, dass das vollständige Protein sich in seiner Sekundärstruktur signifikant vom vorhergesagten Wert unterscheidet, was vermutlich auf eine fehlende Glykosylierung im bakteriellen System zurückzuführen ist. In der Tat wurde gefaltetes Protein voller Länge im Säugetierzellen-Expressionssystem erhalten. Selbst für den in vitro exprimierten emST-MSP1D1-Komplex zeigten die CD-Spektren eine Random-Coil-Struktur, welche einen ungefalteten Zustand darstellt. In diesem Fall war auch die Nanodisc-Umgebung nicht ausreichend, um einen gefalteten Zustand des Proteins aufrechtzuerhalten.

In Säugetierzellen wurde das emST in Form von emST-HSP-Komplexen isoliert. Dies lieferte die Erkenntnis, dass sich das isolierte Protein im ER in einem Zwischenzustand befand. Die ER-Lokalisierung wurde sowohl durch konfokale mikroskopische Lokalisierungsanalyse unter Verwendung eines mCherry-Konstrukts als auch durch subzelluläre Fraktionierungsanalyse bestätigt. Die Untersuchung der Glykosylierung hat gezeigt, dass die auf emST und seinen Varianten vorhandenen Glykaneinheiten offensichtlich für die Prozessierung unterschiedlich zugänglich waren, wobei das mCherry-Konstrukt am wenigsten prozessiert war. Die CD-Analyse beider Komplexe zeigte eine Sekundärstruktur nahe den vorhergesagten Werten, was darauf hinwies, dass das HSP als Co-Chaperon in der Lage war emST in einem richtig gefalteten Zustand zu halten.

Der Helixanteil war signifikant erhöht, wenn Cholesterol (CHS) zu dem mit Detergens gereinigten emST gegeben wurde, welches nach der Solubilisierung mit Detergens einen niedrigen Helixanteil aufwies. Die vermutete Relevanz von CHS für die

Aufrechterhaltung der Faltung konnte hierdurch gezeigt werden. Die Wiederherstellung der Sekundärstruktur von emST erwies sich jedoch als unvollständig, was darauf hinwies, dass eine Abweichung von der ordnungsgemäßen intrazellulären Prozessierung von emST irreversible Änderungen in der Proteinstruktur verursachte.

In dieser Arbeit wurden erstmals die HSP-Komplexe des Zielproteins isoliert. Diese HSP Komplexe waren bisher unbeschrieben. Ihre Entdeckung stellt eine Erweiterung des COPII-Austausch Modells für den Transport von Membranproteinen dar.

Die Ausbeute von ca. 5-7 μg / g Zellpellet ermöglichte die Charakterisierung der biochemischen und biophysikalischen Eigenschaften, insbesondere hinsichtlich der Faltungsverlauf des Proteins. Die Komplexe werden weitere Studien ermöglichen, die für den Transport- und Faltungsprozess von Bedeutung sind, und stellen ein geeignetes Ziel für pharmazeutische Interventionen bei AHD dar.

Bibliography

1. Moro, P. and P.M. Schantz, Echinococcosis: a review. *International journal of Infectious diseases*, 2009. 13(2): p. 125-133.
2. McManus, D.P., et al., Echinococcosis. *The Lancet*, 2003. 362(9392): p. 1295-1304.
3. Deplazes, P., et al., Global distribution of alveolar and cystic echinococcosis. *Advances in parasitology*, 2017. 95: p. 315-493.
4. Venyo, A.K.-G., Hydatid Cyst of the Prostate Gland: A Review and Update. *Progress in Men's Health*, 2021. 1(1): p. 10-20.
5. Torgerson, P.R., et al., The global burden of alveolar echinococcosis. *PLoS Negl Trop Dis*, 2010. 4(6): p. e722.
6. Nakao, M., et al., Geographic pattern of genetic variation in the fox tapeworm *Echinococcus multilocularis*. *Parasitology international*, 2009. 58(4): p. 384-389.
7. Ito, A., et al., Histopathological, serological, and molecular confirmation of indigenous alveolar echinococcosis cases in Mongolia. *The American journal of tropical medicine and hygiene*, 2010. 82(2): p. 266-269.
8. Konyaev, S.V., et al., Genetic diversity of *Echinococcus* spp. in Russia. *Parasitology*, 2013. 140(13): p. 1637.
9. Knapp, J., et al., *Echinococcus multilocularis* in Svalbard, Norway: microsatellite genotyping to investigate the origin of a highly focal contamination. *Infection, genetics and evolution*, 2012. 12(6): p. 1270-1274.
10. Yamasaki, H., et al., Genetic analysis of *Echinococcus multilocularis* originating from a patient with alveolar echinococcosis occurring in Minnesota in 1977. *The American journal of tropical medicine and hygiene*, 2008. 79(2): p. 245-247.
11. Gesy, K.M. and E.J. Jenkins, Introduced and native haplotypes of *Echinococcus multilocularis* in wildlife in Saskatchewan, Canada. *Journal of wildlife diseases*, 2015. 51(3): p. 743-748.
12. Massolo, A., et al., *Echinococcus multilocularis* in North America: the great unknown. *Parasite*, 2014. 21.
13. Kern, P., et al., European echinococcosis registry: human alveolar echinococcosis, Europe, 1982-2000. *Emerging infectious diseases*, 2003. 9(3): p. 343.

14. Otero-Abad, B., et al., Mathematical modelling of *Echinococcus multilocularis* abundance in foxes in Zurich, Switzerland. *Parasites & vectors*, 2017. 10(1): p. 1-12.
15. Hifumi, T., et al., Relationship between hepatic grayish-white solid nodules in horses imported from Canada and larval *Echinococcus multilocularis* infection. *The Canadian Veterinary Journal= La Revue Veterinaire Canadienne*, 2021. 62(3): p. 285-288.
16. Baumann, S., et al., Worldwide literature on epidemiology of human alveolar echinococcosis: a systematic review of research published in the twenty-first century. *Infection*, 2019: p. 1-25.
17. Dezsasny, B., et al., Emerging human alveolar echinococcosis in Hungary (2003–2018): a retrospective case series analysis from a multi-centre study. *BMC Infectious Diseases*, 2021. 21(1): p. 1-15.
18. Toews, E., et al., A global assessment of *Echinococcus multilocularis* infections in domestic dogs: proposing a framework to overcome past methodological heterogeneity. *International Journal for Parasitology*, 2021.
19. Grimm, J., et al., Establishing and evaluation of a polymerase chain reaction for the detection of *Echinococcus multilocularis* in human tissue. *PLoS neglected tropical diseases*, 2021. 15(2): p. e0009155.
20. Svrckova, P., et al., Disseminated cerebral hydatid disease (multiple intracranial echinococcosis). *Practical neurology*, 2019. 19(2): p. 156-163.
21. Ozdemir, N.G., et al., *Echinococcus alveolaris*: presenting as a cerebral metastasis. *Turkish neurosurgery*, 2012. 22(4): p. 448.
22. Bulakci, M., et al., Disseminated alveolar hydatid disease resembling a metastatic malignancy: a diagnostic challenge report of two cases. *Case reports in radiology*, 2014. 2014.
23. Santivavaez, S.J., et al., Absence of brain involvement and factors related to positive serology in a prospective series of 61 cases with pulmonary hydatid disease. *The American journal of tropical medicine and hygiene*, 2008. 79(1): p. 84-88.
24. Bellanger, A.P., et al., Investigating new serological and tissue markers for the follow up of patients operated for alveolar echinococcosis. *Parasite immunology*, 2021: p. e12827.

25. Zhao, Y., et al., Characterizing dynamic changes of plasma cell-free *Echinococcus granulosus* DNA before and after cystic echinococcosis treatment initiation. *Genomics*, 2021: p. 576-582.
26. Rao, M.R., et al., Nanosuspension coated multiparticulates for controlled delivery of albendazole. *Drug Development and Industrial Pharmacy*, 2021: p. 1-36.
27. Ezzatkah, F., A.K. Khalaf, and H. Mahmoudvand, Copper nanoparticles: Biosynthesis, characterization, and protoscolicidal effects alone and combined with albendazole against hydatid cyst protoscoleces. *Biomedicine and Pharmacotherapy*, 2021. 136: p. 111257.
28. Kouguchi, H., et al., In vivo efficacy of combination therapy with albendazole and atovaquone against primary hydatid cysts in mice. 2021.
29. Weingartner, M., et al., Albendazole reduces endoplasmic reticulum stress induced by *Echinococcus multilocularis* in mice. *bioRxiv*, 2021.
30. Golriz, M., et al., Case Report: Successful DaVinci-Assisted Major Liver Resection for Alveolar Echinococcosis. *Frontiers in Surgery*, 2021. 8: p. 33.
31. Takenaka, Y., et al., Long-term Follow-up of a Patient with Portal Hypertension and Hepatic Failure Due to Hepatic Hydatid Disease. *Internal Medicine*, 2021: p. 6397-20.
32. Jenkins, D.J., et al., Detection of *Echinococcus granulosus* coproantigens in Australian canids with natural or experimental infection. *Journal of Parasitology*, 2000. 86(1): p. 140-145.
33. Laurimaa, L., *Echinococcus multilocularis* and other zoonotic parasites in Estonian canids. 2016, Tartu.
34. Hildreth, M., et al., Failure to identify alveolar echinococcosis in trappers from South Dakota in spite of high prevalence of *Echinococcus multilocularis* in wild canids. *Journal of Parasitology*, 2000. 86(1): p. 75-77.
35. Avcioglu, H., et al., First molecular characterization of *Echinococcus multilocularis* in Turkey. *Vector-Borne and Zoonotic Diseases*, 2016. 16(9): p. 627-629.
36. Thompson, R., *Biology and systematics of Echinococcus. Echinococcus and hydatid disease*, 1995.
37. Thompson, R., *The biology of Echinococcus and hydatid disease*. 1986.
38. Organization, W.H., *World Health Organization-WHO*. 2000.

39. Guislain, M.-H., et al., Ecological and biological factors involved in the transmission of *Echinococcus multilocularis* in the French Ardennes. *Journal of helminthology*, 2008. 82(2): p. 143-151.
40. Stieger, C., et al., Spatial and temporal aspects of urban transmission of *Echinococcus multilocularis*. *Parasitology*, 2002. 124(6): p. 631.
41. Hegglin, D., F. Bontadina, and P. Deplazes, Human wildlife interactions and zoonotic transmission of *Echinococcus multilocularis*. *Trends in parasitology*, 2015. 31(5): p. 167-173.
42. Giraudoux, P., et al., Transmission ecology of *Echinococcus multilocularis* in wildlife: what can be learned from comparative studies and multiscale approaches Report of the Hokkaido Institute of Public Health, 2002. 52: p. 115-115.
43. Knapp, J., et al., Real time PCR to detect the environmental faecal contamination by *Echinococcus multilocularis* from red fox stools. *Veterinary Parasitology*, 2014. 201(1-2): p. 40-47.
44. Stien, A., et al., Intestinal parasites of the Arctic fox in relation to the abundance and distribution of intermediate hosts. *Parasitology*, 2010. 137(1): p. 149.
45. Dyachenko, V., et al., *Echinococcus multilocularis* infections in domestic dogs and cats from Germany and other European countries. *Veterinary parasitology*, 2008. 157(3-4): p. 244-253.
46. Martinek, K., et al., *Echinococcus multilocularis* in European wolves (*Canis lupus*). *Parasitology Research*, 2001. 87(10): p. 838-839.
47. Kapel, C., et al., Reproductive potential of *Echinococcus multilocularis* in experimentally infected foxes, dogs, raccoon dogs and cats. *International journal for parasitology*, 2006. 36(1): p. 79-86.
48. Catalano, S., et al., *Echinococcus multilocularis* in urban coyotes, Alberta, Canada. *Emerging infectious diseases*, 2012. 18(10): p. 1625.
49. Leiby, P.D. and D.C. Kritsky, *Echinococcus multilocularis*: a possible domestic life cycle in central North America and its public health implications. *The Journal of parasitology*, 1972. 58(6): p. 1213-1215.
50. Petavy, A., S. Deblock, and S. Walbaum, Life cycles of *Echinococcus multilocularis* in relation to human infection. *The Journal of parasitology*, 1991: p. 133-137.

51. Vervaeke, M., et al., Implications of increased susceptibility to predation for managing the sylvatic cycle of *Echinococcus multilocularis*. *Parasitology*, 2006. 132(6): p. 893.
52. Rausch, R.L. and J. Bernstein, *Echinococcus vogeli* sp. (Cestoda: Taeniidae) from the bush dog, *Speothos venaticus* (Lund). 1972.
53. Hitchman, R.B., et al., Improved expression of secreted and membrane targeted proteins in insect cells. *Biotechnology and applied biochemistry*, 2010. 56(3): p. 85-93.
54. Ibrahim, M., et al., Livestock hydatid disease (cystic hydatidosis) in Libya: a review. *American Journal of Animal and Veterinary Sciences*, 2016. 11(2): p. 70-84.
55. Tamarozzi, F., P. Deplazes, and A. Casulli, Reinventing the Wheel of *Echinococcus granulosus sensu lato* Transmission to Humans. *Trends in Parasitology*, 2020.
56. Camicia, F., et al., The nervous and prenervous roles of serotonin in *Echinococcus* spp. *International journal for parasitology*, 2013. 43(8): p. 647-659.
57. Freissmuth, M., T. Stockner, and S. Sucic, SLC6 transporter folding diseases and pharmacochaperoning. *Targeting Trafficking in Drug Development*, 2017: p. 249-270.
58. Sloley, B.D., Metabolism of monoamines in invertebrates: the relative importance of monoamine oxidase in different phyla. *Neurotoxicology*, 2004. 25(1-2): p. 175-183.
59. Catto, B.A. and E.A. Ottesen, Serotonin uptake in schistosomules of *Schistosoma mansoni*. *Comparative Biochemistry and Physiology Part C: Comparative Pharmacology*, 1979. 63(2): p. 235-242.
60. Moreno, M.S. and J. Barrett, Monoamine oxidase in adult *Hymenolepis diminuta* (Cestoda). *Parasitology*, 1979. 78(1): p. 1-5.
61. Ribeiro, P. and R.A. Webb, The occurrence, synthesis and metabolism of 5-hydroxytryptamine and 5-hydroxytryptophan in the cestode *Hymenolepis diminuta*: A high performance liquid chromatographic study. *Comparative Biochemistry and physiology. C, Comparative Pharmacology and Toxicology*, 1984. 79(1): p. 159-164.
62. Frazer, A. and J. Hensler, Serotonin involvement in physiological function and behaviour. 1999, Lippincott-Raven, Philadelphia, Pa, USA.

63. Young, S.N. and M. Leyton, The role of serotonin in human mood and social interaction: insight from altered tryptophan levels. *Pharmacology Biochemistry and Behavior*, 2002. 71(4): p. 857-865.
64. Li, D. and L. He, Meta-analysis supports association between serotonin transporter (5-HTT) and suicidal behavior. *Molecular psychiatry*, 2007. 12(1): p. 47-54.
65. Fanciulli, G., et al., Serotonin pathway in carcinoid syndrome: Clinical, diagnostic, prognostic and therapeutic implications. *Reviews in Endocrine and Metabolic Disorders*, 2020: p. 1-14.
66. Ranganathan, R., S.C. Cannon, and H.R. Horvitz, MOD-1 is a serotonin-gated chloride channel that modulates locomotory behaviour in *C. elegans*. *Nature*, 2000. 408(6811): p. 470-475.
67. Brownlee, D., et al., Immunocytochemical localization of serotonin (5-HT) in the nervous system of the hydatid organism, *Echinococcus granulosus* (Cestoda, Cyclophyllidea). *Parasitology*, 1994. 109(2): p. 233-241.
68. Fairweather, I., et al., Serotonergic and peptidergic nerve elements in the protoscolex of *Echinococcus granulosus* (Cestoda, Cyclophyllidea). *Parasitology research*, 1994. 80(8): p. 649-656.
69. Backstram, T. and S. Winberg, Serotonin coordinates responses to social stress What we can learn from fish. *Frontiers in neuroscience*, 2017. 11: p. 595.
70. Kristensen, A.S., et al., SLC6 neurotransmitter transporters: structure, function, and regulation. *Pharmacological reviews*, 2011. 63(3): p. 585-640.
71. Ayka, A. and A.O. Sehirli, The role of the SLC transporters protein in the neurodegenerative disorders. *Clinical Psychopharmacology and Neuroscience*, 2020. 18(2): p. 174.
72. Englund, G., et al., Regional levels of drug transporters along the human intestinal tract: co-expression of ABC and SLC transporters and comparison with Caco-2 cells. *European Journal of Pharmaceutical Sciences*, 2006. 29(3-4): p. 269-277.
73. Hellsberg, E., et al., A structural model of the human serotonin transporter in an outward-occluded state. *PloS one*, 2019. 14(6): p. e0217377.
74. Hediger, M.A., et al., The ABCs of solute carriers: physiological, pathological and therapeutic implications of human membrane transport proteins. *Pflagers Archiv*, 2004. 447(5): p. 465-468.

75. Barnes, N.M., et al., The 5-HT₃ receptor the relationship between structure and function. *Neuropharmacology*, 2009. 56(1): p. 273-284.
76. Colas, C., P.M.-U. Ung, and A. Schlessinger, SLC transporters: structure, function, and drug discovery. *Medchemcomm*, 2016. 7(6): p. 1069-1081.
77. Liu, X., SLC family transporters. *Drug Transporters in Drug Disposition, Effects and Toxicity*, 2019: p. 101-202.
78. Lin, L., et al., SLC transporters as therapeutic targets: emerging opportunities. *Nature reviews Drug discovery*, 2015. 14(8): p. 543-560.
79. Perland, E. and R. Fredriksson, Classification systems of secondary active transporters. *Trends in pharmacological sciences*, 2017. 38(3): p. 305-315.
80. Sijben, H.J., et al., A study of the dopamine transporter using the TRACT assay, a novel in vitro tool for solute carrier drug discovery. *Scientific reports*, 2021. 11(1): p. 1-14.
81. van Munster, B.C., et al., The association of the dopamine transporter gene and the dopamine receptor 2 gene with delirium, a meta analysis. *American Journal of Medical Genetics Part B: Neuropsychiatric Genetics*, 2010. 153(2): p. 648-655.
82. Lee, A.K., et al., Effect of high-fat feeding on expression of genes controlling availability of dopamine in mouse hypothalamus. *Nutrition*, 2010. 26(4): p. 411-422.
83. Jardetzky, O., Simple allosteric model for membrane pumps. *Nature*, 1966. 211(5052): p. 969-970.
84. Zhang, Y.-W., B.E. Turk, and G. Rudnick, Control of serotonin transporter phosphorylation by conformational state. *Proceedings of the National Academy of Sciences*, 2016. 113(20): p. E2776-E2783.
85. Kolds, H., et al., Ligand induced conformational changes of the human serotonin transporter revealed by molecular dynamics simulations. *PloS one*, 2013. 8(6): p. e63635.
86. Coleman, J.A., E.M. Green, and E. Gouaux, X-ray structures and mechanism of the human serotonin transporter. *Nature*, 2016. 532(7599): p. 334-339.
87. Coleman, J.A. and E. Gouaux, Structural basis for recognition of diverse antidepressants by the human serotonin transporter. *Nature structural & molecular biology*, 2018. 25(2): p. 170-175.
88. Coleman, J.A., et al., Serotonin transporter ibogaine complexes illuminate mechanisms of inhibition and transport. *Nature*, 2019. 569(7754): p. 141-145.

89. Ben-Zvi, A., et al., Mfsd2a is critical for the formation and function of the blood brain barrier. *Nature*, 2014. 509(7501): p. 507-511.
90. Jeschke, G., A comparative study of structures and structural transitions of secondary transporters with the LeuT fold. *European Biophysics Journal*, 2013. 42(2-3): p. 181-197.
91. Perez, C. and C. Ziegler, Mechanistic aspects of sodium-binding sites in LeuT-like fold symporters. *Biological chemistry*, 2013. 394(5): p. 641-648.
92. Quick, M., et al., The LeuT-fold neurotransmitter: sodium symporter MhsT has two substrate sites. *Proceedings of the National Academy of Sciences*, 2018. 115(34): p. E7924-E7931.
93. Kazmier, K., D.P. Claxton, and H.S. Mchaourab, Alternating access mechanisms of LeuT-fold transporters: trailblazing towards the promised energy landscapes. *Current opinion in structural biology*, 2017. 45: p. 100-108.
94. Khafizov, K., et al., A study of the evolution of inverted-topology repeats from LeuT-fold transporters using AlignMe. *Biochemistry*, 2010. 49(50): p. 10702-10713.
95. Joseph, D., et al., Structure and gating dynamics of Na⁺/Cl⁻ coupled neurotransmitter transporters. *Frontiers in molecular biosciences*, 2019. 6: p. 80.
96. Yamashita, A., et al., Crystal structure of a bacterial homologue of Na⁺/Cl⁻ dependent neurotransmitter transporters. *Nature*, 2005. 437(7056): p. 215-223.
97. Rosenberg, M.F., et al., Three-dimensional structure of P-glycoprotein: the transmembrane regions adopt an asymmetric configuration in the nucleotide-bound state. *Journal of Biological Chemistry*, 2005. 280(4): p. 2857-2862.
98. Wang, X., et al., Study of two G-protein coupled receptor variants of human trace amine-associated receptor 5. *Scientific reports*, 2011. 1: p. 102.
99. Norregaard, L., et al., Delineation of an endogenous zinc binding site in the human dopamine transporter. *The EMBO journal*, 1998. 17(15): p. 4266-4273.
100. Stockner, T., et al., Mutational analysis of the high-affinity zinc binding site validates a refined human dopamine transporter homology model. *PLoS Comput Biol*, 2013. 9(2): p. e1002909.
101. Asjad, H.M.M., Trafficking, folding and pharmacological rescue of dopamine transporter mutants linked with infantile parkinsonism-dystonia. 2017, Medical University of Vienna.

102. Korkhov, V.M., et al., The conserved glutamate (Glu136) in transmembrane domain 2 of the serotonin transporter is required for the conformational switch in the transport cycle. *Journal of Biological Chemistry*, 2006. 281(19): p. 13439-13448.
103. El-Kasaby, A., et al., A cytosolic relay of heat shock proteins HSP70-1A and HSP90 monitors the folding trajectory of the serotonin transporter. *Journal of Biological Chemistry*, 2014. 289(42): p. 28987-29000.
104. Asjad, H.M., et al., Pharmacochaperoning in a *Drosophila* model system rescues human dopamine transporter variants associated with infantile/juvenile parkinsonism. *Journal of Biological Chemistry*, 2017. 292(47): p. 19250-19265.
105. El-Kasaby, A., et al. How does the carboxyl terminus assist folding and ER export of the serotonin transporter? in *BMC Pharmacology and Toxicology*. 2012. Springer.
106. Bhat, S., A.H. Newman, and M. Freissmuth, How to rescue misfolded SERT, DAT and NET: targeting conformational intermediates with atypical inhibitors and partial releasers. *Biochem Soc Trans*, 2019. 47(3): p. 861-874.
107. Beerepoot, P., V.M. Lam, and A. Salahpour, Pharmacological chaperones of the dopamine transporter rescue dopamine transporter deficiency syndrome mutations in heterologous cells. *Journal of Biological Chemistry*, 2016. 291(42): p. 22053-22062.
108. Taguchi, K., et al., Role of the E3 ubiquitin ligase HRD1 in the regulation of serotonin transporter function. *Biochemical and Biophysical Research Communications*, 2020.
109. Miles, J.S. and C.R. Wolf, Principles of DNA cloning. *BMJ: British Medical Journal*, 1989. 299(6706): p. 1019.
110. Mullis, K.B., The polymerase chain reaction (Nobel Lecture). *Angewandte Chemie International Edition in English*, 1994. 33(12): p. 1209-1213.
111. Fisher, C.L. and G.K. Pei, Modification of a PCRBased Site-Directed Mutagenesis Method. *Biotechniques*, 1997. 23(4): p. 570-574.
112. Deng, W.P. and J.A. Nickoloff, Site-directed mutagenesis of virtually any plasmid by eliminating a unique site. *Analytical biochemistry*, 1992. 200(1): p. 81-88.
113. Carter, P., Site-directed mutagenesis. *Biochemical Journal*, 1986. 237(1): p. 1.
114. Sarkar, G. and S.S. Sommer, The " megaprimer" method of site-directed mutagenesis. *BioTechniques*, 1990. 8(4): p. 404-407.

115. Henrich, E., et al., Membrane protein production in Escherichia coli cell-free lysates. *FEBS letters*, 2015. 589(15): p. 1713-1722.
116. Haberstock, S., et al., A systematic approach to increase the efficiency of membrane protein production in cell-free expression systems. *Protein expression and purification*, 2012. 82(2): p. 308-316.
117. Lyukmanova, E., et al., Lipid protein nanodiscs for cell-free production of integral membrane proteins in a soluble and folded state: comparison with detergent micelles, bicelles and liposomes. *Biochimica et Biophysica Acta (BBA)-Biomembranes*, 2012. 1818(3): p. 349-358.
118. Henrich, E., V. Dastsch, and F. Bernhard, Screening for lipid requirements of membrane proteins by combining cell-free expression with nanodiscs. *Methods in enzymology*, 2015. 556: p. 351-369.
119. Miliara, X., et al., Structural determinants of lipid specificity within Ups/PRELI lipid transfer proteins. *Nature communications*, 2019. 10(1): p. 1-15.
120. Rues, R.-B., et al., Membrane protein production in E. coli lysates in presence of preassembled nanodiscs, in *Heterologous Gene Expression in E. coli*. 2017, Springer. p. 291-312.
121. Roos, C., et al., High-level cell-free production of membrane proteins with nanodiscs, in *Cell-Free Protein Synthesis*. 2014, Springer. p. 109-130.
122. MacVicar, T., et al., Lipid signalling drives proteolytic rewiring of mitochondria by YME1L. *Nature*, 2019. 575(7782): p. 361-365.
123. Schwarz, D., et al., Preparative scale cell-free expression systems: new tools for the large scale preparation of integral membrane proteins for functional and structural studies. *Methods*, 2007. 41(4): p. 355-369.
124. Bayburt, T.H., Y.V. Grinkova, and S.G. Sligar, Self-assembly of discoidal phospholipid bilayer nanoparticles with membrane scaffold proteins. *Nano letters*, 2002. 2(8): p. 853-856.
125. Denisov, I.G., et al., Directed self-assembly of monodisperse phospholipid bilayer Nanodiscs with controlled size. *Journal of the American Chemical Society*, 2004. 126(11): p. 3477-3487.
126. Gopal, G.J. and A. Kumar, Strategies for the production of recombinant protein in Escherichia coli. *The protein journal*, 2013. 32(6): p. 419-425.

127. Hemamalini, N., S. Ezhilmathi, and A.A. Mercy, Recombinant protein expression optimization in *Escherichia coli*: A review. *Indian Journal of Animal Research*, 2020. 54(6).
128. Arya, R., et al., Optimization of culture parameters and novel strategies to improve protein solubility. *Insoluble Proteins*, 2015: p. 45-63.
129. Joseph, B.C., et al., An overview of the parameters for recombinant protein expression in *Escherichia coli*. *Journal of Cell Science and Therapy*, 2015. 6(5): p. 1.
130. Akiba, H. and K. Tsumoto, Expression in bacteria and refolding, in *Advanced Methods in Structural Biology*. 2016, Springer. p. 3-23.
131. Felberbaum, R.S., The baculovirus expression vector system: A commercial manufacturing platform for viral vaccines and gene therapy vectors. *Biotechnology journal*, 2015. 10(5): p. 702-714.
132. Steele, K.H., et al., Improving the baculovirus expression vector system with vankyrin enhanced technology. *Biotechnology progress*, 2017. 33(6): p. 1496-1507.
133. Palomares, L.A., M. Realpe, and O.T. Ramirez, An overview of cell culture engineering for the insect cell-baculovirus expression vector system (BEVS). *Animal Cell Culture*, 2015: p. 501-519.
134. Mori, K., et al., Efficient production of antibody Fab fragment by transient gene expression in insect cells. *Journal of bioscience and bioengineering*, 2017. 124(2): p. 221-226.
135. Shen, X., et al., A simple plasmid-based transient gene expression method using High Five cells. *Journal of biotechnology*, 2015. 216: p. 67-75.
136. Bleckmann, M., et al., Identifying parameters to improve the reproducibility of transient gene expression in High Five cells. *PloS one*, 2019. 14(6).
137. Puente-Massaguer, E., M. Lecina, and F. Gáñdia, Nanoscale characterization coupled to multi-parametric optimization of Hi5 cell transient gene expression. *Applied microbiology and biotechnology*, 2018. 102(24): p. 10495-10510.
138. Lung, O., et al., Pseudotyping *Autographa californica* multicausid nucleopolyhedrovirus (AcMNPV): F proteins from group II NPVs are functionally analogous to AcMNPV GP64. *Journal of virology*, 2002. 76(11): p. 5729-5736.
139. Slack, J. and B.M. Arif, The baculovirus occlusion derived virus: virion structure and function. *Advances in virus research*, 2006. 69: p. 99-165.

140. Wu, W. and A.L. Passarelli, *Autographa californica* multiple nucleopolyhedrovirus Ac92 (ORF92, P33) is required for budded virus production and multiply enveloped occlusion-derived virus formation. *Journal of virology*, 2010. 84(23): p. 12351-12361.
141. Cardarelli, F., et al., The intracellular trafficking mechanism of Lipofectamine-based transfection reagents and its implication for gene delivery. *Scientific reports*, 2016. 6(1): p. 1-8.
142. Longo, P.A., et al., Transient mammalian cell transfection with polyethylenimine (PEI). *Methods in enzymology*, 2013. 529: p. 227-240.
143. Boussif, O., et al., A versatile vector for gene and oligonucleotide transfer into cells in culture and in vivo: polyethylenimine. *Proceedings of the National Academy of Sciences*, 1995. 92(16): p. 7297-7301.
144. Benslimane, C., et al., Insights into the central metabolism of *Spodoptera frugiperda* (Sf9) and *Trichoplusia ni* (Tn5) insect cells by radiolabeling studies. *Biotechnology progress*, 2005. 21(1): p. 78-86.
145. Rhiel, M., C.M. Mitchell Logean, and D.W. Murhammer, Comparison of *Trichoplusia ni* BTITn5B14 (high five[™]) and *Spodoptera frugiperda* Sf9 insect cell line metabolism in suspension cultures. *Biotechnology and bioengineering*, 1997. 55(6): p. 909-920.
146. Cadena-Herrera, D., et al., Validation of three viable-cell counting methods: manual, semi-automated, and automated. *Biotechnology Reports*, 2015. 7: p. 9-16.
147. Hitchman, R.B., R.D. Possee, and L.A. King, Baculovirus expression systems for recombinant protein production in insect cells. *Recent patents on biotechnology*, 2009. 3(1): p. 46-54.
148. Hitchman, R.B., et al., Genetic modification of a baculovirus vector for increased expression in insect cells. *Cell biology and toxicology*, 2010. 26(1): p. 57-68.
149. Gamez-Sebastian, S., J. Laípez-Vidal, and J.M. Escribano, Significant productivity improvement of the baculovirus expression vector system by engineering a novel expression cassette. *PLoS One*, 2014. 9(5): p. e96562.
150. Dyson, M.R., *Fundamentals of expression in mammalian cells. Advanced Technologies for Protein Complex Production and Characterization*, 2016: p. 217-224.
151. Joeger, V., K. Bażssow, and T. Schirrmann, Transient recombinant protein expression in mammalian cells. *Animal cell culture*, 2015: p. 27-64.

152. Oluwole, A.O., et al., Formation of lipid-bilayer nanodiscs by diisobutylene/maleic acid (DIBMA) copolymer. *Langmuir*, 2017. 33(50): p. 14378-14388.
153. Gulamhussein, A.A., et al., A comparison of SMA (styrene maleic acid) and DIBMA (di-isobutylene maleic acid) for membrane protein purification. *Biochimica et Biophysica Acta (BBA)-Biomembranes*, 2020. 1862(7): p. 183281.
154. Smith, S.M., Strategies for the purification of membrane proteins, in *Protein Chromatography*. 2011, Springer. p. 485-496.
155. Lee, B.-K., et al., Affinity purification and characterization of a G-protein coupled receptor, *Saccharomyces cerevisiae* Ste2p. *Protein expression and purification*, 2007. 56(1): p. 62-71.
156. Cummins, P.M., K.D. Rochfort, and B.F. O Connor, Ion-exchange chromatography: basic principles and application, in *Protein chromatography*. 2017, Springer. p. 209-223.
157. Yamamoto, S., K. Nakanishi, and R. Matsuno, *Ion-exchange chromatography of proteins*. 1988: CRC Press.
158. Ladner, C.L., et al., Visible fluorescent detection of proteins in polyacrylamide gels without staining. *Analytical biochemistry*, 2004. 326(1): p. 13-20.
159. de Moreno, M.R., J.F. Smith, and R.V. Smith, Silver staining of proteins in polyacrylamide gels: increased sensitivity through a combined Coomassie blue-silver stain procedure. *Analytical biochemistry*, 1985. 151(2): p. 466-470.
160. Demchenko, A.V., *Handbook of chemical glycosylation: advances in stereoselectivity and therapeutic relevance*. 2008: John Wiley and Sons.
161. Zhang, H., et al., Identification and quantification of N-linked glycoproteins using hydrazide chemistry, stable isotope labeling and mass spectrometry. *Nature biotechnology*, 2003. 21(6): p. 660-666.
162. Maley, F., et al., Characterization of glycoproteins and their associated oligosaccharides through the use of endoglycosidases. *Analytical biochemistry*, 1989. 180(2): p. 195-204.
163. Fecher-Trost, C., et al., The in vivo TRPV6 protein starts at a non-AUG triplet, decoded as methionine, upstream of canonical initiation at AUG. *Journal of Biological Chemistry*, 2013. 288(23): p. 16629-16644.

164. Francelle, L., T.F. Outeiro, and G.A. Rappold, Inhibition of HDAC6 activity protects dopaminergic neurons from alpha-synuclein toxicity. *Scientific reports*, 2020. 10(1): p. 1-14.
165. Kelly, S.M., T.J. Jess, and N.C. Price, How to study proteins by circular dichroism. *Biochimica et Biophysica Acta (BBA)-Proteins and Proteomics*, 2005. 1751(2): p. 119-139.
166. Bonifacino, J.S. and B.S. Glick, The mechanisms of vesicle budding and fusion. *cell*, 2004. 116(2): p. 153-166.
167. Wyles, J.P., C.R. McMaster, and N.D. Ridgway, Vesicle-associated membrane protein-associated protein-A (VAP-A) interacts with the oxysterol-binding protein to modify export from the endoplasmic reticulum. *Journal of Biological Chemistry*, 2002. 277(33): p. 29908-29918.
168. Itin, C., R. Schindler, and H.-P. Hauri, Targeting of protein ERGIC-53 to the ER/ERGIC/cis-Golgi recycling pathway. *The Journal of cell biology*, 1995. 131(1): p. 57-67.
169. Puthenveedu, M.A., et al., GM130 and GRASP65-dependent lateral cisternal fusion allows uniform Golgi-enzyme distribution. *Nature cell biology*, 2006. 8(3): p. 238-248.
170. Rohrer, J., et al., The targeting of Lamp1 to lysosomes is dependent on the spacing of its cytoplasmic tail tyrosine sorting motif relative to the membrane. *The Journal of cell biology*, 1996. 132(4): p. 565-576.
171. Rubino, M., et al., Selective membrane recruitment of EEA1 suggests a role in directional transport of clathrin-coated vesicles to early endosomes. *Journal of Biological Chemistry*, 2000. 275(6): p. 3745-3748.
172. Echard, A., et al., Interaction of a Golgi-associated kinesin-like protein with Rab6. *Science*, 1998. 279(5350): p. 580-585.
173. Ullrich, O., et al., Rab11 regulates recycling through the pericentriolar recycling endosome. *The Journal of cell biology*, 1996. 135(4): p. 913-924.
174. Kozieł, K., et al., Plasma membrane associated membranes (PAM) from Jurkat cells contain STIM1 protein: is PAM involved in the capacitative calcium entry? *The international journal of biochemistry & cell biology*, 2009. 41(12): p. 2440-2449.

175. Pichler, H., et al., A subfraction of the yeast endoplasmic reticulum associates with the plasma membrane and has a high capacity to synthesize lipids. *European journal of biochemistry*, 2001. 268(8): p. 2351-2361.
176. Mamuti, W., et al., *Echinococcus multilocularis*: developmental stage-specific expression of Antigen B 8-kDa-subunits. *Experimental parasitology*, 2006. 113(2): p. 75-82.
177. Worms, D., et al., Expression, purification and stabilization of human serotonin transporter from *E. coli*. *Protein expression and purification*, 2019. 164: p. 105479.
178. Green, E.M., J.A. Coleman, and E. Gouaux, Thermostabilization of the human serotonin transporter in an antidepressant-bound conformation. *PloS one*, 2015. 10(12).
180. Sharma, D., et al., *M. tuberculosis* ferritin (Rv3841): potential involvement in Amikacin (AK) and Kanamycin (KM) resistance. *Biochemical and biophysical research communications*, 2016. 478(2): p. 908-912.
181. Lee, J., et al., Generating in vivo cloning vectors for parallel cloning of large gene clusters by homologous recombination. *PLoS One*, 2013. 8(11): p. e79979.
182. Matsumura, I., M.J. Olsen, and A.D. Ellington, Optimization of heterologous gene expression for in vitro evolution. *Biotechniques*, 2001. 30(3): p. 474-476.
183. Inagaki, S., R. Ghirlando, and R. Grishammer, Biophysical characterization of membrane proteins in nanodiscs. *Methods*, 2013. 59(3): p. 287-300.
184. Bayburt, T.H. and S.G. Sligar, Membrane protein assembly into Nanodiscs. *FEBS letters*, 2010. 584(9): p. 1721-1727.
185. Marty, M.T., et al., Probing the Lipid Annular Belt by GasPhase Dissociation of Membrane Proteins in Nanodiscs. *Angewandte Chemie International Edition*, 2016. 55(2): p. 550-554.
186. Wilde, M., et al., Tn 38, high five and Sf 9 evaluation of host virus interactions in three different insect cell lines: baculovirus production and recombinant protein expression. *Biotechnology letters*, 2014. 36(4): p. 743-749.
187. Krishnamurthy, H. and E. Gouaux, X-ray structures of LeuT in substrate-free outward-open and apo inward-open states. *Nature*, 2012. 481(7382): p. 469-474.
188. Baker, J.D., et al., Hsp90 heterocomplexes regulate steroid hormone receptors: from stress response to psychiatric disease. *International journal of molecular sciences*, 2019. 20(1): p. 79.

189. Bhat, S., et al., Tropane-Based Ibogaine Analog Rescues Folding-Deficient Serotonin and Dopamine Transporters. *ACS Pharmacology & Translational Science*, 2020.
190. Bhat, S., et al., A tropane-based ibogaine analog rescues folding-deficient SERT and DAT. *bioRxiv*, 2020.
191. Oluwole, A.O., et al., Solubilization of membrane proteins into functional lipid bilayer nanodiscs using a diisobutylene/maleic acid copolymer. *Angewandte Chemie International Edition*, 2017. 56(7): p. 1919-1924.
192. Navratna, V. and E. Gouaux, Insights into the mechanism and pharmacology of neurotransmitter sodium symporters. *Current opinion in structural biology*, 2019. 54: p. 161-170.
193. Mueller, I.R., et al., Conformational dynamics of the human serotonin transporter during substrate and drug binding. *Nature communications*, 2019. 10(1): p. 1-13.
194. Hasenhuettl, P.S., et al., A kinetic account for amphetamine-induced monoamine release. *Journal of General Physiology*, 2018. 150(3): p. 431-451.
195. Haase, J., et al., Serotonin transporter associated protein complexes are enriched in synaptic vesicle proteins and proteins involved in energy metabolism and ion homeostasis. *ACS chemical neuroscience*, 2017. 8(5): p. 1101-1116.
196. El-Kasaby, A., et al., Mutations in the carboxyl-terminal SEC24 binding motif of the serotonin transporter impair folding of the transporter. *Journal of Biological Chemistry*, 2010. 285(50): p. 39201-39210.
197. Litvinov, D.Y., E.V. Savushkin, and A.D. Dergunov, Intracellular and plasma membrane events in cholesterol transport and homeostasis. *Journal of lipids*, 2018. 2018.
198. Ikonen, E., Mechanisms of cellular cholesterol compartmentalization: recent insights. *Current opinion in cell biology*, 2018. 53: p. 77-83.
199. Wastner, D. and K. Solanko, How cholesterol interacts with proteins and lipids during its intracellular transport. *Biochimica et Biophysica Acta (BBA)-Biomembranes*, 2015. 1848(9): p. 1908-1926.
200. Raffy, S. and J. Teissie, Control of lipid membrane stability by cholesterol content. *Biophysical journal*, 1999. 76(4): p. 2072-2080.

201. Guex, N., M.C. Peitsch, and T. Schwede, Automated comparative protein structure modeling with SWISS MODEL and Swiss PdbViewer: A historical perspective. *Electrophoresis*, 2009. 30(S1): p. S162-S173.
202. Waterhouse, A., et al., SWISS-MODEL: homology modelling of protein structures and complexes. *Nucleic acids research*, 2018. 46(W1): p. W296-W303.
203. Bienert, S., et al., The SWISS-MODEL Repository new features and functionality. *Nucleic acids research*, 2017. 45(D1): p. D313-D319.
204. Kornfeld, R. and S. Kornfeld, Assembly of asparagine-linked oligosaccharides. *Annual review of biochemistry*, 1985. 54(1): p. 631-664.
205. Freeze, H.H. and C. Kranz, Endoglycosidase and glycoamidase release of N linked glycans. *Current protocols in molecular biology*, 2010. 89(1): p. 17.13 A. 1-17.13 A. 25.
206. Rogala-Koziarska, K., L.u. Samluk, and K.A. Nacz, Amino acid transporter SLC6A14 depends on heat shock protein HSP90 in trafficking to the cell surface. *Biochimica et Biophysica Acta (BBA)-Molecular Cell Research*, 2019. 1866(10): p. 1544-1555.
207. Kikkert, M., et al., Human HRD1 is an E3 ubiquitin ligase involved in degradation of proteins from the endoplasmic reticulum. *Journal of Biological Chemistry*, 2004. 279(5): p. 3525-3534.

Abbreviations

ATP	Adenosinetriphosphate
CD	Circular Dichroism
COPII	coat protein II
CV	Column volume
DAT	dopamine transporter
DLS	Dynamic light scattering
DMSO	dimethyl sulfoxide
DNA	Deoxyribonucleic acid
<i>E. coli</i>	<i>Escherichia coli</i>
EDTA	Ethylendiethyltetraacetic acid
ER	Endoplasmic reticulum

ERAD	ER-associated protein degradation
ERGIC	ER–Golgi intermediate compartment
HSP	heat shock protein
IMAC	Immobilized metal affinity chromatography
IPTG	Isopropyl β -D-1-thiogalactopyranoside
LAMP2	lysosome-associated membrane protein
M_w	Molecular weight
MS	Mass spectrometry
MS/MS	Tandem MS
Na^+	sodium ion
NET	norepinephrine transporter
OD	Optical density
PAGE	Polyacrylamide gel electrophoresis
PBS	Phosphate buered saline
PCR	Polymerase chain reaction
PFA	paraformaldehyde
PMSF	Phenylmethanesulfonyl fluoride
PVDF	Polyvinylidene difluoride
SDS	Sodium dodecyl sulfate
SEC	Size exclusion chromatography
ST	serotonin transporter
SLC6	solute carrier 6
SSRIs	selective serotonin reuptake inhibitors
TCEP	Tris (2-chlorethyl) phosphine
TEMED	Tetramethylethylenediamine
TM	Transmembrane
Tris	Tris (hydroxymethyl) aminomethane
UV	Ultraviolet
VAP-A	vesicle-associated membrane protein-associated protein-A
WT	wild type
β -ME	β -Mercaptoethanol

Appendix I: DNA and protein sequences

emST DNA Sequence

ATG GAA GAT CAG TCC CTC AAG AGC TGC AAC CTG CAG GAC GCT ACC CCT TCT TTG GTG GAC GCT
GTG GTG GTG GAA ACC GCT GAG GCT GTG GTC ACT AAG GTG GAA CGC AAG CGC GAG AAG TGG GAT
ACC AAG ATC GAC TTC CTG CTG TCC GTG ATC GGT TTC GCT GTG GAC CTG GGC AAT ATC TGG CGT
TTC CCC TAC ATC TGC TAC CAG AAC GGT GGC GAG CAC CGT ATC TGC GCT TTC TTG ATC CCC TAC
CTG CTC ATG TAC ATC TTC GGT GGC CTG CCT CTG TTC TAC CTC GAG CTG GCT CTG GGA CAG TTC
CAG CGT TCC GGT TGC ATC TCT GTG TGG TCC CGC ATC TGC CCA TTC TTC ACC GGA CTC GGT TAC
GGT ATC TGC ATC ATT GCT AGC TAC ACC GCC TGG TAC TAC AAC ACC GTG ATC TCT TGG GCC CTG
TTC TAC ATG TTC GAC TCC ATG CGT CTG CGT CTG CCC TGG GAC TCT TGC GAC AAC TGG TGG AAC
ACC CCT AAG ACC TGC ATC ACC GTG TAC CAA AAG CTG GTC ACC GGT GCT AAC TCC TCC GAT ATC
GCT GAC TCC GAC GCT TCT AAC ACC CTG CAC GCT GTG AAC ACC ACC GGT TAC TAC TCC TCC ACC
GAG CAG TAC TTC TAC AAC CGT GTG CTG CAG ATC CAG CTG TCC GAC GGT TTC AAC AAG CTG GGC
ACC ATC CGT TGG GAA GTC GCT CTG TGC CTG CTG GCT GTG TTC ACC CTG GTG TAC TTC GCT CTC
TGG AAG GGT GTC AAG TCC TCC GGC AAG GCT GTG TGG ATC ACC GCT ACT CTG CCT TAC GTG ATC
CTG TTC ATC CTG CTG ATC CGC GGA CTG ACC CTG AGG GGT TCT CTG ATG GGT ATC CAG TAC TAC
CTG CTG CCT GAC TTC GGT CGT CTG AAG TCC ATC GAA GTG TGG AAC GCT GCT GCT TCC CAG ATC
TTC TTC TCC CTC GGT CCT GGT TTC GGC GTG CTG CTG GCT TTG GCT TCC TAC AAC CGC TTC CGT
AAC AAC TGC TAC TAC GAC GCT ATG CTG ACC TCC GCT ATC AAC TGC GGA ACC TCC TTC CTG TCC
GGT TTC GTG GTG TTC TCC GTG CTG GGT CAC ATG TGC TAC CGT ATG AAC CGT ACC ATG GAC ACC
GTG GCT AAC GAG GGT CCC AGC CTG GTG TTC ATT GCT TAC CCC GAG GCT ATC GCT ACC CTG CCT
GGT TCC ACT TTC TGG GCT ATC ATC TTC ATG CTG ATG CTG ATC ACC CTG GGC CTC GAC TCC ACC
TTC GGT GGA TTG GAA GCT ATC ATC ACC GCT CTG CTG GAC CGT TGG CCT AAG CTG AGA AAG CGT
CGC GAG ATC GTG GTG CTC ATC ATG ATC ATC TAC TGC TAC GTG GGT GCT CTG CCT ACC ACC ACC
AAC GGT GGT TAC TAC ATC TTG ACC CTG TTC GAC ACC TAC GGC GCT CCC TTC TCC ATC TTG TTC ATC
GTG TTC TGC GAG TGC GTG GCC CTG TGC TGG TGT TAC GGT GTC GGT CGT TTC ACC CGT GAC ATC
GAG TCC ATG CTG GGT TTC AAG CCC GGA TGG TTC TGG CGC ATC TGC TGG GCT GTT ATC TCC CCT
GCT TTC ATG CTG GGC ATC TTT ATC CTG AAC ATC ACT TTC TTC AGG CCG CCT GAG ATC ACC GTG
ATG GGC AAG ACT GTG CGT GCT GAC ACT TGG GTG CAC GTG GTG TCT TGG ATG CTC GTG TTC TCC
TCT CTG GTC ACT ATC CCC ATC TTC GCT GTC GTG ACC TTC TGC TCC GCT CGT GGT TCC TTC AAA
GAG CGC CTG AAG TCC CTG TTC ACT CCC GGT ATC CGT CCT TCC TTC TCC GAC TTC CAC GTT CAC
CCC AAC TCT CAC AAG AAG CAA GAA ATC AAG GAC AAG GAC GAG GAA CAG GTG GCC AAG TCT GCT
GAA GCT GTG GAC GAC ACT CAG TCC GAA GGC GAC GAA GGT

emST Protein Sequence

MEDQSLKSCNLQDATPSLVDAVVVETA EAVVTKVERKREKWDTKIDFLLSVIGFAVDLGNIWRFPHYICYQNGGEHR
ICAFLLPYLLMYIFGGLPLFYLELALGQFQRSGCISVWSRICPFFTGLGYGICIIASYTAWYYNTVISWALFYMFDSMR
LRLPWDSCDNWWNTPKTCITVYQKLVGTGANSSDIADSDASNTLHAVNTTGYYSSTEQYFYNRVLQIQLSDGFNKL

GTIRWEVALCLLAVFTLVYFALWKGVKSSGKAVWITATLPYVILFILLIRGLTLRGSLMGIQYLLPDFGRLKSIEVWN
AAASQIFFSLGPGFGVLLALASYNRFRNNCYDAMLTSAINCGTSFSLSGFVVFVSLGHMCMYRMRNRTMDTVANEGP
SLVFIAYPEAIATLPGSTFWAIIFMLMLITLGLDSTFGGLEAITALLDRWPKLRKRREIVLIMIIYCYVGALPTTTNNG
YYILTLFDTYGAPFSILFVFCCEVALWCYGVGRFTRDIESMLGFKPGWFWRICWAVISPAFMLGIFILNITFFRPPE
ITVMGKTVRADTWVHVVSWMMLVFSSLVTIPIFAVWTFCSARGSFKERLKSLFTPGIRPSFSDFHVHPNSHKKQEIKD
KDEEQVAKSAEAVDDTQSEGDEG

emST-tm2 DNA Sequence

ATG GAA GAT CAG TCC CTC AAG AGC TGC AAC CTG CAG GAC GCT ACC CCT TCT TTG GTG GAC GCT
GTG GTG GTG GAA ACC GCT GAG GCT GTG GTC ACT AAG GTG GAA CGC AAG CGC GAG AAG TGG GAT
ACC AAG ATC GAC TTC CTG CTG TCC GTG ATC GGT TTC GCT GTG GAC CTG GGC AAT ATC TGG CGT
TTC CCC TAC ATC TGC gcc CAG AAC GGT GGC GAG CAC CGT ATC TGC GCT TTC TTG ATC CCC TAC CTG
CTC ATG TAC ATC TTC GGT GGC CTG CCT CTG TTC TAC CTC GAG CTG GCT CTG GGA CAG TTC CAG
CGT TCC GGT TGC ATC TCT GTG TGG TCC CGC ATC TGC CCA TTC TTC ACC GGA CTC GGT TAC GGT
ATC TGC ATC ATT GCT AGC TAC ACC GCC TGG TAC TAC AAC ACC GTG ATC TCT TGG GCC CTG TTC
TAC ATG TTC GAC TCC ATG CGT CTG CGT CTG CCC TGG GAC TCT TGC GAC AAC TGG TGG AAC ACC
CCT AAG ACC TGC ATC ACC GTG TAC CAA AAG CTG GTC ACC GGT GCT AAC TCC TCC GAT ATC GCT
GAC TCC GAC GCT TCT AAC ACC CTG CAC GCT GTG AAC ACC ACC GGT TAC TAC TCC TCC ACC GAG
CAG TAC TTC TAC AAC CGT GTG CTG CAG ATC CAG CTG TCC GAC GGT TTC AAC AAG CTG GGC ACC
ATC CGT TGG GAA GTC GCT CTG TGC CTG CTG GCT GTG TTC ACC CTG GTG TAC TTC GCT CTC TGG
AAG GGT GTC AAG TCC TCC GGC AAG GCT GTG TGG ATC ACC GCT ACT CTG CCT TAC GTG gcc CTG
TTC ATC CTG CTG ATC CGC GGA CTG ACC CTG AGG GGT TCT CTG ATG GGT ATC CAG TAC TAC CTG
CTG CCT GAC TTC GGT CGT CTG AAG TCC ATC GAA GTG TGG AAC GCT GCT GCT TCC CAG ATC TTC
TTC TCC CTC GGT CCT GGT TTC GGC GTG CTG CTG GCT TTG GCT TCC TAC AAC CGC TTC CGT AAC
AAC TGC TAC TAC GAC GCT ATG CTG ACC TCC GCT ATC AAC TGC GGA ACC TCC TTC CTG TCC GGT
TTC GTG GTG TTC TCC GTG CTG GGT CAC ATG TGC TAC CGT ATG AAC CGT ACC ATG GAC ACC GTG
GCT AAC GAG GGT CCC AGC CTG GTG TTC ATT GCT TAC CCC GAG GCT ATC GCT ACC CTG CCT GGT
TCC ACT TTC TGG GCT ATC ATC TTC ATG CTG ATG CTG ATC ACC CTG GGC CTC GAC TCC ACC TTC
GGT GGA TTG GAA GCT ATC ATC ACC GCT CTG CTG GAC CGT TGG CCT AAG CTG AGA AAG CGT CGC
GAG ATC GTG GTG CTC ATC ATG ATC ATC TAC TGC TAC GTG GGT GCT CTG CCT ACC ACC ACC AAC
GGT GGT TAC TAC ATC TTG ACC CTG TTC GAC ACC TAC GGC GCT CCC TTC TCC ATC TTG TTC ATC GTG
TTC TGC GAG TGC GTG GCC CTG TGC TGG TGT TAC GGT GTC GGT CGT TTC ACC CGT GAC ATC GAG
TCC ATG CTG GGT TTC AAG CCC GGA TGG TTC TGG CGC ATC TGC TGG GCT GTT ATC TCC CCT GCT
TTC ATG CTG GGC ATC TTT ATC CTG AAC ATC ACT TTC TTC AGG CCG CCT GAG ATC ACC GTG ATG
GGC AAG ACT GTG CGT GCT GAC ACT TGG GTG CAC GTG GTG TCT TGG ATG CTC GTG TTC TCC TCT
CTG GTC ACT ATC CCC ATC TTC GCT GTC GTG ACC TTC TGC TCC GCT CGT GGT TCC TTC AAA GAG
CGC CTG AAG TCC CTG TTC ACT CCC GGT ATC CGT CCT TCC TTC TCC GAC TTC CAC GTT CAC CCC
AAC TCT CAC AAG AAG CAA GAA ATC AAG GAC AAG GAC GAG GAA CAG GTG GCC AAG TCT GCT GAA
GCT GTG GAC GAC ACT CAG TCC GAA GGC GAC GAA GGT

emST-tm2 Protein Sequence

MEDQSLKSCNLQDATPSLVDVAVVETA EAVVTKVERKREKWDTKIDFLLSVIGFAVDLGNIWRFYPYIC AQNGGEHR
ICAFILPYLLMYIFGGLPLFYLELALGQFQRSGCISVWSRICPFFTGLGYGICIIASYTAWYYNTVISWALFYMFDSMR

LRLPWDSCDNWWNTPKTCITVYQKLVGTGANSSDIADSDASNTLHAVNTTGYYSSTEQYFYNRVLQIQLSDGFNKL
GTIRWEVALCLLAVFTLVYFALWKGVKSSGKAVWITATLPYV^{AL}FILLIRGLTLRGLSMGIQYLLPDFGRLKSIEVW
NAAASQIFFSLGPGFGVLLALASYNRFRNNCYDAMLTSAINCGTSFLSGFVVFVSVLGHMCMYRMNRTMDTVANEG
PSLVFIAYPEAIATLPGSTFWAIIFMLMLITLGLDSTFGGLEAIITALLDRWPKLKRREIVLMIICYV GALPTTTNG
GYYILTLFDTYGAPFSILFIVFCECVALCWYGVGRFTRDIESMLGFKPGWFWRICWAVISPAFMLGIFILNITFFRPP
EITVMGKTVRADTWVHVVSWMMLVFSSLVTIPIFAVVTFCSARGSFKERLKS LFTP GIRPSFSD FHVHPNSHKKQEIK
DKDEEQVAKSAEAVDDTQSEGDEG

emST-mCherry DNA Sequence

ATG GAA GAT CAG TCC CTC AAG AGC TGC AAC CTG CAG GAC GCT ACC CCT TCT TTG GTG GAC GCT
GTG GTG GTG GAA ACC GCT GAG GCT GTG GTC ACT AAG GTG GAA CGC AAG CGC GAG AAG TGG GAT
ACC AAG ATC GAC TTC CTG CTG TCC GTG ATC GGT TTC GCT GTG GAC CTG GGC AAT ATC TGG CGT
TTC CCC TAC ATC TGC TAC CAG AAC GGT GGC GAG CAC CGT ATC TGC GCT TTC TTG ATC CCC TAC
CTG CTC ATG TAC ATC TTC GGT GGC CTG CCT CTG TTC TAC CTC GAG CTG GCT CTG GGA CAG TTC
CAG CGT TCC GGT TGC ATC TCT GTG TGG TCC CGC ATC TGC CCA TTC TTC ACC GGA CTC GGT TAC
GGT ATC TGC ATC ATT GCT AGC TAC ACC GCC TGG TAC TAC AAC ACC GTG ATC TCT TGG GCC CTG
TTC TAC ATG TTC GAC TCC ATG CGT CTG CGT CTG CCC TGG GAC TCT TGC GAC AAC TGG TGG AAC
ACC CCT AAG ACC TGC ATC ACC GTG TAC CAA AAG CTG GTC ACC GGT GCT AAC TCC TCC GAT ATC
GCT GAC TCC GAC GCT TCT AAC ACC CTG CAC GCT GTG AAC ACC ACC GGT TAC TAC TCC TCC ACC
GAG CAG TAC TTC TAC AAC CGT GTG CTG CAG ATC CAG CTG TCC GAC GGT TTC AAC AAG CTG GGC
ACC ATC CGT TGG GAA GTC GCT CTG TGC CTG CTG GCT GTG TTC ACC CTG GTG TAC TTC GCT CTC
TGG AAG GGT GTC AAG TCC TCC GGC AAG GCT GTG TGG ATC ACC GCT ACT CTG CCT TAC GTG ATC
CTG TTC ATC CTG CTG ATC CGC GGA CTG ACC CTG AGG GGT TCT CTG ATG GGT ATC CAG TAC TAC
CTG CTG CCT GAC TTC GGT CGT CTG AAG TCC ATC GAA GTG TGG AAC GCT GCT GCT TCC CAG ATC
TTC TTC TCC CTC GGT CCT GGT TTC GGC GTG CTG CTG GCT TTG GCT TCC TAC AAC CGC TTC CGT
AAC AAC TGC TAC TAC GAC GCT ATG CTG ACC TCC GCT ATC AAC TGC GGA ACC TCC TTC CTG TCC
GGT TTC GTG GTG TTC TCC GTG CTG GGT CAC ATG TGC TAC CGT ATG AAC CGT ACC ATG GAC ACC
GTG GCT AAC GAG GGT CCC AGC CTG GTG TTC ATT GCT TAC CCC GAG GCT ATC GCT ACC CTG CCT
GGT TCC ACT TTC TGG GCT ATC ATC TTC ATG CTG ATG CTG ATC ACC CTG GGC CTC GAC TCC ACC
TTC GGT GGA TTG GAA GCT ATC ATC ACC GCT CTG CTG GAC CGT TGG CCT AAG CTG AGA AAG CGT
CGC GAG ATC GTG GTG CTC ATC ATG ATC ATC TAC TGC TAC GTG GGT GCT CTG CCT ACC ACC ACC
AAC GGT GGT TAC TAC ATC TTG ACC CTG TTC GAC ACC TAC GGC GCT CCC TTC TCC ATC TTG TTC ATC
GTG TTC TGC GAG TGC GTG GCC CTG TGC TGG TGT TAC GGT GTC GGT CGT TTC ACC CGT GAC ATC
GAG TCC ATG CTG GGT TTC AAG CCC GGA TGG TTC TGG CGC ATC TGC TGG GCT GTT ATC TCC CCT
GCT TTC ATG CTG GGC ATC TTT ATC CTG AAC ATC ACT TTC TTC AGG CCG CCT GAG ATC ACC GTG
ATG GGC AAG ACT GTG CGT GCT GAC ACT TGG GTG CAC GTG GTG TCT TGG ATG CTC GTG TTC TCC
TCT CTG GTC ACT ATC CCC ATC TTC GCT GTC GTG ACC TTC TGC TCC GCT CGT GGT TCC TTC AAA
GAG CGC CTG AAG TCC CTG TTC ACT CCC GGT ATC CGT CCT TCC TTC TCC GAC TTC CAC GTT CAC
CCC AAC TCT CAC AAG AAG CAA GAA ATC AAG GAC AAG GAC GAG GAA CAG GTG GCC AAG TCT GCT
GAA GCT GTG GAC GAC ACT CAG TCC GAA GGC GAC GAA GGT GGT AGC TCC GGT ACT AGT GTG AGC
AAG GGC GAG GAG GAT AAC ATG GCC ATC ATC AAG GAG TTC ATG CGC TTC AAG GTG CAC ATG GAG
GGC TCC GTG AAC GGC CAC GAG TTC GAG ATC GAG GGC GAG GGC GAG GGC CGC CCC TAC GAG GGC
ACC CAG ACC GCC AAG CTG AAG GTG ACC AAG GGT GGC CCC CTG CCC TTC GCC TGG GAC ATC CTG

TCC CCT CAG TTC ATG TAC GGC TCC AAG GCC TAC GTG AAG CAC CCC GCC GAC ATC CCC GAC TAC
TTG AAG CTG TCC TTC CCC GAG GGC TTC AAG TGG GAG CGC GTG ATG AAC TTC GAG GAC GGC GGC
GTG GTG ACC GTG ACC CAG GAC TCC TCC CTG CAG GAC GGC GAG TTC ATC TAC AAG GTG AAG CTG
CGC GGC ACC AAC TTC CCC TCC GAC GGC CCC GTA ATG CAG AAG AAG ACC ATG GGC TGG GAG GCC
TCC TCC GAG CGG ATG TAC CCC GAG GAC GGC GCC CTG AAG GGC GAG ATC AAG CAG AGG CTG AAG
CTG AAG GAC GGC GGC CAC TAC GAC GCT GAG GTC AAG ACC ACC TAC AAG GCC AAG AAG CCC GTG
CAG CTG CCC GGC GCC TAC AAC GTC AAC ATC AAG TTG GAC ATC ACC TCC CAC AAC GAG GAC TAC
ACC ATC GTG GAA CAG TAC GAA CGC GCC GAG GGC CGC CAC TCC ACC GGC GGC ATG GAC GAG CTG
TAC AAG

emST-mCherry Protein Sequence

MEDQSLKSCNLQDATPSLVDVVVETAEAVVTKVERKREKWDTKIDFLLSVIGFAVDLGNIWRFYICYQNGGEHR
ICAFILIPYLLMYIFGGLPLFYLELALGQFQRSGCISVWSRICPFFTGLGYGICIIASYTAWYYNTVISWALFYMFD
SMR LRLPWDSNDNWWNTPKTCITVYQKLVGTANSSDIADSDASNTLHVNNTTGYYSSTEQYFYNRVLQIQLSDGF
NKL GTIRWEVALCLLAVFTLVYFALWKGVKSSGKAVWITATLPYVILFILLIRGLTLRGSLMGIQYYLLPDFGRL
KSIEVWN AAASQIFFSLGPGFGVLLALASYNRFRNNCYDAMLTSAINCGTSFSLSGFVVFVSLGHMCMYRMR
TMDTVANEGP SLVFIAYPEAIATLPGSTFWAIIIFMLMLITLGLDSTFGGLEAIIALLDRWPKLRKRREIV
VLIMIIYCYVGALPTTTNGG YYILTLFDYTGAPFSILFIVFCECVLWCYGVGRFTRDIESMLGFKPGWFW
RICWAVISPAFMLGIFILNITFFRPPE ITVMGKTVRADTWVHVSWMLVFSSLVTIPIFAVVTFC
SARGSFKERLKSIFTPGIRPSFSDFHVHPNSHKKQEIKD KDEEQVAKSAEAVDDTQSEGDEGGSSGLV
SKGEEDNMAIIEFMRFKVHMEGSVNGHEFEIEGEGEGRPYEGTQ TAKLKVTKGGPLPFAWDILSPQF
MYGSKAYVKHPADIPDYLKLSFPEGFKWERVMNFEDGGVVTVTQDSSLQDG EFIYKVKLRGTNFP
SDGPMQKKTMGWEASSERMYPEDGALKGEIKQRLKLDGGHYDAEVKTTYKAKKPVQLP GAYNVNIKLDIT
SHNEDYTIVEQYERAEGRHSTGGMDELYK

Appendix II: Alignment of ST

CLUSTAL O(1.2.4) multiple sequence alignment

```

hSERT  METTPLNSQKQLSACEDGEDCQENGVLQKVVPTPGDKVESGQISNGYSAVPSPGAGDDTR 60
emSERT ME-----DQSLKSCN-----LQDA-----TPS----LV 19
      **      :..*.:*:*      **..      :*.*

hSERT  HSIPATTTTLVAELHQGERETWGKKVDFLLSVIGYAVDLGNVWRFPYICYQNGGG----A 116
emSERT DAVVVETAEAHVTKVERKREKWDTKIDFLLSVIGFAVDLGNVWRFPYICYQNGGEHRICA 79
      .:: . *:* * . : : **.*..*:*:*****:*****:*****:***** *

hSERT  FLLPYTIMAIFGGIPLFYMELALGQYHRNGCISIWKICPIFKGIGYAICIIAFYIASYY 176
emSERT FLIPYLLMYIFGGLPLFYLELALGQFQRSQCISVWSRICPFFTGLGYGICIIASYTAWYY 139
      **:* * :* *****:*****:*****:*.*****:* :*****:*.**.* ***** * * **

hSERT  NTIMAWALYLISSFTDQLPWTSCKNSWNTGNCT-NYFS-----EDNITWTLH 223
emSERT NTVISWALFYMFDMSMLRRLPWDSCDNWNTPKTCITVYQKLVGTANSDDIADSDASNTLH 199
      **:::***:*:..*:* : *** **.* *** : . : . : : : : **

hSERT  -----STSPAEEFYTRHVLQIHRSKGLQDLGGISWQLALCIMLIFTVIYFSIWKGVKTS 277
emSERT AVNTTGYYSSTEQYFYNRVLQIQLSDFGNKLGITIRWEVALCLLAVFTLVYFALWKGVKSS 259
      * :*::: .:*****: *.*::** * *::*****: :*:*:*:*:*****:*

hSERT  GKVVVWTATFPYIILSVLLVRGATLPGAWRGVLFYLPKNWQKLEETGVWIDAAAQIFFSL 337
emSERT GKAVWITATLPYVILFILLIRGLTLRGLMGIQYLLPDFGRLKSIEVWNAASQIFFSL 319
      **.**:***:*:*:* :*:** ** *:* *:* ** *:::* . ** **:******

hSERT  GPGFGVLLAFASYNKFNNNCYQDALVTSVNCMTSFFVSGFVIFTVLGYMAEMRNEVDVSEV 397
emSERT GPGFGVLLALASYNFRNRCYDAMLTSAINCGTSFSLSGFVVFVSLGHMCMYRMRNTMD-T 378
      *****:*****:*.***** **::**.:** *****:*****:*****:* . * . : .

hSERT  AKDAGPSLLFITAYAEAIANMPASTFFAIIFFLMLITLGLDSTFAGLEGVITAVLDEFPHV 457
emSERT VANEGPSLVFIAYPEAIATLPGSTFWAIIIFMLMLITLGLDSTFGGLEAIITALLDRWPKL 438
      . : *****:*:* * ***.:.*.***:*****:*****.***.:***:**.:::

hSERT  WAKRRERFVLAVVITCFFGSLVTLTFFGAYVVKLLEEYATGPAVLTVALIEAVAVSWFYG 517
emSERT R-KRREIVVLIMIICYV GALPTTTNGGYIILTFDITYGAPFSILFIVFCECVALCWCYG 497
      **** .** :* *:*:* * * ** *:::*.:: *.: :* :.: *.*:* * **

hSERT  ITQFCRDVKEMLGFSPGWFWRICWVAISPLFLLFI--ICSFLMSPPQLRLFQY--NYPYW 573
emSERT VGRFTRDIESMLGFKPGFWFWRICWAVISPAFMLGIFILNITFFRPPEITVMGKTVRADTW 557
      : :* **::.****.*****.*** *:* * : : : **:: : : . *

hSERT  SIILGYCIGTSSFICIPYIAYRLIITPGTFKERIIKSITPETPTEIPCGDIRLNAV--- 630
emSERT VHVVSWMLVFSSLVTIPIFAVVTFCARGSFKERLKSFLTGPGRPSFSDFHVHPNSHKKQ 617
      :::: : **:: ** : . : : *:*****: . :** .: .: : *

hSERT  -----
emSERT EIKDKDEEQVAKSAEAVDDTQSEGDEG 644

```

Figure II.0.1 MUSCLE alignment of emST and hST sequences.

E. multilocularis (Fox tapeworm), A0A068XWX1; Homo sapiens (Human), P31645; Figure generated alignment in CLUSTAL software.

Appendix III: Primers

Table III.0.1 Primers for cloning

Name	Sequence	Tm °C
emST 1200bp R	GTA GCG ATA GCC TCG GG	58
emST 800bp F	TGG ATC ACC GCT ACT CTG	58
emST Nde1 F	CAC GTG TCT TGT CCG CGG TAC C	72
emST Hind3 R	CGT AAG CTT TTA ATG GTG ATG GTG ATG GTG ATG GTG ATG GTG ACC GGA GCT ACC ACC TT	176
emST EcoR1 F	CAC GTG TCT TGT CCG CGG TAC C	67
emST Hind3 R	CGT AAG CTT TTA ATG GTG ATG GTG ATG GTG ATG GTG ATG GTG ACC GGA GCT ACC ACC TT	79
emST pOpiE2 R AvrII	AAA TAT CCT AGG TTA TTA AGC AGG GGC CAC C	59
pTT5emST NDeI Rev	GGT GGC GAA TTC GCT AGA GAT	59
pOpiE2emST NDeI Rev	GGT GGC GGA TCC TCG AAC A	64
pTT5-emST For	cca agt tta aac gga tct cta gcg ATG GAA GAT CAG TCC CTC AA	73
pTT5-emST Rev	aga ggt cga ggt cgg ggg atc CTA TTA TTA AGC AGG GGC CAC CT	79
pOpiE2-emST For	AGT TGA ACA GCA TCT GTT CGA GAT GGA AGA TCA GTC CCT CAA	74
pOpiE2-emST Rev	TCA AAA TAT ATG TAT AAC CTG ACT ATT ATT AAG CAG GGG CCA CCT	70
PS2_Nde1_new	GGA ATT Cca tat gCT GAC CTT TAT GGC GA	67
PS2_Xho1_no tta	CCG ctc gag AAT ATA CAG CTG ATG	62
PS2_Rho_Xho1	GGG CTC GAG CTA TTA AGC TGG CGC CAC CTG GGA AGT CTC GGT GCC GGA GGA GCC AAT ATA CAG CTG ATG GCT GG	86

emST pO2 noRho Spe1 R	GGA CTA GTA CCG GAG CTA CCA CCT T	60
Avr2 mCh C Rho R	GTA TAA CCT GAG GCC TAG GG	58
T2S pOpiE2 BamH1 R	GGG GAA GAT TCG TTG AAG G	57
T2S pOpiE2 Spe1 F	GAA ATT CAA GAC TCC CAG AAC	56
pTT5BA-B BamH1 R	GGA CTG ATC TTC CAT GGT G	57
pTT5BA-B Avr2mch F	CCC CTG CTT AAT AAC CTA GG	57
pO2_T2S-Crho Ins F	tca caa gtg gct cca gcc tga GGT ACC CCT AGG CCT CAG	60
pO2_T2S-Crho Ins R	agt ctc ggt tcc gga cga tcc CTT GTA CAG CTC GTC CAT G	57
pQE2 emST C Rho F	ggt ggc ccc tgc tTA AAA GAT TAA TTA AAT TGA AGG CCG C	73
pQE2 emST C Rho R	tga gaa gtc tca gtA CCG GAG CTA CCA CCT TC	71
emST pOpiE2 F BamH1	CGC gga tcc GCC ACC ATG GAA GAT CAG T	68
emST pOpiE2 R Bsu36I	AAA TAT CCT nAG GTT ATT AAG CAG GGG CCA CC	69
pTT5emST NDeI Rev	GGT GGC GAA TTC GCT AGA GAT	62
pOpiE2emST NDeI Rev	GGT GGC GGA TCC TCG AAC A	64
Fwd emST NdeI	CGC CAC ATA TGG AAG ATC	54
Rev emST HindIII	GCA AGC TTT TAA TGG TGA TG	55
pET27b emST C Rho F	ggc ccc tgc tta ata aAA GCT TGC GGC CGC ACT C	66
pET27b emST C Rho R	acc tga gaa gtc tca gtA CCG GAG CTA CCA CCT TC	71
Fwd emST I273A	GCC TTA CGT Ggc cCT GTT CAT CC	65
Rev emST I273A	AGA GTA GCG GTG ATC CAC	58
Fwd emST N605A	CTT TAT CCT Ggc aAT CAC TTT CTT CAG GCC	68
Rev emST N605A	ATG CCC AGC ATG AAA GCA	66

Fwd emST Cdel Rho pQE2	ttc tca ggt ggc ccc tgc tTA AAA GAT TAA TTA AAT TGA AGG CCG	63
Rev emST Cdel Rho pQE2	gtc tca gta ccg gag cta ccG GAG AAG GAA GGA CGG AT	61
Fwd emST Ndel M pQE2	atg GAA CGC AAG CGC GAG AAG	67
Rev emST Ndel M pQE2	TCT CCT CTT TAA TGA ATT CTG TGT G	62
Fwd emST Y69A	CTA CAT CTG Cgc cCA GAA CGG TG	63
Rev emST Y69A	GGG AAA CGC CAG ATA TTG	60
Fwd emST Loop del	GAC GCT TCT AAC ACC CTG	58
Rev emST Loop del	CAG CTT TTG GTA CAC GGT	59

T_m values were calculated from Thermo Scientific Web Tools-T_m Calculator

Appendix IV: Protocols

Osmotic shock:

Periplasmic fraction removal: Cell pellets were resuspended in sucrose buffer with a ratio of 5 mL per gram cell pellet and homogenized by glass porter before pelleting down at $7,000 \times g$ for 30 min at 4 °C. The pellet was re-suspended in 5 mM $MgSO_4$. The mixture was then incubated on ice for 10 min, centrifuged at $4500 \times g$ for 20 min at 4 °C and the pellet was collected for cell lysis.

Transformation:

The plasmids were transformed into 100 μ L aliquots of competent cells by 42 °C heat-shock treatment. The transformants were selected on an LB agar plate with 50 μ g/ml kanamycin. After overnight incubation at 37 °C

Competence cells:

Streak out the *E.coli* strain on an LB plate to isolate colonies and incubate at 37 degrees °C overnight (16-20 hours). Use a sterile inoculating loop to collect cells from a single colony and inoculate 50 ml sterile Grow at 37 °C overnight (16-20 hours) in a shaker incubator. Also place 2 flasks of 250 ml in the incubator to equilibrate the temperature of the medium. Add 25 ml of the overnight culture to each 250 ml LB flask. Place another flask of 150 ml LB medium in the incubator to equilibrate the temperature of the medium. Grow the cultures to $OD_{650} = 0.2$ (not dense approximately 3 hours). Add 75 ml of equilibrated LB medium to each flask and continue incubating for 30 minutes. Then pellet the cells at 5000 rpm for 10 minutes. Decant supernatant and resuspend the cells in 87.5 ml ice cold 100 mM $MgCl_2$. Hold on ice for 5 minutes. Transfer the cells to a pre-chilled sterile large centrifuge falcon tube. Spin for 10 minutes with 4000 rpm at 4 °C. Decant the supernatant and resuspend the cells in 17.5 ml of ice cold 100 mM $CaCl_2$. Hold on ice for 20 minutes. Pellet as above 4000 rpm for 10 minutes. Decant the supernatant and resuspend the cell pellet in 3.5 ml of a solution that is 85% v/v 100 mM $CaCl_2$ and 15% v/v glycerol (100%). For each culture processed chill approximately 15 labeled eppendorf tubes. Pipet 300 μ l cells into each tube. Transfer the frozen competent cell aliquots to -80 °C.

Acknowledgments

I would like to thank the China scholarship council (CSC) program and Forschungszentrum Juelich for financial support during my Ph.D. study.

I would like to thank the following people, without whom I would not have been able to complete this research and have made it through my Ph.D. degree.

I would like to express my sincere gratitude to my advisor Prof. Dr. Jörg Labahn for providing guidance and feedback throughout this project and for the continuous support of my Ph.D. also for rescuing me when I stuck in the confusing experimental results.

I sincerely thank Dr. Udaya K Tiruttani S, for every meeting and conversation were inspiring me to think more logically. I am truly grateful for his supervision over the four years, for his support, encouragement, and patience.

I am thankful to my colleagues, Dr. Ge Yang for their insightful comments on my project whenever necessary. And Dr. Daniel Worms for guiding me when I joined the group. Furthermore, I like to thank Abhilasha Kerkmann, Chengcheng Tao, Aziz Tume, Nishika Sabharwal and Lukas Lim for their great support in our lab. It has been so nice to be lab mates with them.

I also want to thank Dr. Jan Kubicek and Dr. Barbara Maertens from Cube Biotech for preparing the Nanodisc and insect cell cultures. I would like to thank Dr. Joop van den Leute from the Helmholtz Centre for Infection for providing insect and mammalian cell cultures. I also would like to thank Maria Marta Garcia Alai, Stephan Niebling, from Facilities of CSSB, Hamburg for help with Nanotemper and Roland Thünauer with confocal microscopy.

I would like to thank my family for their continuous and unparalleled love and for giving me the experiences that have made me who I am. I am grateful to my parent who supported me spiritually throughout my Ph.D. study and my whole life.

Erklärung

Ich erkläre, dass ich die vorliegende Arbeit selbständig und ohne unerlaubte Hilfe verfasst habe. Die vorliegende Arbeit wurde weder in der jetzigen oder in ähnlicher Form bei einer anderen Institution eingereicht. Es wurden zuvor keine Promotionsversuche unternommen

Hamburg,

Weihou Guo